STRUCTURE, LOW TEMPERATURE CONDUCTIVITY, AND SUPERCONDUCTING PROPERTIES OF NIOBIUM-SILICON COMPOSITE FILMS

by

Michael Wayne Denhoff

B.Sc. University of Calgary, 1976

M.Sc. Simon Fraser University, 1981

A THESIS SUBMITTED IN PARTIAL FULFILLMENT OF

THE REQUIREMENTS FOR THE DEGREE OF

DOCTOR OF PHILOSOPHY

in the Department

of

Physics

SIMON FRASER UNIVERSITY

March 1985

APPROVAL

Name: Michael Wayne Denhoff

Degree: Doctor of Philosophy

Title of Thesis: Structure, Low Temperature Conductivity, and Superconducting Properties of Niobium-Silicon Composite Films

Examining Committee:

Chairman: J. C. Irwin

S. Gygax
Senior Supervisor

R. F. Frindt

B. Heinrich

M. Plischke

B. P. Clayman

M. R. Beasley
External Examiner
Professor
Department of Applied Physics
Stanford University, Stanford, CA

Date Approved: March 14, 1985

PARTIAL COPYRIGHT LICENSE

I hereby grant to Simon Fraser University the right to lend my thesis, project or extended essay (the title of which is shown below) to users of the Simon Fraser University Library, and to make partial or single copies only for such users or in response to a request from the library of any other university, or other educational institution, on its own behalf or for one of its users. I further agree that permission for multiple copying of this work for scholarly purposes may be granted by me or the Dean of Graduate Studies. It is understood that copying or publication of this work for financial gain shall not be allowed without my written permission.

Title of Thesis/Project/Extended Essay

Structure, Low Temperature Conductivity and Superconducting Properties of Niobium-Silicon Composite Films

Author: _____
(signature)

Michael Denhoff
(name)

19 March 1985
(date)

ABSTRACT

Niobium-silicon thin films have been fabricated using a dual electron gun, ultra high vacuum evaporator. Films with a layered or modulated structure were made as well as coevaporated niobium-silicon films with uniform composition. Transmission electron microscopy shows that both thin film materials are polycrystalline and have the niobium crystal structure. Sputtering-Auger depth profiles show that there is a large amount of interdiffusion at the niobium- silicon interfaces.

Superconducting critical temperatures and critical magnetic fields were measured. An empirical relationship was found between the critical temperature and the bulk resistivity for the layered thin films. It is not clear what the theoretical explanation for this relation is. Temperature dependent conductivity and magnetoconductivity measurements were made on three and two dimensional films. These data are analyzed using superconducting fluctuation, weak localization, and electron-electron interaction theories. Good agreement between theory and experiment was obtained, giving values for the inelastic scattering time and for the spin orbit scattering time.

ACKNOWLEDGEMENTS

The author wishes to thank his supervisor Dr. Suso Gygax for his suggestions and guidance throughout this project, and especially for his invaluable help in writing this manuscript. His generousity in sending the author to conferences where knowledge vital to this thesis was obtained is greatly appreciated.

Russell Barton is thanked for his help in the design and construction of the vacuum system. Russ, along with Dr. Gygax built the high field cryostat which was used to make the conductivity measurements.

The author thanks Dr. A. E. Curzon for the TEM micrographs and diffraction patterns and for his help in interpreting these results.

Thanks also go to Dr. B. Heinrich for many helpful discussions about vacuum systems and for the Auger-sputtering depth profiles.

Helpful discussions on thin film depostion techniques and the properties of thin films with Dr. Bob Hammond, J. M. Graybeal, and Dr. M. R. Beasley all of Stanford University are acknowledged. Special thanks go to Dr. Beasley for sending the author recent literature concerning the influence of localization on superconductivity.

Finally, many thanks go to the author's wife, Pat Kalyniak, for her patience and support.

TABLE OF CONTENTS

LIST OF TABLES

LIST OF FIGURES

I. Introduction

The study of electronic properties of composite structures has had a profound impact in the field of semiconductors. It is interesting to investigate to what extent superconducting properties can be influenced by this novel fabrication technique. Of particular interest is the Nb-Si system since it has the promise of merging existing Si technology with high T_c superconducting properties. Towards this end we built an ultra high vacuum system containing e-gun evaporators. We then determined the structure of the composite films using TEM and Auger spectroscopy and measured the superconducting properties. Finally we studied in detail the influence of disorder and dimensionality which become important in these thin films. In particular, the recently developed theories of superconducting fluctuations, weak localization, and electron-electron interactions were used to analyse the normal state conductivity and superconducting properties of coevaporated Nb:Si and layered Nb/Si films. These effects are essential for a complete understanding of the properties of these films and they allow the determination of the inelastic scattering time τ_i and the spin orbit scattering time τ_{so}. There remain however a number of outstanding problems as will be explained in the relevant sections.

This thesis is organized as follows. Chapter 2 gives a description of the vacuum system which we built and the procedures used to make the Nb-Si thin films. The structure of these films is investigated in Chapter 3. Both transmission electron microscopy and Auger/sputtering depth profiles were used.

The low temperature electrical properties of our Nb-Si films are given in Chapter 4. There is a relationship between the critical temperature and the resistivity. Similar observations have been made many times in the literature. This relationship is not completely understood and inspired us to look more carefully at the electronic properties. In this chapter, we use our measurements of ρ, T_c, and H_{c2} to determine a number of the electronic parameters for three of our films. Then measurements of temperature dependent and field dependent conductivity above T_c are given along with a qualitative description.

In Chapter 5, we present a detailed analysis of the conductivity in terms of superconducting fluctuations, localization, and electron-electron interactions. One must have a qualitative understanding of these theories before one can even begin a quantitative analysis. This is given as an introduction to Chapter 5. Then the data for three Nb/Si films is analysed. The complicated theoretical formulae used are given along with the analysis. This is done so that the reasons for choosing a particular formula can be explained. At the end of

the chapter, the shape of the critical field curves is discussed along with possible effects that localization may have on superconductivity.

In the last chapter we give a summary and present the main conclusions reached in this thesis.

II. Ultra High Vacuum Evaporator

The physical vapor deposition of Nb and Si poses a number of problems. Nb has a high melting temperature of 2497 C and must be heated to an even higher temperature of 2657 C to give a reasonable evaporation rate [Shapira and Lichtman (1979)]. Si is highly reactive when in the liquid state, so that the container will quickly contaminate the Si evaporant. Both of these problems can be overcome by using electron beam heated sources which are contained in a water cooled copper hearth. Both Nb and Si are good getters. This means that a film deposited in a poor vacuum will contain a large amount of impurities from the residual gas in the vacuum. In order to obtain a clean thin film an ultra high vacuum is necessary. We designed and built this evaporator to satisfy these requirements.

A drawing showing the components of the evaporator is given in Fig. 2-1. The vacuum system is constructed of stainless steel and has copper gasketted, knife-edge seals. Pumping is done by a titanium getter pump and a 50 liter per second ion pump . A 50 l/s pump is rather small, because it must keep up with the large outgassing during the evaporation of Nb. This resulted in pressures during Nb evaporation of about 3 to 7×10^{-7} torr, even though pressures with the evaporators off were about 2×10^{-9} torr. This was achieved without a bakeout of the vacuum system.

This system contains two electron gun evaporators. One is a Thermionics electron gun source model # 100-0051. The source of electrons, in this gun, is a filament at the side. The electron beam is focussed and bent in a 270° arc by a permanent magnet. One of three evaporation sources can be placed in the electron beam by turning a handle outside the vacuum system. This electron gun has a maximum output of 4 Kwatts.

A second evaporation source was built using an electrostatically focussed gun made by Veeco, model # VeB-6. This gun is aimed at a target which sits on a water cooled copper pedestal. When a Nb target was used, the bottom of the Nb would get hot enough to melt the copper at a few contact points. These points would then greatly increase the amount of heat conducted from the target and consequently reduce the evaporation rate. This was remedied by hard soldering a 0.010 inch thick tungsten sheet onto the top of the pedestal and placing the evaporation target on the tungsten. Both evaporation sources were encircled with water cooled stainless steel cylinders to shield the vacuum chamber from the heat.

Substrates are held about 8 inches above the evaporation sources in a stainless steel oven. The oven, heated by tungsten filaments, can attain temperatures above 700 C. The temperature is measured using a chromel-alumel thermocouple placed near the substrate holder. An introduction chamber allows the placement or removal of substrates without breaking the vacuum in the main system. The introduction chamber is pumped with a liquid

nitrogen trapped diffusion pump. A magnetically coupled arm can be passed through a gate valve to place the substrate holder in the oven. After sample insertion, the gate valve is closed to allow attainment of ultra high vacuum.

Film thickness is monotored using a Kronos model # ADS 200 quartz crystal thickness monitor. The quartz crystal is placed next to the substrate holder. The calibration of the Kronos monitor was checked by also measuring the thickness of a few films over 1000 Å thick using a Taylor-Hobson Talysurf model 3 surface profiler. The two thickness measurements agreed within a few percent.

The Kronos deposition monitor performed well when the Thermionic e-gun was operating. Unfortuately, it would not operate properly when the Veeco gun was on, even at low power levels. The cause of this is probably due to electrons from the Veeco gun scattering off the evaporation target onto the quartz crystal. A charge build-up on the crystal would cause unstable oscillation. Two attempts were made to prevent this. A grounded copper screen was placed in front of the crystal in hopes that it would collect most of the electrons. Also a permanent magnet was positioned to try to deflect the electrons. Neither method was successful in solving the problem.

The substrates used were either microscope slides cut into 1/2 inch by 1/2 inch squares or "flame polished" sapphire squares of the same size. Two substrates (usually one of each type) could be mounted side by side in the substate holder. The

substrates were first cleaned by scrubbing them in hot soapy water. They were then rinsed in hot tap water, distilled water, and finally ethanol. The substrates were blown dry and immediately placed into the vacuum system. The final cleaning step was baking at over 300 C in the ultra high vacuum.

The following procedure was used to deposit the thin films. With a shutter covering the substrates, the electron guns were operated for about ten minutes at a power level higher than what would be used during the actual deposition. The vacuum system was then allowed to cool off for 15 to 30 minutes. The shutter was opened and the substrate oven was brought up to the required temperature. Then, the thin film was deposited using one or both electron guns.

Films composed of Nb and Si layers were made using only the Thermionic gun, so that the quartz crystal thickness meter could be used. The sources were 99.9% pure Nb and 99.99% pure Si. In each case a Si layer was deposited first in order to isolate the Nb from the substrate. Then by turning the handle on the Thermionic gun the evaporation target was changed from Si to Nb. This takes about 15 seconds. A Nb layer is then deposited. This procedure was repeated until the desired number of layers were built up. Evaporation rates for both materials were about 100 Å per minute. During the evaporation of Nb the electron gun was operated at a power of about 2 Kwatts and the vacuum pressure was 5 to 7×10^{-7}torr. The pressure was 2 to 3×10^{-7}torr during Si evaporation using a power of 300 watts. A quadrapole mass

spectrometer showed hydrogen, water, and carbon dioxide in the base vacuum as would be expected. There was also a series of peaks at 13, 14, 15, and 16 atomic mass units. This looked like the signature of ethane which is shown in the appendix of [O'Hanlon (1980)]. When the electron guns were operated the largest increase of residual gas was at these hydrocarbon peaks.

A series of films were made with a single layer of Nb, about 250 Å thick, sandwiched between two 60 Å thick Si layers. The Si layers were used to isolate the Nb layer from the substrate and the atmosphere, and so that a single layer of Nb would have the same boundaries as Nb layers in a multilayer structure. For microcsope glass substrates it was found that the films with the highest superconducting critical temperature T_c were made with the substrate oven at about 300 C. It is assumed that at lower temperatures the Nb absorbs contaminents from the vacuum during evaporation. For substrate temperatures above 400 C the surface of the glass substrate would melt. Films deposited on sappire substrates had the same T_c as the companion glass film for substrate temperatures of 300 C and less. At higher temperatures (up to 600 C), the films on sapphire had slightly higher T_c's than the 300 C films. It was decided to use a substrate temperature of 300 C in the deposition of films throughout this study. We used the lowest temperature which gave films with good superconducting properties while at the same time minimizing diffusion between layers.

Coevaporated Nb:Si films were made using the Thermionic gun to evaporate Nb and the Veeco gun to evaporate Si. With a shutter in front of the substrates, the two sources were warmed up and stabilized. The shutter is then opened to deposit the film. Although the power to the e-guns was kept constant, this does not guarantee constant evaporation rates. The rates can easily change 5 to 10% during the few minutes of evaporation [Hammond et al (1975)]. The coevaporated films will likely have variations in composition of 5 to 10%. After the substrates are cooled from 300 C to 100 C (in about 10 minutes) a thin layer of about 50 Å of Si was deposited on top to protect the film from the atmosphere.

As previously mentioned, the quartz crystal thickness monitor did not work properly while the Veeco gun was operating. The thickness of the coevaporated films was determined using a Talysurf surface profile. This measurement also gives the composition of the film. This is possible because the Nb and Si sources were about 4 inches apart. Because of the shadowing by the substrate holder there is a thin strip of pure Nb on one side of the evaporated film and a thin strip of Si on the other side. The Talysurf profile shows this as steps. The compostion of the film can be determined from the height of the steps. The uncertainties of these measurements is about 10%.

Four probe resistance measurements and SQUID magnetometer measurements were made with the Nb/Si films. In order to facilitate these measurements, the Nb/Si films were evaporated

through masks made of 0.005 inch Mo sheet. The masks gave a four probe pattern in the central region of the subtrates and small circles in the corners of the substrates. The corners could be broken off and provided disc shaped samples for the magnetometer. Electrical connections were made to the four probe pattern using indium solder. Cleanliness is important for this and it was best to do the soldering immediately after the sample is removed from the vacuum system.

If a mask was used for the coevaporated films, there would be a thin strip of pure Nb on one side of the four probe pattern due to the shadowing. This is undesirable as the thin Nb strip dominates the resistive measurements. For this reason masks were not used for the coevaporated materials. Instead a four probe pattern was formed using a photolithographical technique.

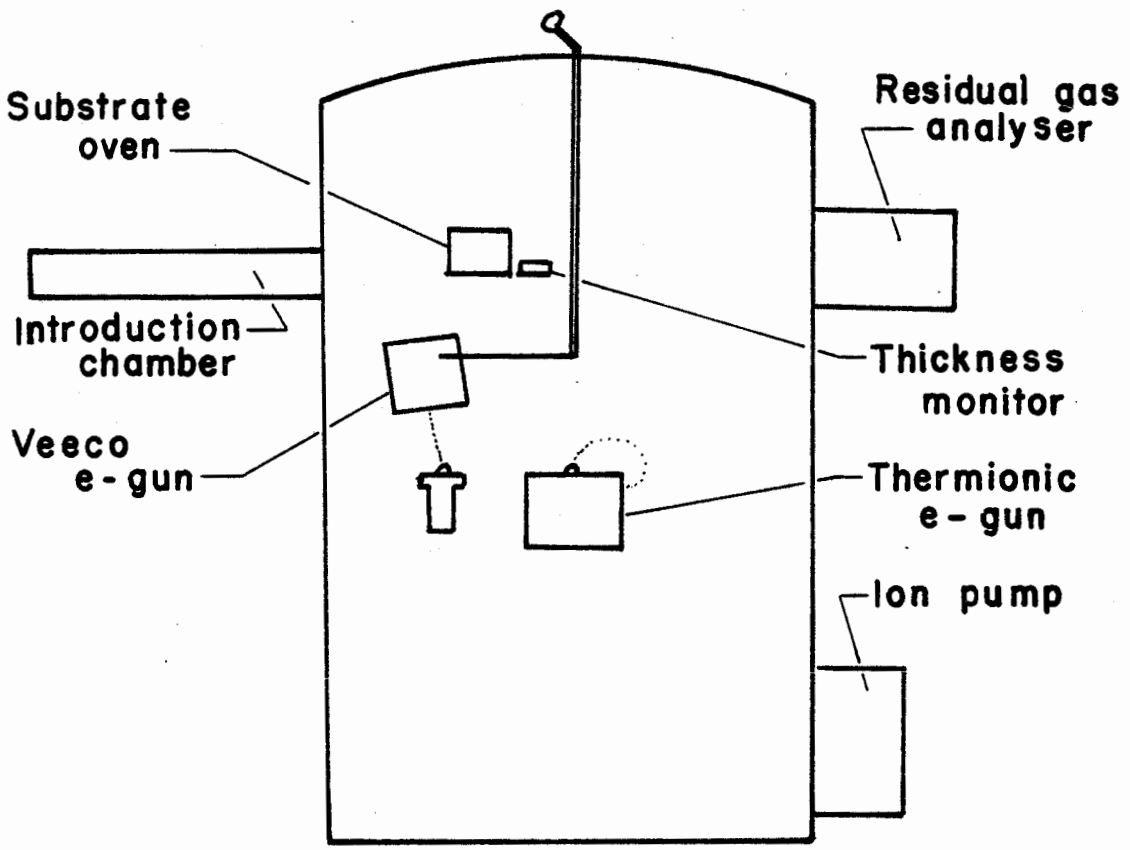

FIG. 2-1: Ultra high vacuum evaporator.

III. Material Analysis

Two basic techniques were used to investigate the structure and composition of the Nb/Si films. One was transmission electron microscopy, which was used to find the crystal structure and the size and orientation of the crystallites. The electron microscope was a Philips EM 300. The second technique used argon ion sputtering in conjunction with Auger electron spectroscopy. It gives the film composition as a function of depth. Two instruments were used to do Auger analysis. One was the analysis chamber in a PHI-400 Molecular Beam Epitaxy system. The second was a PHI-595 scanning Auger microscope. Many of the results in this chapter have been reported elsewhere [Denhoff et al (1985)].

1) Electron microscopy

Samples used in transmission electron microscopy must be thin enough for the electrons to pass through. This means that the samples must be less than about 400 Å thick. They were prepared using the following technique. A thick ($\sim$1 μm) copper film was evaporated onto a glass substrate in a separate evaporator. This substrate was then placed into the ultra high vacuum chamber and a Nb/Si film deposited on the copper with a substrate temperature of 300 C. The copper film was easily

removed from the glass using tweezers. A very weak solution of nitric acid was used to disolve the copper. Neither Nb nor Si are attacked by nitric acid. The remaining Nb/Si film would break up into small flakes floating on the water. They were picked up using a fine copper grid. After drying, this grid could be placed directly into the transmission electron microscope.

Fig. 3-1 shows a bright field TEM image of a Si181/Nb180/Si136 thin film (The numbers give the respective layer thickness in Å. Deposition sequence is from left to right). It is polycrystalline with crystallites on the order of 100 Å in size. The large features seen in this photograph are replicas of defects in the original Cu film. They are not intrinsic to the Nb/Si film. The black regions in the TEM image are crystallites which are in an orientation which transmits less of the electron beam. When the sample was tilted slightly the black spots on the image turned lighter and different crystallites showed up as black. This indicated that this film has a continuous polycrystalline structure rather than crystallites surrounded by an amorphous material. Fig. 3-2 also shows the diffraction pattern from this film. It is the body centered cubic pattern of Nb. A calibration diffraction pattern was made from an Al film. This gave a lattice constant of 3.3±0.1 Å for the Nb film, which is the published value for pure Nb. The diffraction rings are uniform in density indicating that the crystallites have a random orientation. That is, there is a

lack of texture in this film.

A TEM image of a film with a thinner Nb layer (Si37/Nb57/Si43) is shown in Fig. 3-3. The crystallites shown here are smaller than for the thicker Nb film, being on the order of 50 Å in size. Scanning across the sample showed that not all areas of the film were crystalline. A region about 1 μm away from the spot where the photo in Fig. 3-3 was taken, gave no diffraction rings at all. The sample is composed of crystalline as well as amorphous areas. This suggests that for very thin layers the Nb is amorphous and as the layers grow the Nb crystallizes.

A coevaporated Nb:Si film about 180 Å thick containing about 20% Si is shown in Fig. 3-4. As can be seen in the TEM image, it is a continuous polycrystalline film. The diffraction pattern in Fig. 3-5 is that of polycrystalline Nb. The uneven density of the rings shows the existence of texture in this film. There is no evidence of crystalline Si. Since the crystallites give the diffraction pattern of pure Nb, it is likely that amorphous Si is sitting in the grain boundaries.

It is usual for Nb thin films to have some degree of texture as is seen with the coevaporated Nb:Si film. The layers of Nb deposited on an amorphous Si layer however, are not textured. This would indicate that a crystalline substrate is the cause of the texturing.

2) Auger depth profiles

A depth profile of a thin film can be obtained by slowly sputtering away the film in an argon ion beam while examining the surface with an Auger electron analyser. We used a 3 KeV argon ion beam. Ion beam sputtering can cause damage to the surface of a thin film. In particular, it can lead to an artificially broadened interface. The effects of the ion beam on a Nb/Si interface were investigated by doing a depth profile of a 135 Å Nb film deposited on a single crystal Si [100] substrate at 300 C. The depth profile is given in Fig. 3-6. It shows a sharp interface about 20 Å thick. The shape of the interface is close to the shape predicted for interface broadening by collisional cascade [Sigmund (1981)]. In this process, the incoming Ar ions add energy to the surface atoms of the film giving rise to a diffusion process which will broaden a sharp interface. There will also be some broadening of the observed interface due to the escape depth of the Auger electrons of about 4 Å. It can be concluded that the actual Nb-Si interface is less than 20 Å thick. This indicates that there is very little diffusion when Nb is deposited onto a single crystal of Si. We can also conclude that the instrumental resolution is about 20 Å.

The data in Fig. 3-6 was obtained using a small sputtering angle (about 15° with respect to the sample surface). Data taken with a large sputtering angle (60°) gave a very broad interface.

It did not have the shape of an interface broadened by the collisional cascade process. A possible explanation is that for a large sputtering angle the argon ions push many Nb atoms deep into the Si substrate. On the other hand argon ions incident at a glancing angle will shear the Nb atoms off and will not knock them inwards. The following depth profiles all use a shallow sputtering angle (15°).

Fig. 3-7 gives the depth profile of a Si300/Nb103/Si85 thin film deposited on a glass substrate at 300 C. There is, evidently, a large amount of interdiffusion of the Nb-Si layers. In fact, there is a high concentration of Si throughout the Nb layer. The difference in sharpness between the Nb interface with the single crystal and amorphous Si is dramatic.

The ratio of peak-to-peak Auger signal for pure Nb to the signal for pure Si from Fig. 3-6 is 0.73±0.05. The standard Auger sensitivities given by Lawrence et al (1978) give a ratio of 0.75. This agrees with our observation. Knowing the Auger sensitivities we can now interpret the data in Fig. 3-7. The Nb concentration rises to a maximum of only 50%.

A film made by depositing the first Si and Nb layer at 300 C and then allowing the substate to cool to 100 C before adding the final Si layer is shown in Fig. 3-8. The "hot" interface is very broad. But the "cool" interface is much narrower. This shows the large effect that the substrate temperature has on the diffusion. Knowing the thickness of the top Si layer and of the Nb layer we can deduce the sputtering rates. The sputtering rate

for Si was 10.5 Å/min and the rate for Nb was 2.6 Å/min. The Si was sputtered away four times faster than the Nb. Anderson and Bay (1981) give sputtering yields of 0.5 Nb/Ar^+ and 1.0 Si/Ar^+ at 3 KeV, so that the sputtering rate for Si should be only twice as high as for Nb. The comparatively higher rate that we see for Si could be due to its amorphous structure.

The depth profile of a film with a multilayered structure is shown in Fig. 3-9. The nominal thickness of the layers as they were deposited is shown at the top of the figure. One can see, especially for the thinner Si layers, that the concentration of Nb stays relatively constant in depth, but there is a strong modulation of the Si concentration with depth. The layered films studied in this thesis are not properly layered but have a modulated structure.

It is interesting to investigate if heavily diffused layered or modulated Nb/Si thin films have similar properties as coevaporated Nb:Si films. It will be seen in Chapters 4 and 5 that the layered films have very different transport and superconducting properties than the coevaporated films.

FIG. 3-1: Bright field TEM image of a Si181/Nb180/Si136 film.

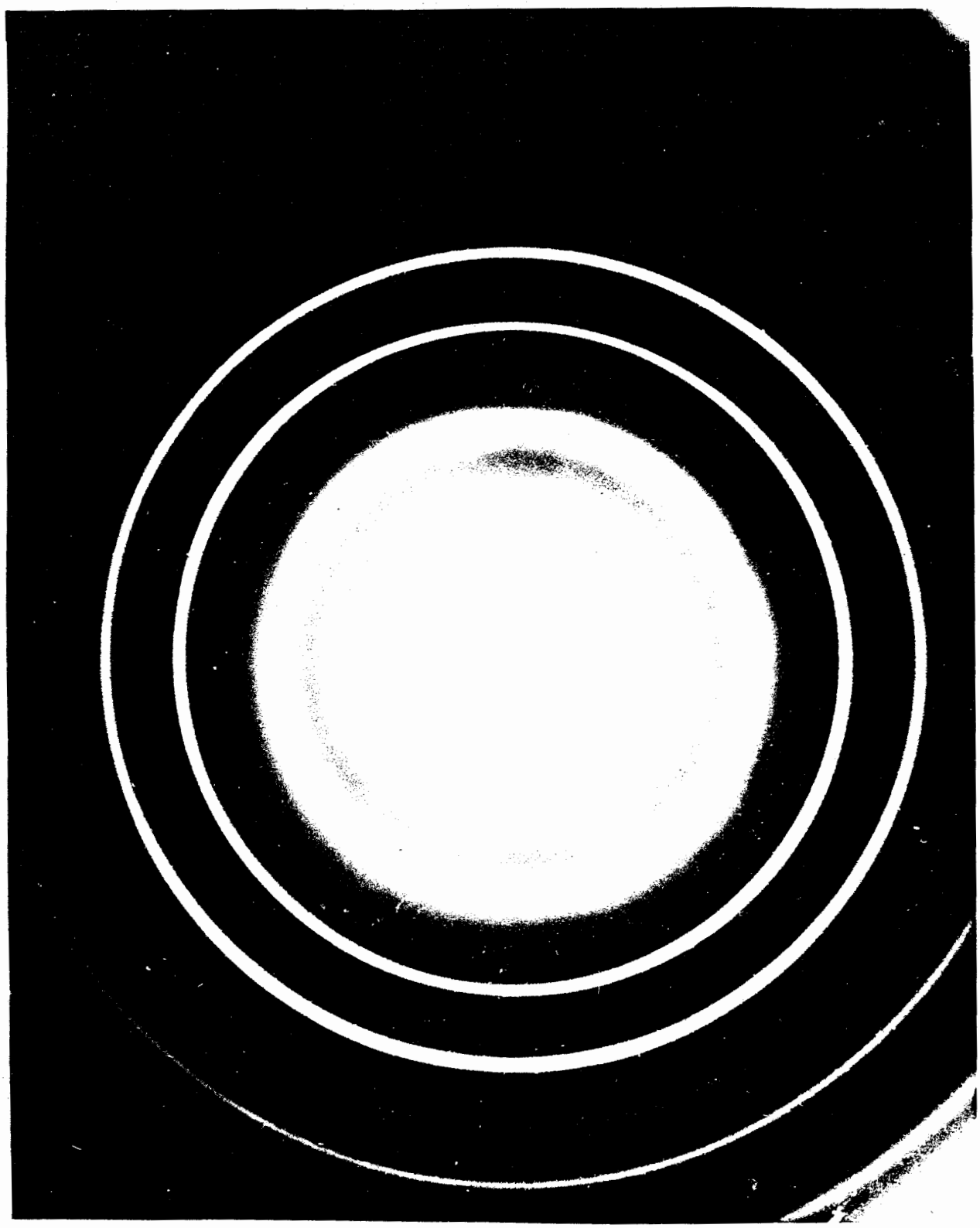

FIG. 3-2: TEM diffraction pattern of the film in Fig. 3-1.

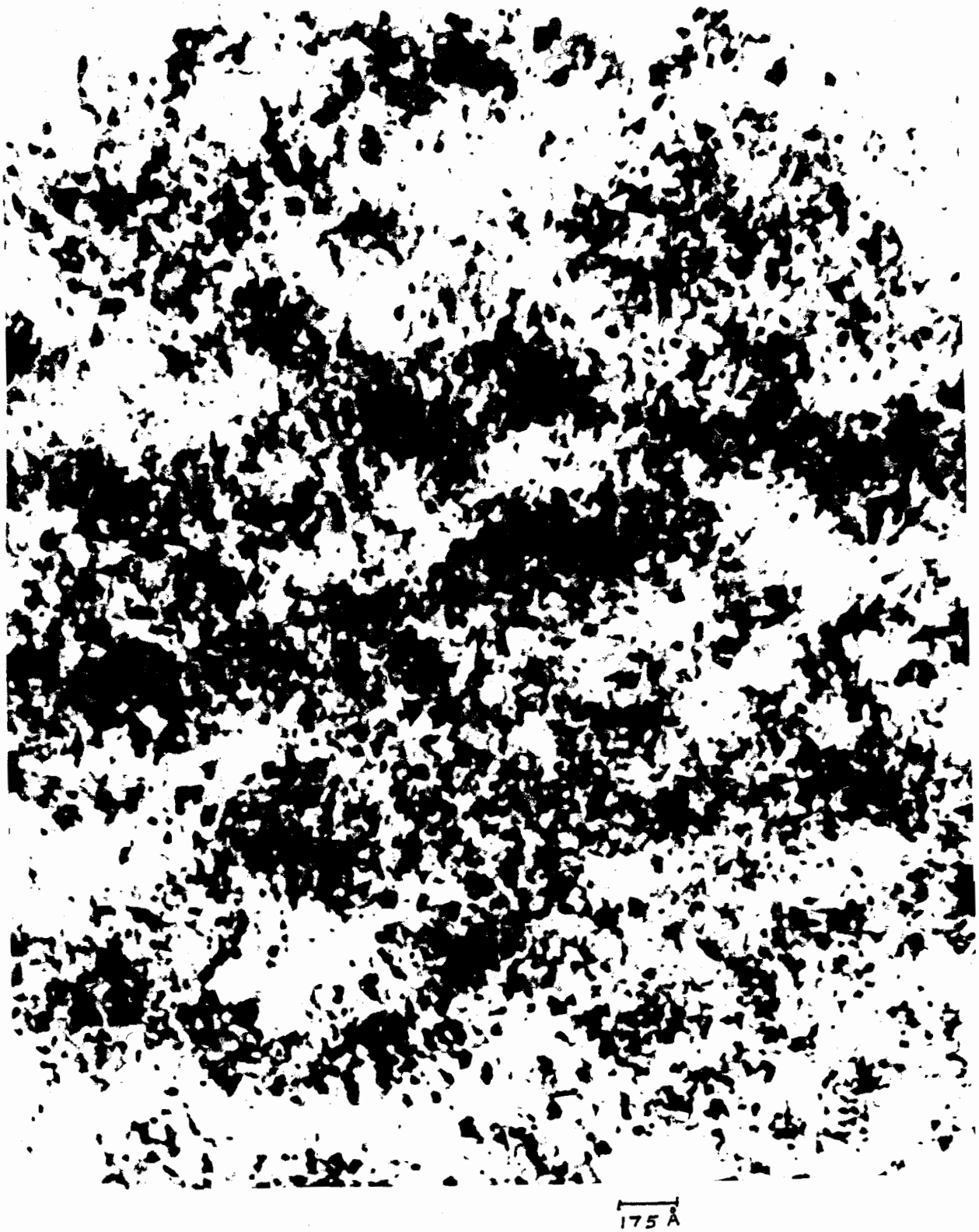

FIG. 3-3: Bright field TEM image of a Si37/Nb57/Si43 film.

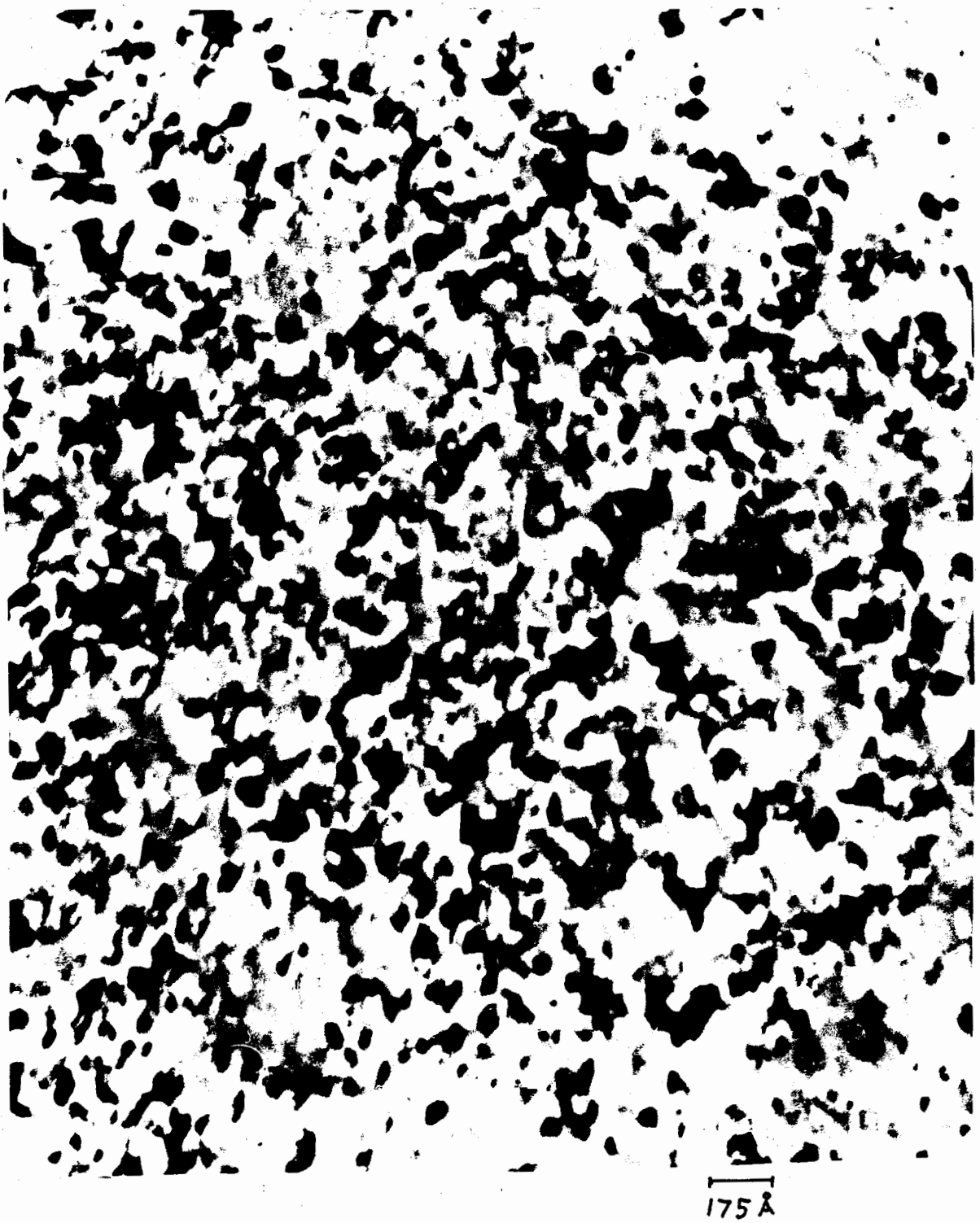

FIG. 3-4: Bright field TEM image of a Nb:Si coevaporated film.

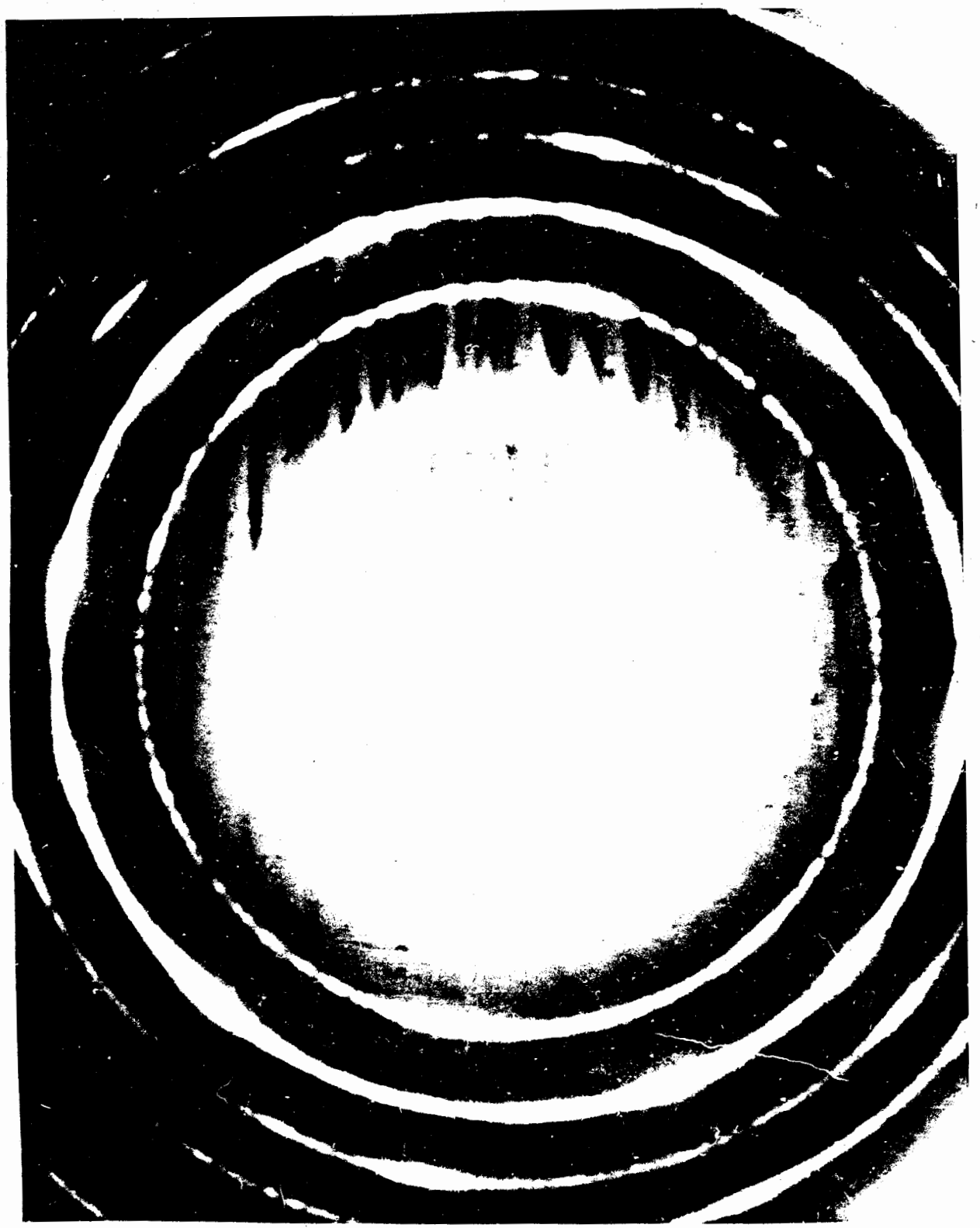

FIG. 3-5: TEM diffraction pattern of the film in Fig. 3-4.

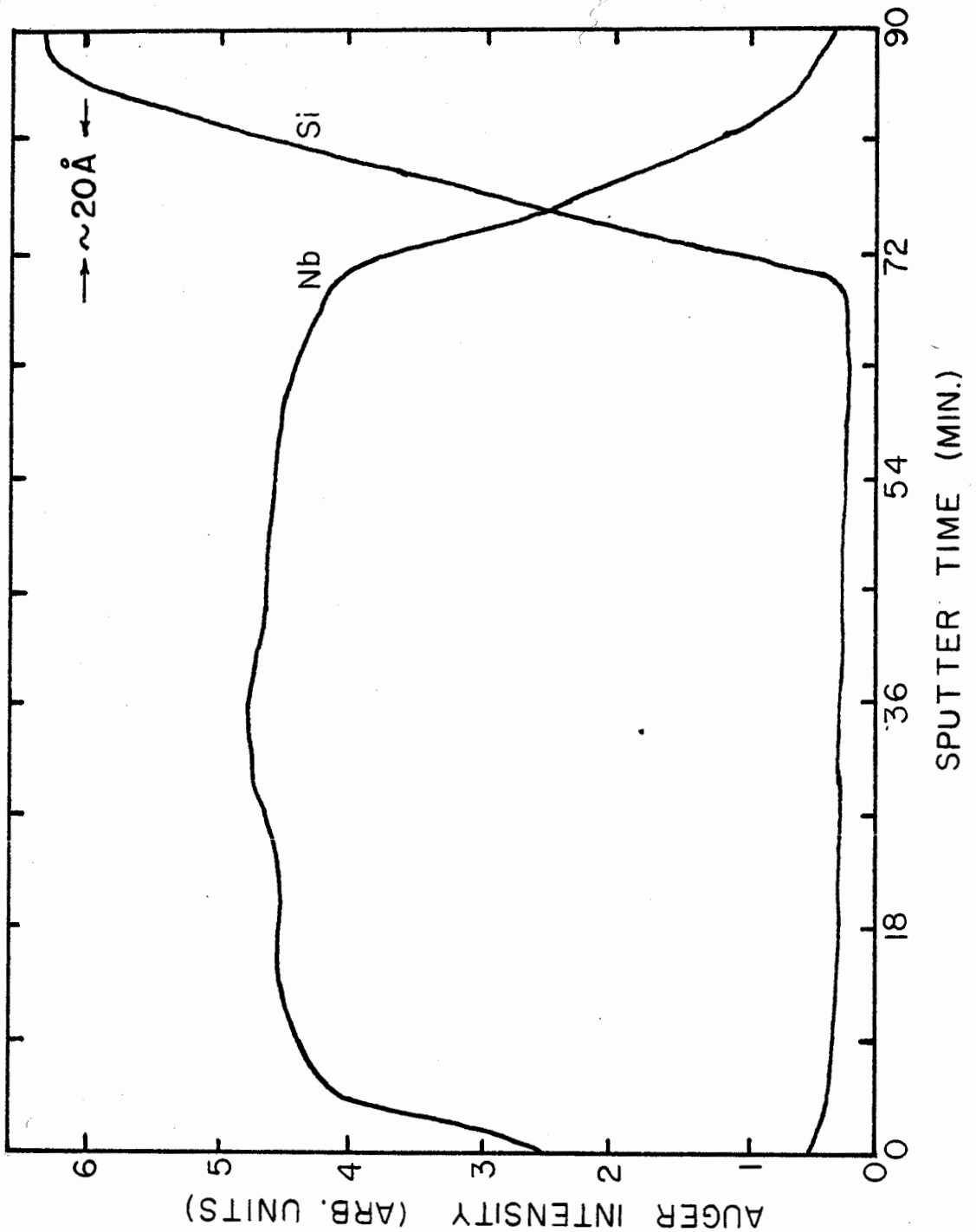

FIG. 3-6: Auger/sputter depth profile of a 135 Å Nb film on a Si[100] substrate.

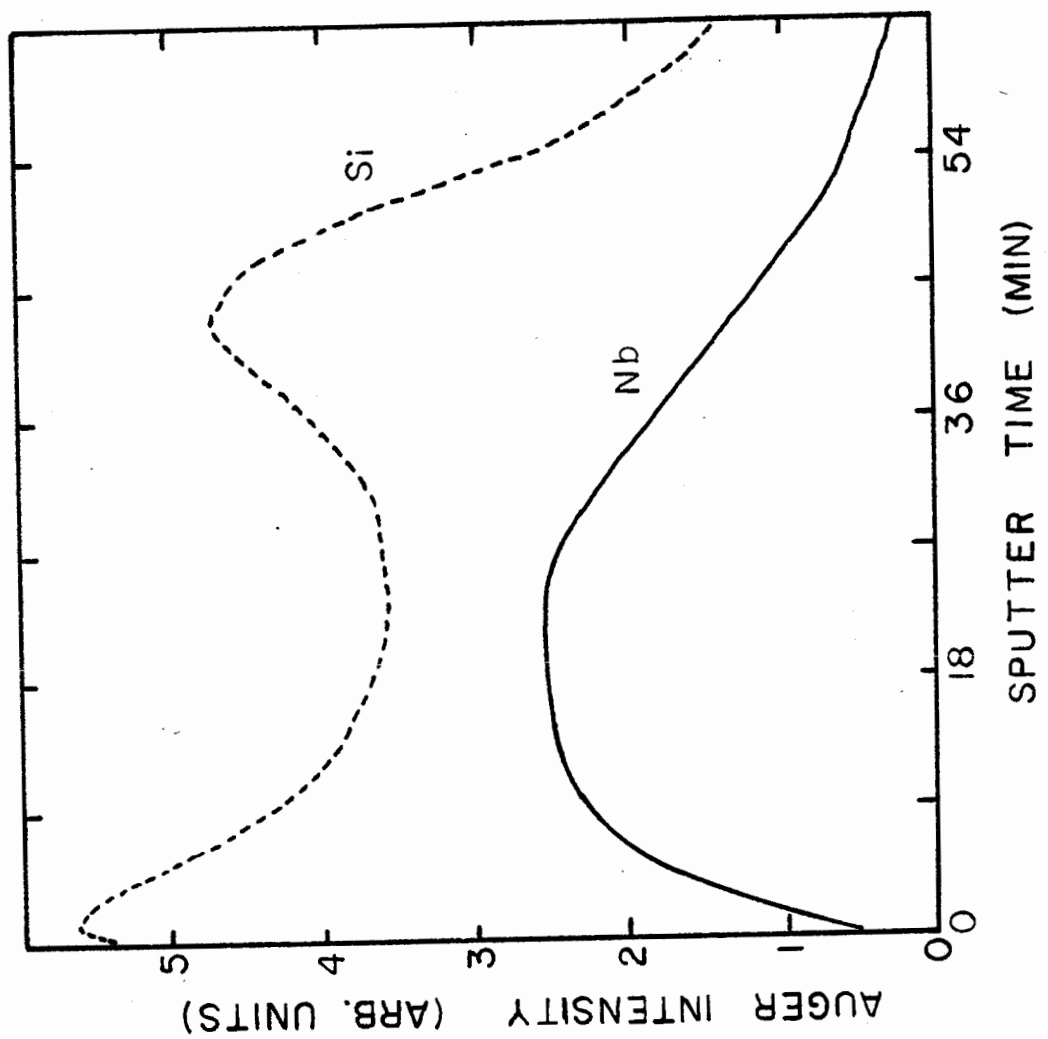

FIG. 3-7: Auger/sputter depth profile of a glass/Si/Nb/Si film.

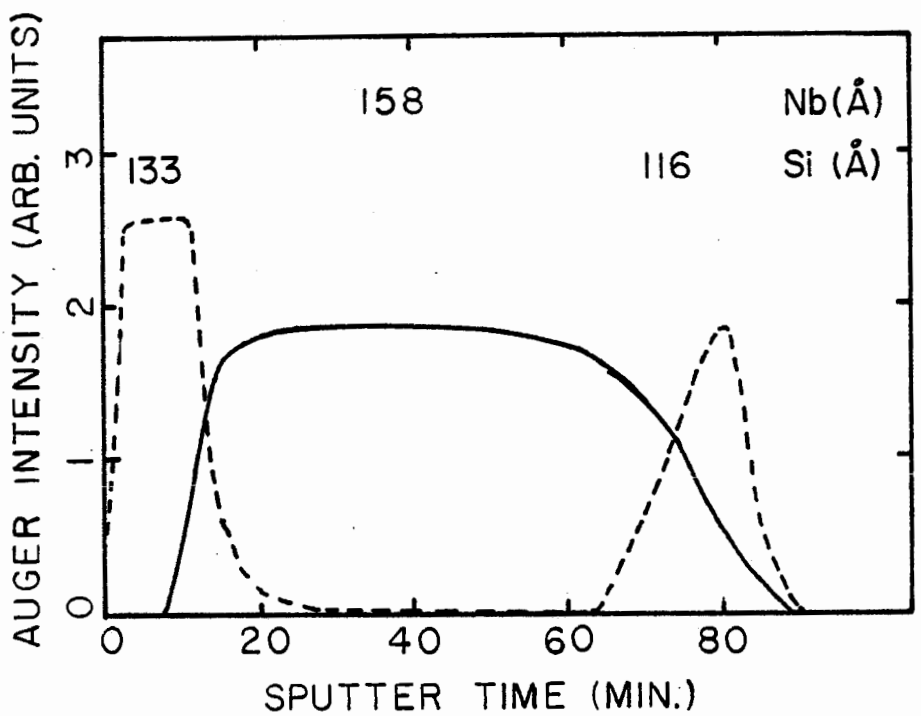

FIG. 3-8: Auger/sputter depth profile of a glass/Si/Nb/coolSi film. The numbers give the nominal thickness of the deposited layers.

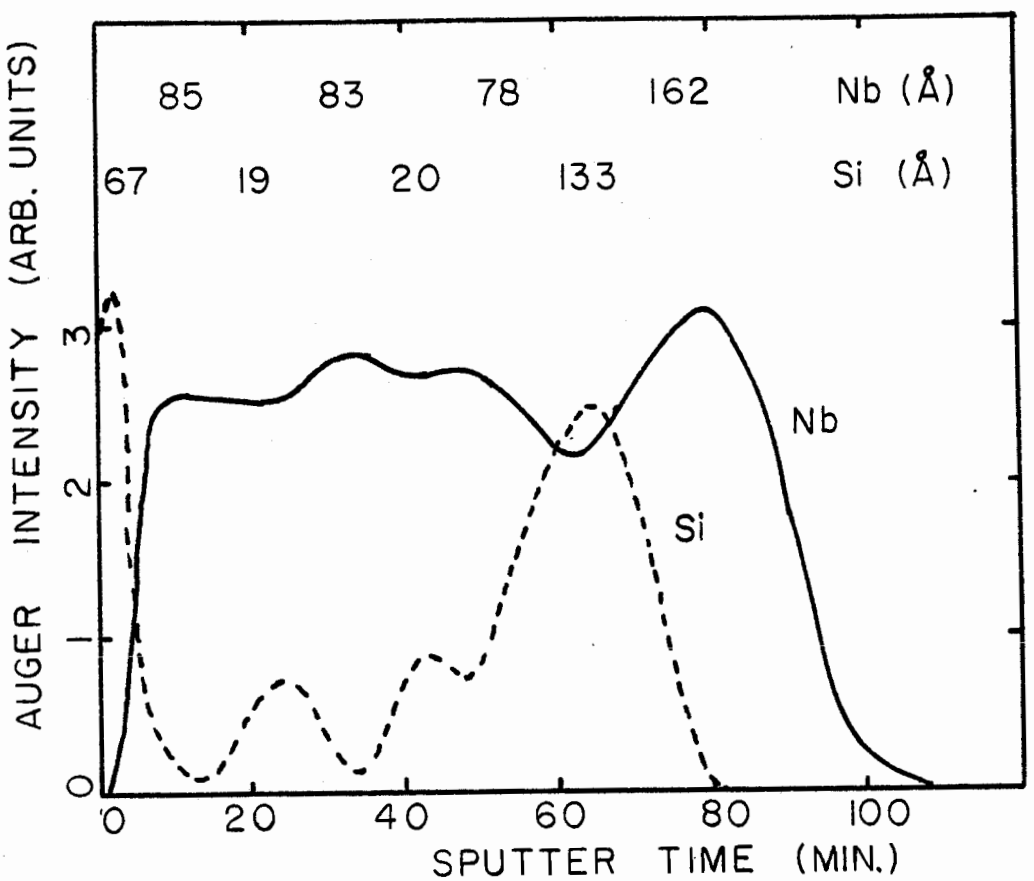

FIG. 3-9: Auger/sputter depth profile of a multilayered film. The numbers give the nominal thickness of the deposited layers.

IV. Low Temperature Measurements

In this chapter low temperature measurements on Nb-Si films are presented. SQUID magnetometer measurements along with four probe resistivity measurements are given in the first section. It was found that there is a relationship between T_c and ρ. The possible origins of this are discussed.

In the next section, results for T_c and H_{c2} from four probe measurements in a high field cryostat are given for three Nb-Si films. A number of superconducting and normal state parameters of the conduction electrons are determined from these measurements.

High sensitivity conductivity and magnetoconductivity measurements on the above three films are described in the final section. Only the qualitative features are discussed in this section. A detailed analysis of these experimental results will be given in Chapter 5.

1) Superconducting critical temperatures

Magnetic measurements were made using a SQUID magnetometer which has been described elsewhere [Denhoff and Gygax (1982)]. The magnetometer measures the magnetization of a sample in small magnetic fields (about 0.1 to 10 oersted). The signal is proportional to the susceptibilty and to the volume of the

sample. Since a superconductor in the Meissner state has a susceptibility of $1/4\pi$, the superconducting volume of the sample can be determined.

A sample the shape of a thin disc, perpendicular to the field, will give a magnetic signal proportional to the radius of the disc. The signal is independent of the thickness of the disc because of demagnetization effects [Denhoff et. al. (1981)]. A sample composed of regions with different critical temperatures does not show a smooth transition as in Fig. 4-1, rather there would be steps in the transition. This was not observed for any of the thin films studied here. If part of a sample does not go superconducting, the height of the transition will not be as large as the transition of a completely superconducting sample of the same size. A few samples were observed to be not completely superconducting above 4.2 K.

An example of a temperature swept superconducting transition is shown in Fig. 4-1. The critical temperature T_c is chosen to be the point where the sample turns completely normal, as shown by the arrow. T_c determined in this way corresponded to the onset of resistivity in the four probe measurement.

The superconducting critical temperatures T_c of several samples, as measured by the SQUID magnetometer, is given in Table 4-1. Also in the table are the resistivities ρ just above the superconducting transition, which were calculated using the thickness of Nb in the film (ie. neglecting the Si thickness even between Nb layers). The samples represented by the full

circles in Fig. 4-2 were made by sequential evaporation of Nb and Si. The crosses are for samples on glass substrates and the full circles on sapphire substrates. The two open circles are coevaporated Nb:Si films on sapphire substrates. A cross on top of a full circle represents fims which were deposited onto sister glass and sapphire substrates at the same time. They have the same T_c and ρ for ρ less than 20 $\mu\Omega$cm. In this range, there is a clear relationship with T_c decreasing rapidly as ρ increases. For ρ above 20 $\mu\Omega$cm, there is a difference between films on sister glass and sapphire substrates. T_c of the films on sapphire continues to decrease rapidly. But for the samples on glass the rate of decrease is much slower. For an even higher ρ (158 $\mu\Omega$cm), the films on sister glass and sapphire substrates again agree. (T_c is less than the 4.2 K liquid helium bath.) The resistance ratio of this film is less than one, which indicates that this film is no longer metallic. The range where sister glass and sapphire substrates give different results is just below this change from metallic to non-metallic behavior. It may be that the different thermal expansivities of the two substrate materials has a large effect on films in this critical region.

Relations between T_c and resistance are often observed, especially for Nb based superconductors. (See for example Ruggiero et al (1982) and Moehlecke and Ovadyahu (1984)). Many reports in the literature give a relationship between T_c and the sheet resistance $R_\square$. But in our data there is no such relationship between T_c and $R_\square$, as can be seen in Fig. 4-2.

The resistivity is influenced by the amount of interdiffusion at the Nb/Si interfaces. This can be seen by considering samples with a single Nb layer with about the same thickness of Nb, but with different Si overlayers. Table 4-1 shows that sample #15, in which all layers were deposited on a 300 C substrate, has a high ρ and a low T_c. A smaller amount of Si next to the sapphire substrate, sample #28, gives a smaller ρ and a higher T_c. An even larger change is seen in sample #29. The substrate was allowed to cool before the top Si layer was deposited. This results in less diffusion and a lower ρ and a higher T_c. All of these samples lie on the same $\rho(T_c)$ curve.

An attempt was made to go to larger ρ and lower T_c by decreasing the thickness of the Nb layer. However, for Nb thicknesses less than 130 Å, the films did not show a single clean superconducting transition. They had a partial transition at about 6 K but did not go completely superconducting until a much lower temperature was reached. These samples are still crystalline but are now behaving like inhomogeneous superconductors [Imry and Strongin (1981)]. A thin layer of Cu (25 Å) next to the Nb layer in sample #27 caused a large increase in ρ and decrease in T_c. The decrease in T_c is too large to be explained by the proximity effect [deGennes (1966)]. The decrease in ρ and its relation with T_c cannot be explained by a proximity effect either. The effect of adding Cu to the films was not studied further.

It was possible to make films with thinner Nb layers having a uniform superconducting transition using a multilayered construction. There is a large amount of diffusion of Nb into Si which gives a modulated structure rather than well defined layers (Chapter 3). Having a larger amount of Si compared to the amount of Nb increases ρ and decreases T_c as can be seen from samples #25, #24, and #23.

Adding more layers had an unexpected effect. Samples #36 and #33 have Nb layers of the same thickness. Sample #33 has thicker Si layers and one would expect it would have a higher ρ and lower T_c than #36. But the opposite is true. #33 has a larger number of layers and it is possible that this could increase T_c, but it would be surprising for the number of layers to have an effect on ρ. It has been suggested [Ruggiero, private communication] that evaporation conditions could improve as more layers are added. The vacuum pressure was observed to increase slightly during the deposition of a thin film. It is not likely that the top layers of sample #33 have a higher T_c than the bottom layers since this would be seen as a broadened transition by the SQUID magnetometer in the case of a field applied parallel to the film. However the temperature of the substrate could get hotter as more layers are deposited, even though the measured temperature of the substate holder stayed constant. This could increase the T_c of the entire sample. Whatever the actual situation is, it is interesting that the increase in T_c, accompanied by an appropriate decrease in ρ, is still keeping

the sample on the observed T_c vs ρ curve. One more observation can be made. Sample #26 has some thinner Nb layers and some thicker ones. There is no indication that the thinner layers have a different T_c than the thicker ones. It appears that the entire sample goes superconducting at the same temperature. Again, this sample is on the T_c vs ρ curve.

There have been many possible explanations for the decrease of T_c with the increase of ρ. Many of these theories such as inhomogeneous superconductors [Imry and Strongin (1981)] are two dimensional and really depend on $R_\square$. These can be discounted as there is no relation between T_c and $R_\square$ observed in our case. (Also these theories give large reductions of T_c only for much larger values of $R_\square$ than those measured for our films.) It is possible that adding Si to Nb reduces the number of conduction electrons. This would increase ρ in proportion to the decrease in $N(E_F)$, the electron density of states at the Fermi level. The mathematical relation is

$$\rho = \frac{e^2 v_F^2 \tau_o}{3\ N(E_F)} \qquad 4\text{-}1$$

where τ_o is the elastic scattering time and v_F is the Fermi velocity. T_c will decrease exponentially with $N(E_F)$ as seen in the relation [McMillan (1968)]

$$T_c = \frac{\omega_D}{1.45} \exp\left(\frac{-1.04\ (1+\lambda)}{\lambda - \mu^*(1+0.62\ \lambda)}\right) \qquad 4\text{-}2$$

where ω is the Debye temperature, $\lambda = VN(E_F)$ is the dimensionless electron-phonon interation constant, and μ^* is the Coulomb

pseudopotential. From Eqn. 4-1 the interaction constant can be written λ=(constant)/ρ. (Assuming that τ_o is unchanged is unreasonable. We make this assumption only to show the large effect that reducing the density of states has on T_c .) Using the values for Nb of ω = 276 K and μ^* = 0.13 and the values for sample #5 of T_c = 9.1 and ρ = 6 $\mu\Omega$cm the constant can be found. Then for a resistivity of ρ = 20 $\mu\Omega$cm Eqn. 4-2 gives $T_c = 5\times10^{-7}$ K. This is very much smaller than the observed T_c of 5 K. The observed T_c vs ρ relation cannot be solely due to a change in the density of states.

T_c can also be reduced by lifetime broadening of electron states at the Fermi surface. Testardi and Mattheis (1978) have calculated this effect for Nb and their result is shown as a dashed line in Fig. 4-2. The agreement between experiment and theory is fairly good for ρ < 20 $\mu\Omega$cm. Life time broadening is likely the cause of the reduction in T_c in this range.

For ρ > 20 $\mu\Omega$cm the drop in T_c is much slower for some of the data than the prediction of the life time broadening theory. Recently there have been calculations made of the decrease in T_c due to quantum effects of elastic scattering in disordered 3-D materials [Anderson et al (1983)] [Fukuyama et al (1984)]. In Chapter 5, we see that these quantum effects are present in our Nb/Si films and they may affect T_c .

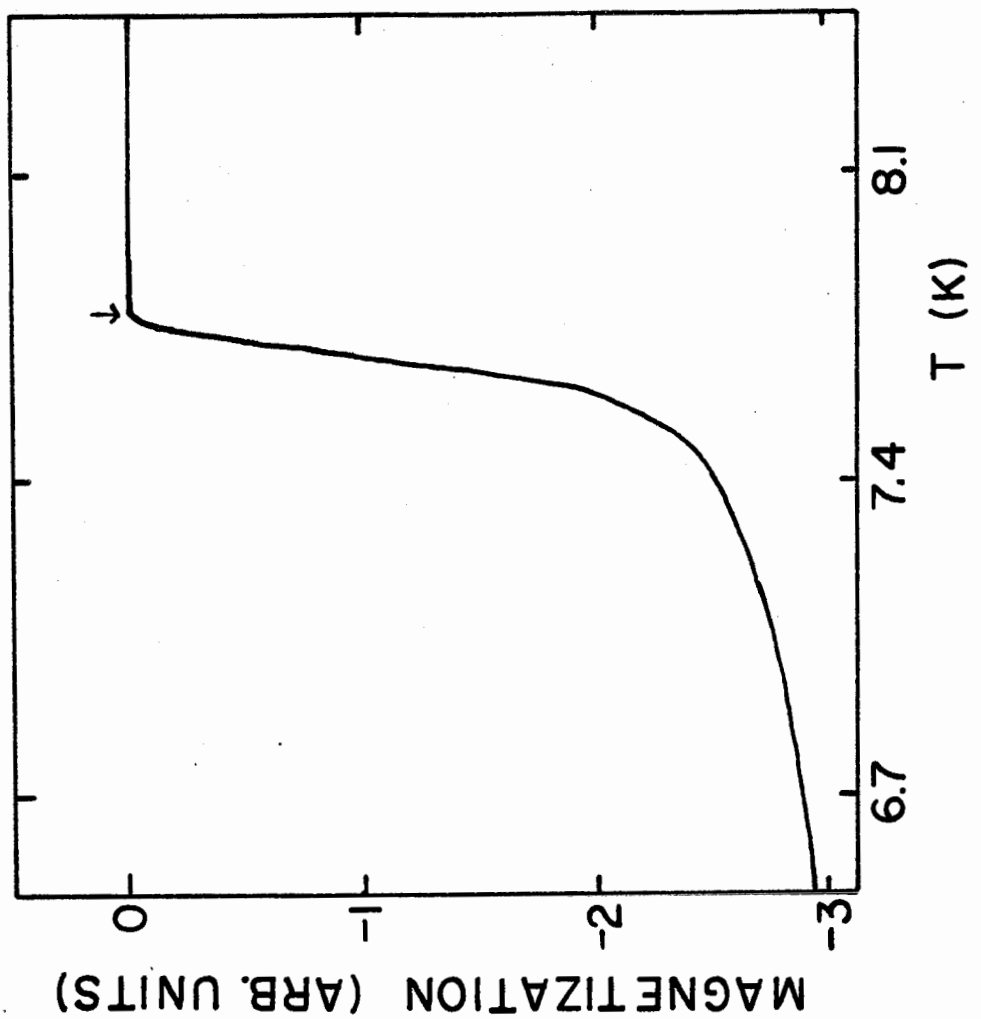

FIG. 4-1: A typical temperature swept magnetic superconducting transition.

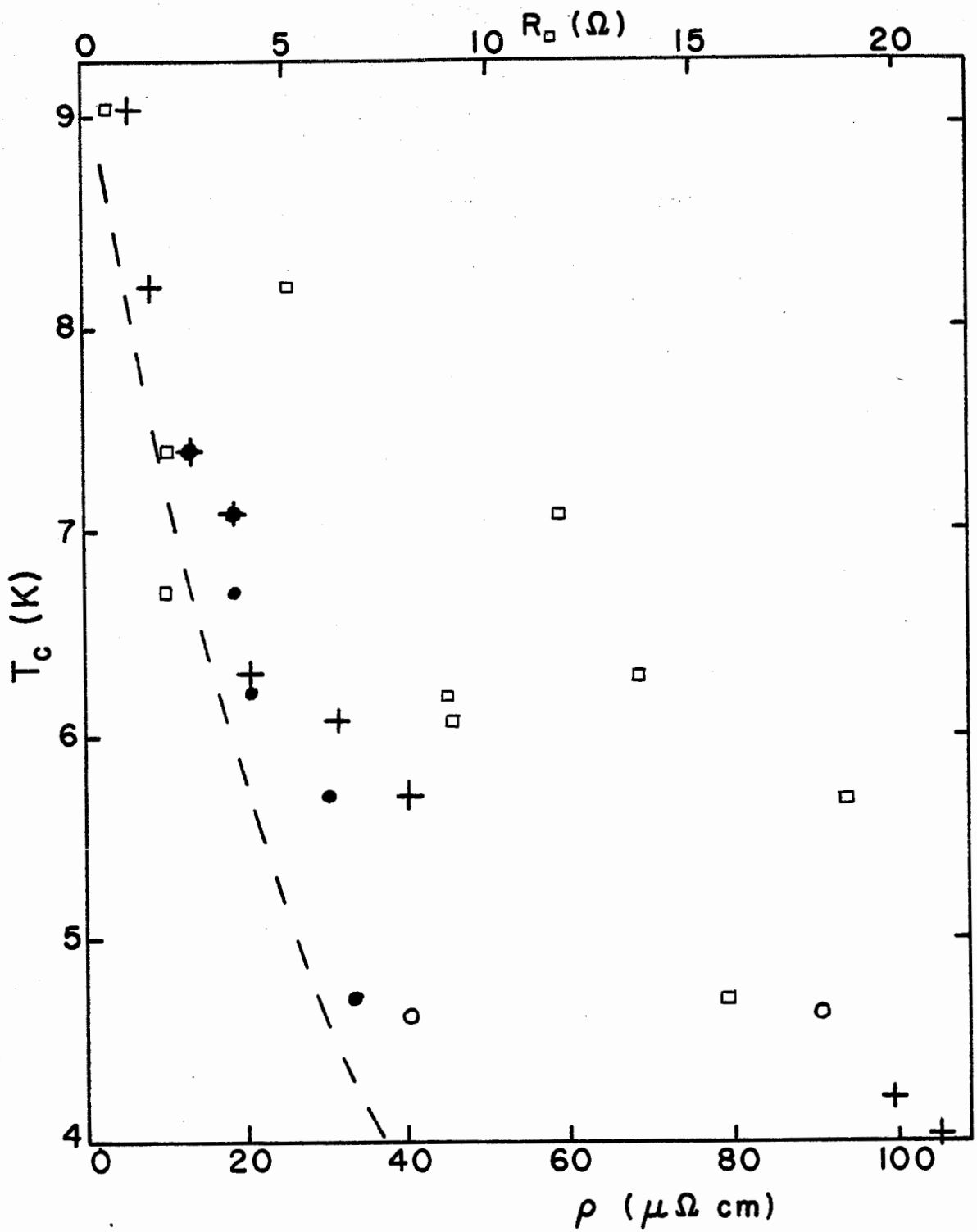

FIG. 4-2: T_c vs ρ for Nb/Si films. The crosses are layered films on glass substrates and the full circles are on sapphire. The two open circles are coevaporated Nb:Si films on sapphire substrates. $R_\square$ vs T_c is plotted as open squares. The dashed line is the lifetime broadening theory by Testardi and Mattheiss (1978).

Table 4-1

Resistance and critical temperature data. The G or S following the sample # signifies a glass or a sapphire substrate. The exponents in the thickness column gives the number of Nb layers. RR is the ratio of the room temperature resistance to the resistance just above the superconducting transition. The uncertainty of the resistivities is 10%.

sample #	thickness Si/Nb (A)	RR	ρ $\mu\Omega$cm	R Ω	T K
5-G	66/1005/57	4.11	6	0.6	9.1
15-G	36/161/61	2.26	22	13.7	6.3
23-G+S	60(65/66)^{3}63	0.97	158	80.9	
24 G	22(70/25)^{3}24	1.25	106.0	50.5	4.0
24-S	"	1.57	33	15.8	4.6
25-G	26(69/12)^{3}25	1.68	39	18.8	5.7
25-S	"	1.90	31	14.8	5.7
26-G	*	1.79	32	9.2	6.1
27-G	63(Cu26)143/70	1.13	100	69.8	4.2
28-G+S	15/155/70	2.50	18	11.7	7.1
29-G	71/158 /cool 68	3.57	5	5.1	8.2
32-G+S	(80/10)^8		13	2.2	7.4
33-S	(81/26)^{11}	2.10	19	2.1	6.7
36-S	54(79/17)^{3}54	-	21	9.0	6.2
50-S	67%Nb:33%Si	1.06	91	15.9	4.5
51-S	80%Nb:20%Si	1.20	40	36.5	4.6

* 31/51/13/49/12/84/13/84/10/63/21

2) Resistive transitions

The temperature dependent resistance and magnetoresistance were measured for several samples. From these measurements the resistivity ρ, superconducting transition temperature T_c, the superconducting coherence length ξ, and the diffusion contant D can be determined. The data is presented and the methods for obtaining the parameters is described in this section. A detailed discussion of the temperature and magnetic field dependence and comparison with theory is given in Chapter 5.

Four probe resistance measurements were made in a high field cryostat. The magnetic field is generated by a 50 KOe superconducting solenoid. The sample and thermometer are enclosed in a copper "isothermal" box. The temperature is controlled by helium gas flow outside the copper box. Four connections are made to the sample using indium solder. The solder will make contact only to the top layer of the layered sample. Because the film is only a few hundred angstroms thick, the resistance from the top layer to the bottom layer is very much smaller than the resistance along the voltage and current leads in the four probe pattern. Therefore the four probe measurement will give the resistance of the entire film.

A typical temperature induced resistive superconducting transition is shown in Fig. 4-3. It is not clear exacly what point on this curve should be used to give T_c. The SQUID

magnetometer measurements correspond to choosing T_c to be the point of initial resistivity. But the rounding of the transition makes this point somewhat ambiguous. One can also find T_c by matching the fluctuation conductivity above T_c to theory. This usually results in a value of T_c which lies in the top part of the resistive transition. In Chapter 5, this method of finding T_c is used for sample #50. It is more usual to operationally define T_c as the midpoint (in height) of the transition. This traditional method will be used here.

If the temperature swept transition is measured in a constant applied field the critical temperature T_c (H) is produced. These measurements can equally be thought of as giving the upper critical field as a function of temperature, $H_{c2}(T)$. A plot of H_{c2}vs T should be linear for temperatures near the critical temperature in the absence of a field, $T_c(0) = T_{co}$. The measured H_{c2} data for samples #50 and #24 are in Figs. 5-12 and 5-13 and are discussed in more detail in Chapter 5. The data for sample #51 is not given.

The temperature independent Ginzburg-Landau coherence length can be determined from [see any textbook on superconductivity, for example Tinkham (1975)]

$$\xi_{GL}(0) = \left[\frac{\phi_o}{2\pi T_c H'_{c2}}\right]^{1/2} \qquad 4-3$$

where $\phi_0 = 2.07\text{x}10^{-7}$ G.cm^2 is the magnetic flux quantum and H'_{c2} is the slope of $H_{c2}(T)$ at T_{co}. This formula is valid for dirty superconductors where $\xi >> l$, and l is the electronic mean free

path. The electronic diffusion constant D can also be obtained using

$$D = \frac{4kc}{\pi e H'_{c2}} \qquad 4\text{-}4$$

where k is Boltsmann's constant and c is the speed of light.

In the case of a layered superconductor the coherence length parallel to the layers is found using fields applied perpendicular to the layers by

$$\xi_{//} = \left[\frac{\phi_o}{2\pi T_c H'_{c2\perp}}\right]^{1/2} \qquad 4\text{-}5$$

Fields applied parallel to the layers give [de Trey et al (1973)]

$$\left[\xi_{//}\,\xi_{\perp}\right]^{1/2} = \left[\frac{\phi_o}{2\pi T_c H'_{c2//}}\right]^{1/2} \qquad 4\text{-}6$$

The anisotropic diffusion constant can be defined in the same way. Experimental values for H'_{c2}, ξ , and D are given in Table 4-2.

Other electronic normal state properties can be found using these results. The density of states at the Fermi surface is given by

$$N(E_F) = \frac{\sigma}{e^2 D} \qquad 4\text{-}7$$

The experimental values for $N(E_F)$ in Table 4-2 agree very closely with each other even though they have different resistivities. The theoretical value for Nb calculated by Mattheiss (1970) is 9.89 states/Ry/atom/spin, which after

converting units is 4.9×10^{34} $cm^{-3} erg^{-1}$. This is somewhat smaller than the experimental result, but the agreement is good enough to assume that the Nb band structure calculations can be used at least approximately, to represent the thin films studied here. Mayadas et al (1972) use Mattheiss' results to find

$$\frac{\ell}{\sigma} = 3.72 \times 10^{-12} \ \Omega \ cm^2 \qquad 4\text{-}8$$

The shortest length the mean free path can have is of the order of a lattice constant. The lattice constant of Nb is 3.3 Å, which is about the same as l for sample #50 (Table 4-2). This indicates that it is a very disordered sample.

It will be important for the analysis in Chapter 5 to know the elastic scattering time. This can be found from

$$\tau_o = \frac{\ell}{v_F} \qquad 4\text{-}9$$

where the Fermi velocity is $6.2 \times 10^7 cm\ s^{-1}$ [Mattheiss (1970)], which is an average over the complicated Fermi surface of Nb. Since Eqn. 4-9 is for a spherical Fermi surface, there is a large degree of uncertainty in our values of τ_o. The results are in Table 4-2.

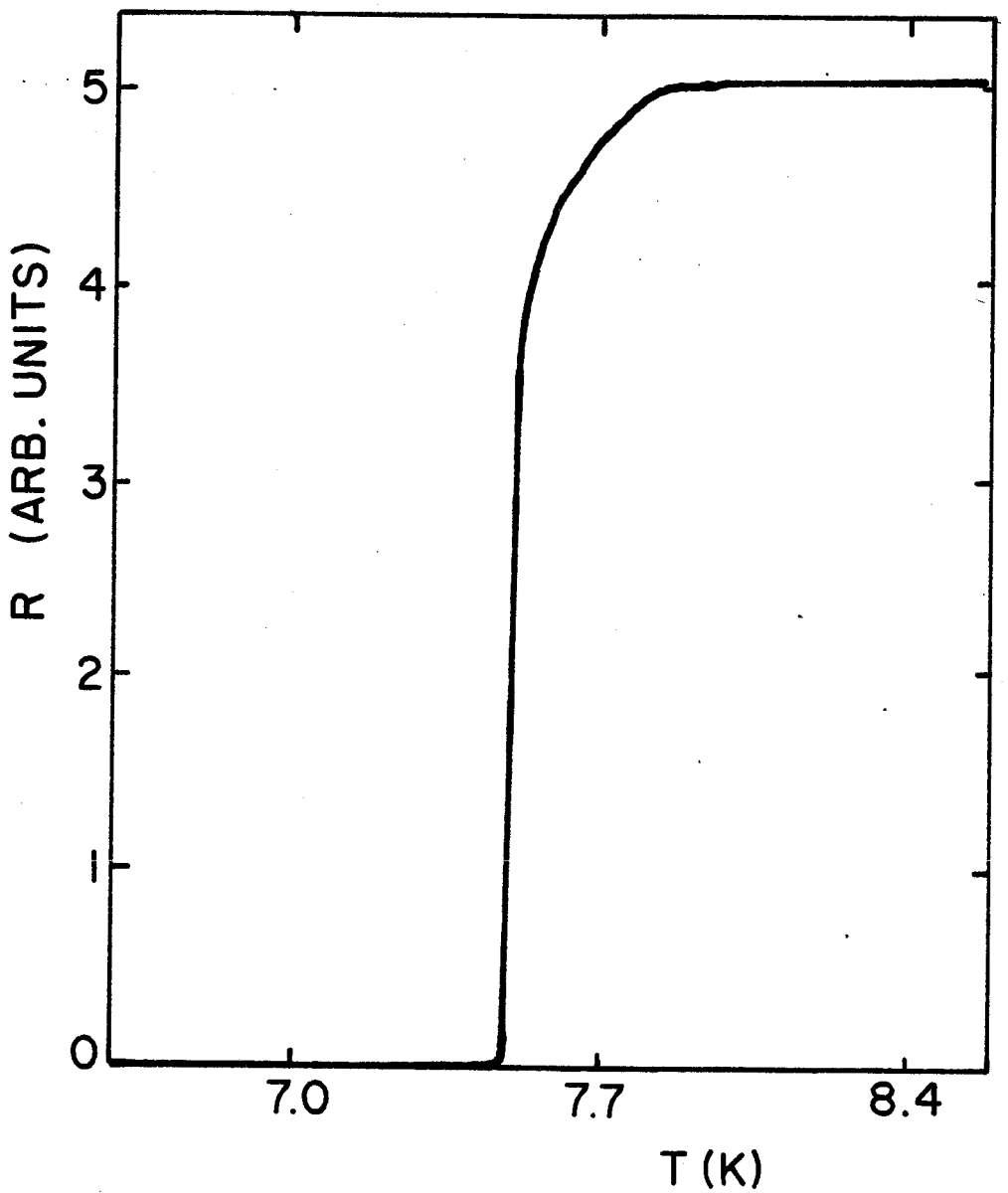

FIG. 4-3: A typical temperature swept resistive superconducting transition.

Table 4-2

Critical fields and transport properties. σ and H each have uncertainties of 5%.

sample	σ	H'_{c2}	$\xi(0)$	D	$N(E_F)$	l	τ_o
#	$\Omega^{-1}cm^{-1}$	KOe/K	Å	cm^2/s	$cm^{-3}erg^{-1}$	Å	s
50	7,400	22.6	57	0.49	5.9×10^{34}	2.8	4.4×10^{-16}
51	19,800	8.2	93	1.34	5.8×10^{34}	7.4	1.2×10^{-15}
24($H_\perp$)	20,800	7.7	96	1.42	5.7×10^{34}	7.7	1.3×10^{-15}
24($H_{//}$)		19.2	38	0.57			

3) Conductivity above T_c

It is interesting to measure the resistivity above T_c and study this in terms of quantum corrections to resistivity as discussed in Chapter 5. The quantum corrections are small compared with the overall resistivity. The four probe resistivity measurement must look for small changes on a large background signal. The measurements made here were sensitive enough to detect a change of 2 parts in 10^5 of the resistivity. These measurements were made using a SHE (model CCS) battery powered constant current source. The voltage signal was fed to a Dana (model 5900) digital microvoltmeter. The analog output was taken from the Dana (which gave a gain of 100), the large background nulled with a battery powered voltage source, and recorded with a Hewlett Packard (model 7046A) x-y recorder. The temperature was measured with a Lake Shore Cryogenics Inc. calibrated carbon-glass resistance thermometer (model #CGR-1-1000). A four probe conductance measurement of the

thermometer was made with a SHE Conductance Bridge (model PCB) and the analog signal fed to the Hewlett Packard x-y recorder. The data for three different types of samples is presented here.

a) Thick coevaporated Nb:Si film

Most conductivity measurements were taken in a constant magnetic field (with the superconducting magnet in the presistent mode) while slowly increasing the temperature. A set of data taken in this manner is shown in Fig. 4-4 for sample #50. This is a 850 Å thick, coevaporated Nb:Si film. Conductivity is plotted against temperature for several values of magnetic field applied perpendicular to the film. A line drawn at constant temperature will give the magnetoconductance. The runs were made starting at zero field going up in the sequence 12.1 KOe., 24.2 KOe.,36.3 KOe. and then back down in the sequence 30.25 KOe., 18.15 KOe., 6.05 KOe. Finally at zero applied field the signal came back to the original value, indicating negligible drift in the electronics. The measuring current used was 0.2 ma, which gives a current density of 450 A/cm and the power dissapation over the 0.65 cm length of the sample was 8×10^{-6} watts. The sapphire substrate is a good thermal conductor and is easily able to carry away this amount of heat. Measurements made using five times less current gave the same results but had a large uncertainty due to noise.

The temperature sweep data shows the conductivity increasing as the temperature decreases towards the critical

temperature. The conductivity goes to infinity at the superconducting transition. As the magnetic field is increased, T_c decreases but the shape of the curves remains about the same. The data for the highest two values of applied field is flat above 9 K. This shows that the temperature dependent conductivity due to phonon or electron-electron scattering (which is not affected by the magnetic field) is negligible on the scale of the figure.

The magnetoconductance can also be measured directly by holding the temperature constant and sweeping the magnetic field. Obtaining a constant temperature was very difficult with the gas flow system so only one magnetoconductance run was performed for each sample. The data for sample #50 is given in Fig. 5-5. The magnetoconductance measured directly agrees exactly with data from the temperature sweeps below an applied field of 20 KOe. The two measurements give slightly different conductivities at higher fields, as shown in Fig. 5-5 and discussed in Chapter 5.

b) Thin coevaporated Nb:Si film

Other coevaporated samples and single Nb layered samples showed the same behavior. Conductance data for sample #51 is presented in Fig. 4-5. This is a coevaporated Nb:Si film with a thickness of 140 Å. There is one qualitative difference between the conductivity of samples #50 and #51. Whereas the high field, high temperature conductivity of sample #50 is approximately

constant, the conductivity in this range for sample #51 still has a small, but significant temperature dependence. This is due to inelastic (phonon or electron-electron) scattering (or possibly weak anti-localization).

c) Multilayered Nb/Si film

Temperature sweep data in a perpendicular applied field, for sample #24, is shown in Fig. 4-6. This is a layered thin film with three 72 Å thick Nb layers sandwiched between four 25 Å thick Si layers. This sample shows very interesting qualitative behavior. As the field is increased the critical temperature decreases, but in contrast to sample #50, the shape of the transition also changes. At the highest fields there is no sign of a superconducting transition. In fact there is a maximum in the conductivity at a temperature of 8.4 K. The curve for 36.3 KOe shows the start of an upturn at the lowest temperatures, indicating the influence of superconductivity. A linear extrapolation of the upper critical field data (Fig. 5-13) gives 35.4 KOe for the critical field at zero temperature. From this it would seem that the conductivity shows superconducting fluctuations even though the sample would never go completely superconducting. The phenomenon of a decreasing conductivity with decreasing temperature at high enough fields to quench the superconductivity has been observed in an amorphous alloy system by [Toyota et al (1984)]. No explanation for this behavior was given. It is, as we show in Chapter 5, due

to quantum interference effects.

At high temperatures, in Fig. 4-6, there is a large temperature dependence in the conductivity in contrast to sample #50. Notice also that there is still an appreciable negative magnetoconductance at the highest temperature. At the highest fields and lowest temperatures, it can be seen that the magnetoconductance changes sign to positive.

The conductivity for the same sample (#24) but with the field applied parallel to the film is shown in Fig. 4-7. It is not surprising that there is no maximum in conductivity here because of the anisotropic nature of the sample. The critical fields in this orientation are much higher than in the perpendicular direction. It was not possible to reach fields high enough to quench superconductivity. It would seem likely that at high enough fields a conductivity maximum would appear.

The magnetoconductivity at high temperatures is quite small. At a temperature of 16 K the 36.3 KOe data lies above the 24.2 KOe data. The magnetoconductance here is positive, which is opposite in sign compared to that observed in perpendicular fields.

Fig. 4-8 shows field sweep data for both perpendicular and parallel fields. This data does agree within uncertainties with the temperature sweep data. It can be seen that the magnetoconductance for fields parallel to the film is much smaller than that for fields perpendicular to the film. This is mainly due to the anisotropic nature of the superconductivity.

It is interesting to note the kink in the perpendicular field data. It occurs at about 35 KOe, which is the extrapolated critical field at zero temperature. There is an abrupt change in the behavior of the electrons at this point.

In Chapter 5 we will analyse the data for these three films in detail. Each of the above mentioned features can be explained.

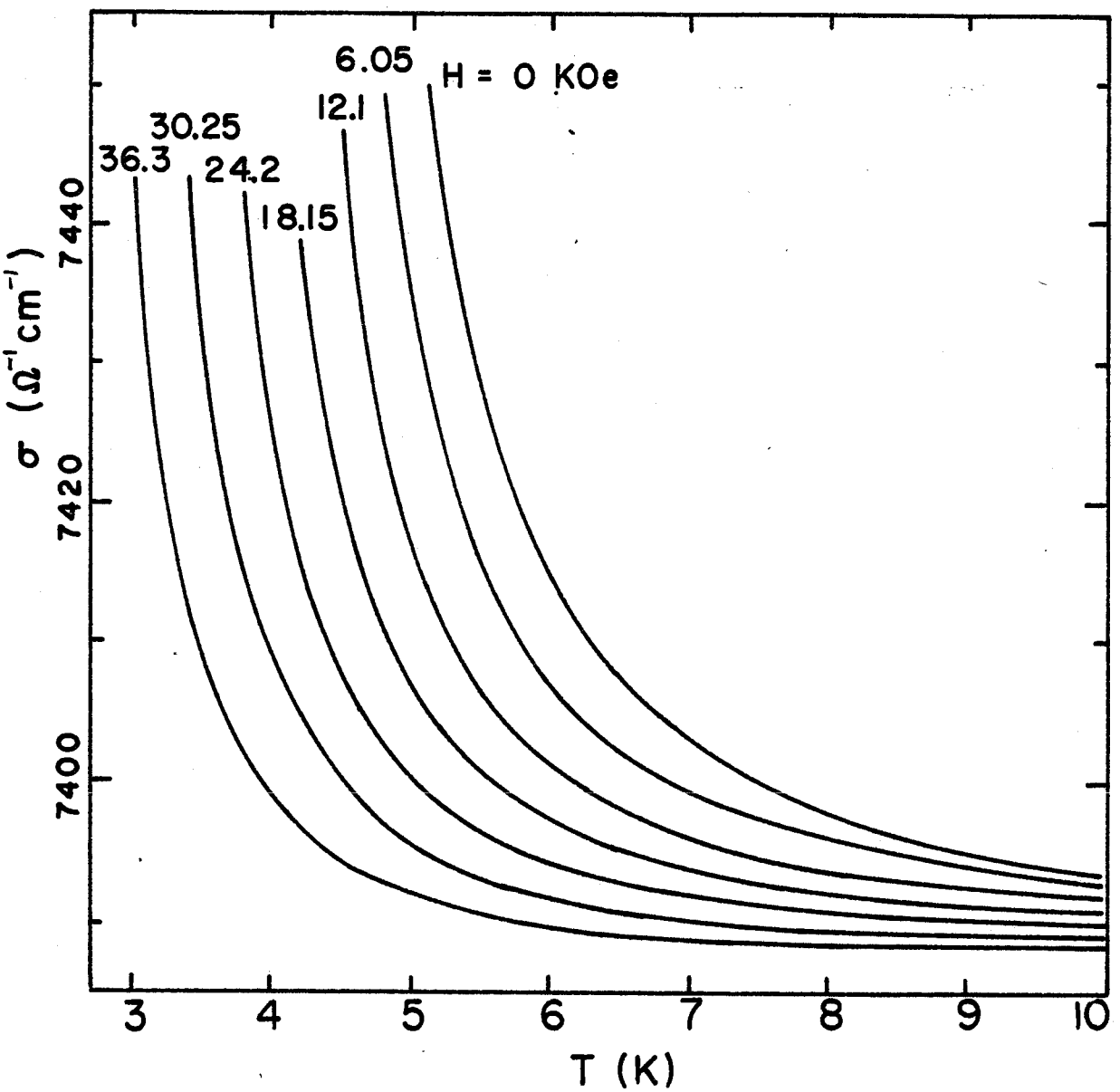

FIG. 4-4: σ vs T for sample #50 (a thick coevaporated Nb:Si film), for several values of perpendicular applied field.

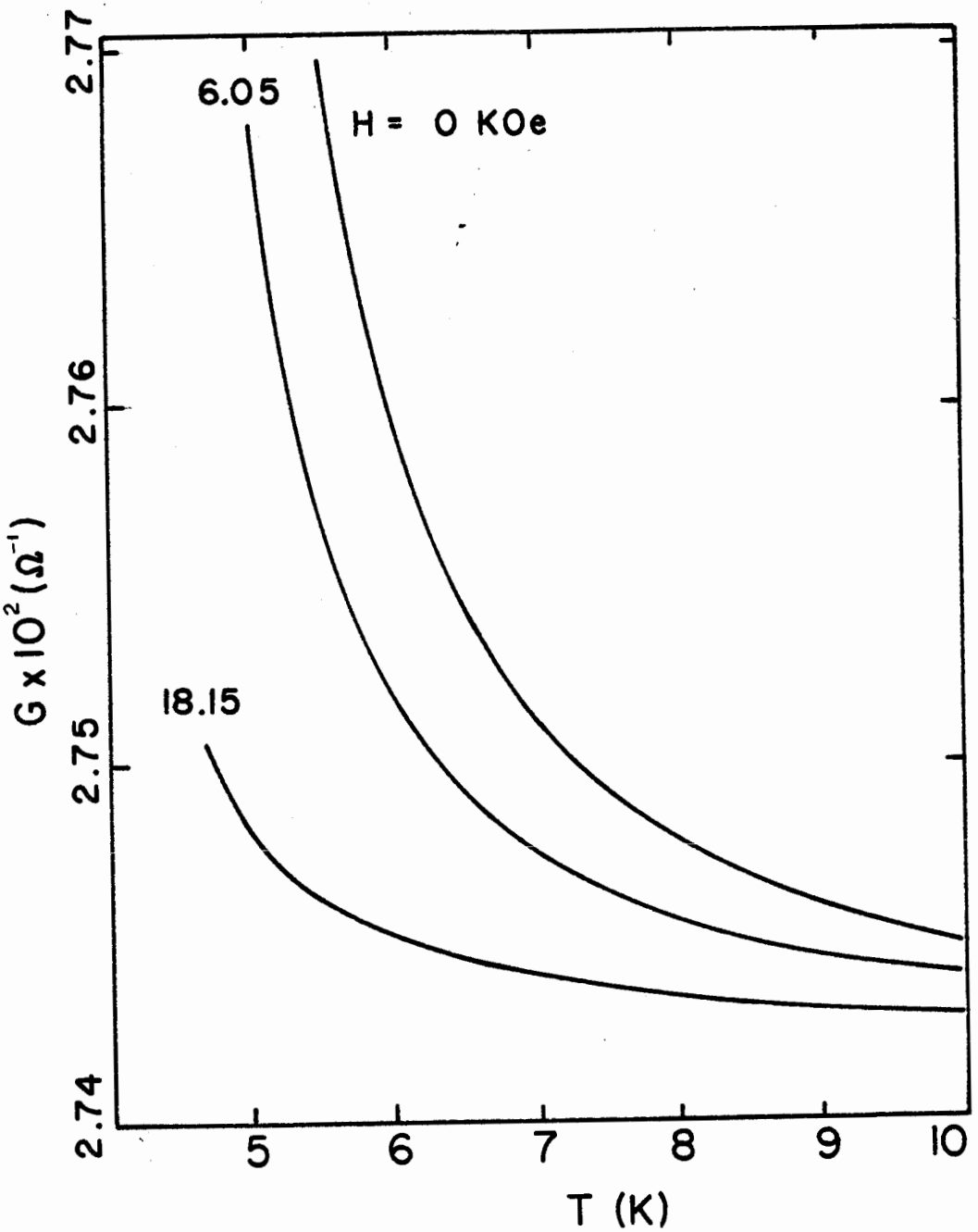

FIG. 4-5: G vs T for sample #51 (thin coevaporated Nb:Si film), for three values of perpendicular applied field.

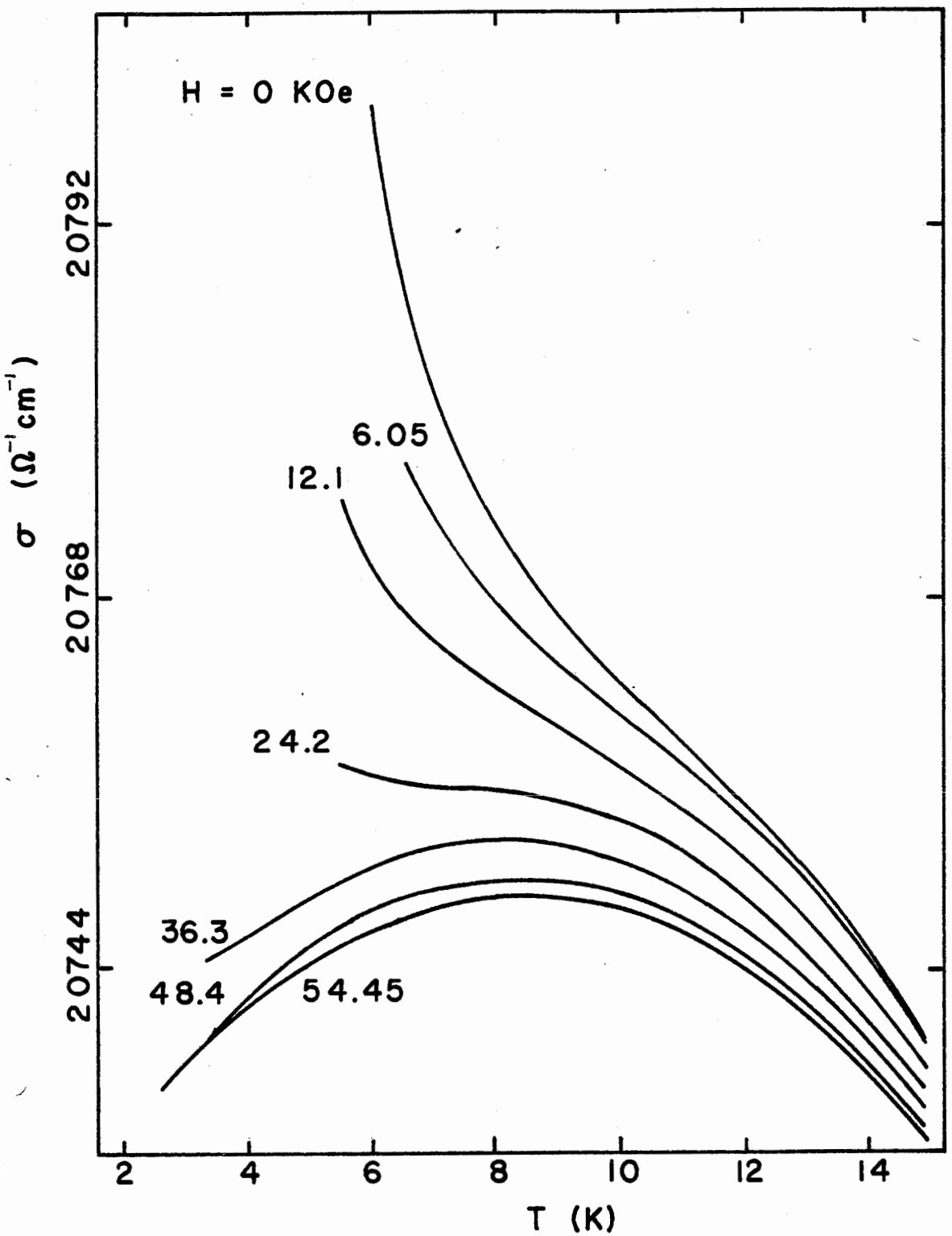

FIG. 4-6: σ vs T for sample #24 (multilayered Nb/Si film), for several values of perpendicular applied field.

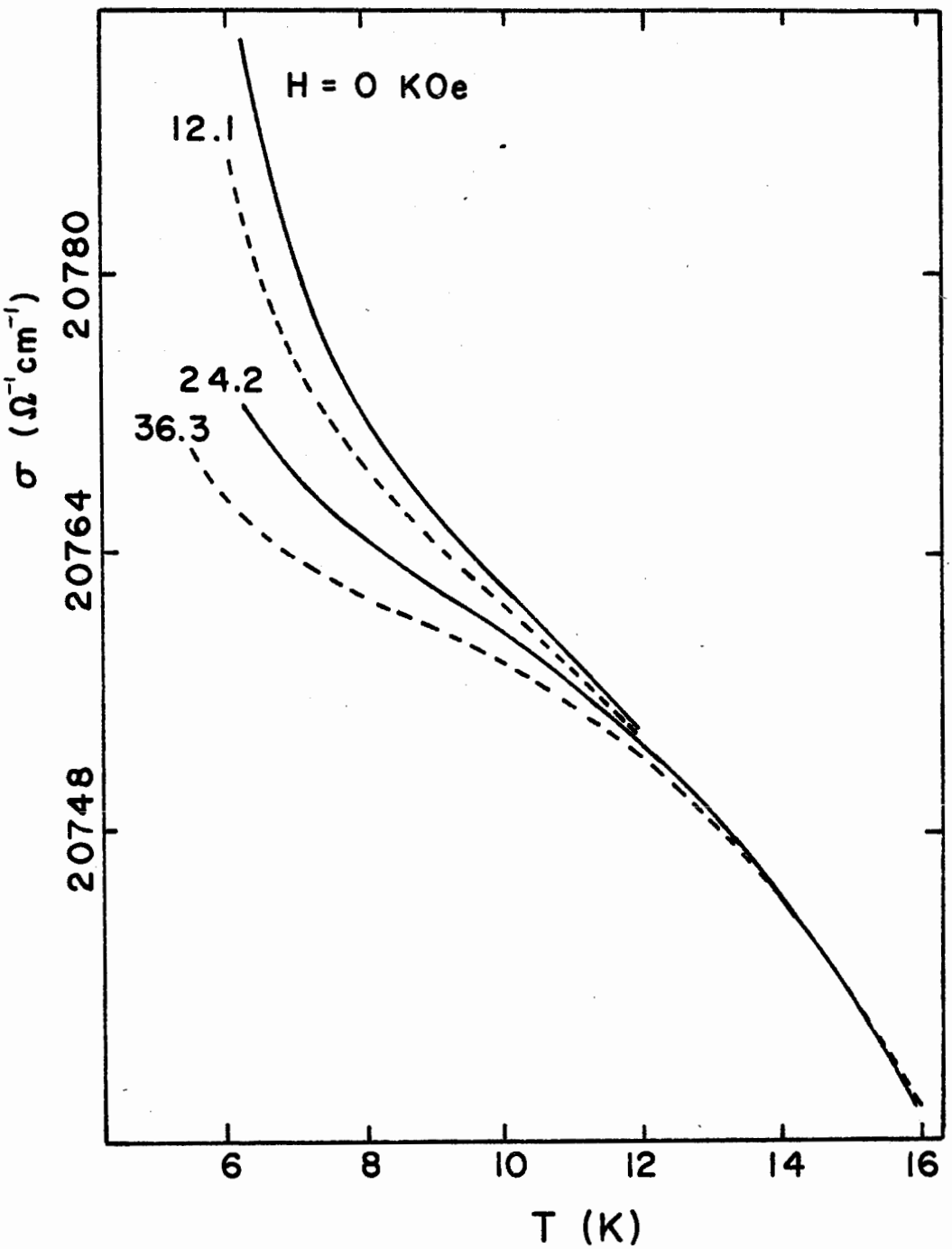

FIG. 4-7: σ vs T for sample #24, for several values of parallel applied field.

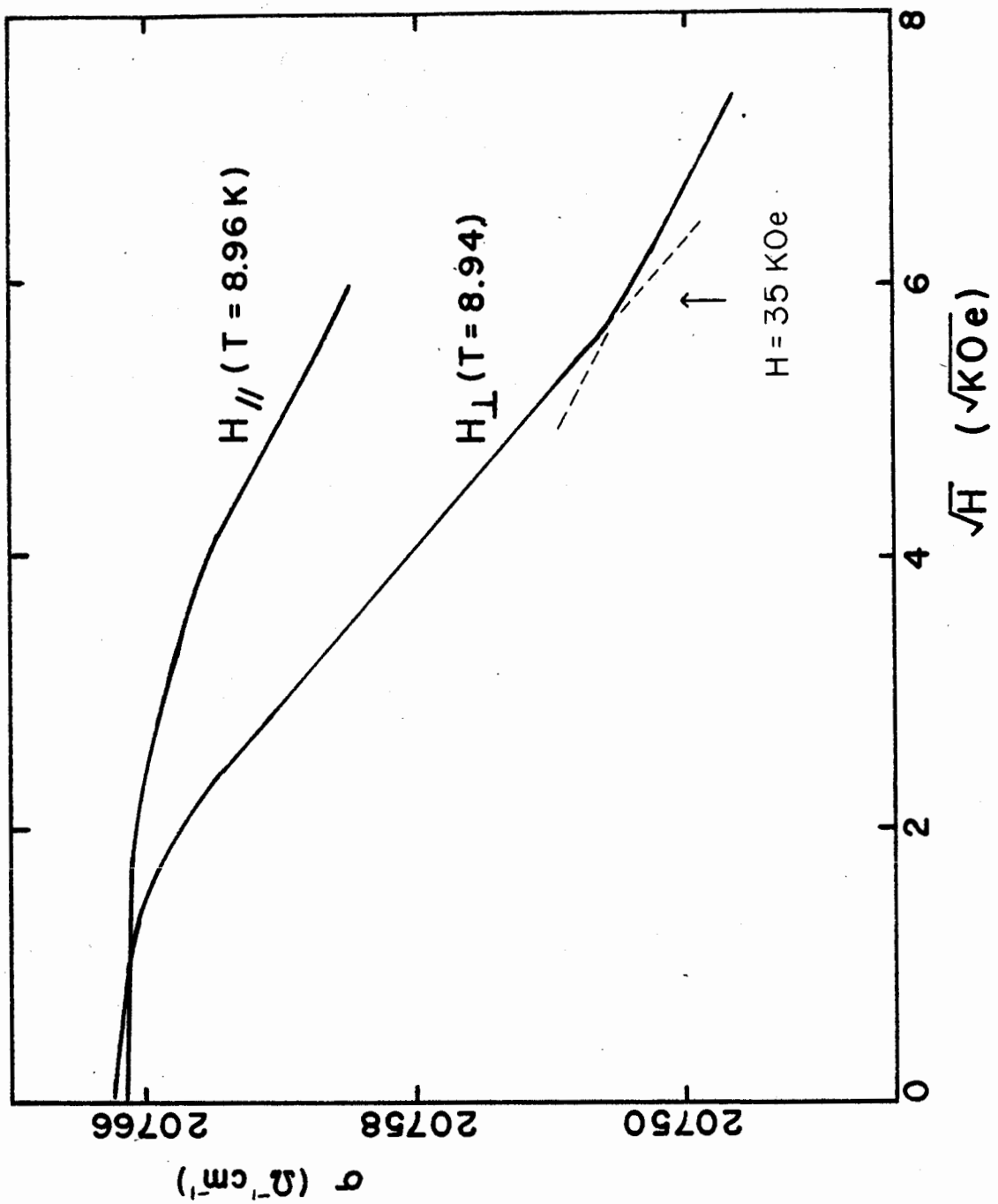

FIG. 4-8: σ vs $H^{1/2}$ for sample #24 for both perpendicular and parallel fields.

V. Quantum Corrections to Conductivity

According to classical theory electrical resistance has two components. One is due to electrons scattering off phonons. This is temperature dependent, decreasing to zero like T^5 at low temperatures. The other part of electrical resistance, the residual resistance, is due to electrons scattering off impurities and imperfections. It is independent of temperature. At low temperatures, the resistance is nearly constant, and is usually identified with the residual resistance.

Theories derive expressions for the conductivity. The conductivity of a disordered metal can be described by classical diffusion, which assumes independent electrons and treats the scattering events as independent. The conductivity is given by the Einstein relation

$$\sigma = e^2 N(E_F) D \qquad 5\text{-}1$$

where D is the diffusion constant. The average distance an electron will diffuse during a time t is equal to $(Dt)^{1/2}$.

The classical theory can also treat magnetoconductance due to orbital effects of electrons on the Fermi surface. The classical magnetoconductance becomes important only when the Landau orbit size is of the order of a mean free path. For disordered materials the mean free path is very small (~10 Å) and the fields necessary to produce appreciable

magnetoconductance effects are very large ($\sim 10^3$ KOe).

There is no fundamental difference between the scattering of electrons due to disorder and scattering due to phonons in classical theory. However, if one is considering the quantum mechanical properties of the electron it is important to note that scattering due to disorder is elastic and that the electron retains its phase coherence. It is characterized by the elastic scattering time τ_o , which is independent of temperature. In contrast, inelastic scattering (due to phonons or electron-electron interactions) causes a loss of phase coherence. The inelastic scattering time τ_i is temperature dependent.

Quantum mechanical effects give additional contributions to classical metallic conductivity. A qualitative description of superconducting fluctuations, weak localization, and electron-electron interactions are discussed in this section. Specific formula will be given as they are needed in the following analysis.

The contribution to conductivity due to superconducting fluctuations above T_c was first calculated by Aslamazov and Larkin (1968). Although enegetically unfavorable, there will be fluctuations into the superconducting state of bubbles with a radius of a coherence length. The smaller the coherence length the greater is the probability for such fluctuations. The superconducting volume will decay back to the normal state in a time proportional to $\epsilon = \ln(T/T_c)$ [Abrahams and Woo (1968)]. These

superconducting droplets will increase the conductivity of the material as a whole.

The conductivity of normal electrons is also increased by the influence of superconducting fluctuations [Maki (1968)] [Thompson (1970)]. This is a sort of proximity effect where a superconducting volume influences the properties of nearby normal regions. The extent of this effect is limited by pair breaking. It has been found [Ebisawa et al (1983)] that the superconducting pairs are broken by inelastic electron interactions.

The classical theory of conductivity assumes that electron collisions with impurities are statistically independent events. But an electron is a quantum mechanical particle and there will be interference between states of opposite momentum (k and -k) as is nicely explained by Bergmann (1983) and Fukuyama (1982). This quantum interference of non-interacting conduction electrons is known as weak localization [Anderson et al (1979)]. It gives a negative contribution to the conductivity. The magnitude of the interference depends on the distance over which the electron retains its phase coherence. Therefore this distance L_i is related to the inelastic scattering time by

$$L_i = [D\tau_i]^{1/2} \qquad 5\text{-}2$$

Notice that both weak localization and Maki-Thompson fluctuations depend on τ_i.

There are two major effects which influence weak localization. First, the presence of spin orbit scattering changes the nature of the interference [Bergmann (1983)]. If the spin of an electron is flipped, then the scattering from a state k to a state -k will see destructive interference rather than constructive. This will reduce the effect of the weak localization. For strong spin orbit coupling where $\tau_{so} << \tau_i$ there will be a net positive contribution to conductivity (weak anti-localization). Second, a magnetic field will change the phase of a charged particle. This will reduce the phase coherence and the quantum interference. There will be a positive magnetoconductance (for zero or small spin orbit scattering) [Altshuler et al (1981)]. The magnetoconductance for weak localization becomes important for fields larger than $H_i = \hbar c/4eD\tau_i$ (on the order of 2 KOe for films studied here).

The dynamically screened Coulomb electron-electron interaction will also give a correction to the conductivity. This correction is the result of interference of inelastic and multiple elastic scattering events [Altshuler and Aronov (1979)]. This is a different phenomenon than weak localization, but it also gives a negative contribution to conductivity and has a similar temperature dependence. Both phenomenae may occur simultaneously in the same material.

Magnetoconductivity due to electron-electron interactions can come from two mechanisms. One is due to the effect of the magnetic field on the orbital motion of the electrons. This

correction comes from the so called particle-particle channel. This additional magnetoconductance becomes important for fields of the order of $H_T = \pi ckT/2eD$ (when the Landau orbit becomes comparable to the thermal diffusion length; ~50 KOe for our films). This usually occurs at a higher field than the characteristic field H for localization effects. Then, there is yet another term in the magnetoconductance which comes from splitting of the spin-up and spin-down bands [Lee and Ramakrishnan (1982)]. This correction is calculated in the particle-hole channel. It becomes important when the spin splitting ($g\mu H/c$) is of order kT, where μ is the Bohr magnetron and g is the Landé factor. This gives a characteristic field of $H_\mu = kT/g\mu$, which is similar in magnitude to the characteristic field for the orbital effect.

In thin films, the quantum processes described above may have a two or three dimensional character depending on the film thickness and the characteristic length of the process. For superconducting fluctuations the characteristic length is the coherence distance ξ. In a thick film the volume of a fluctuation is a sphere of radius ξ. But if the film thickness d is much smaller than ξ, the fluctuating volume will be a disc of radius ξ and thickness d. The conductivity corrections will be different in both magnitude and functional form for the different dimensionalities. By a similar argument, localization effects can be two or three dimensional depending on the characteristic length L_i. The same is true for electron-electron

interactions whose characteristic length is the thermal diffusion length $L_T = [Dh/kT]^{1/2}$.

All of these corrections to the conductivity are present in the materials studied here. Even though the problem is complicated, a careful analysis can separate each of these effects. In this chapter, both qualitative and quantitative analysis of both temperature and field dependent data is used to determine the extent of each type of phenomenon.

The theoretical expressions for localization and electron-electron interactions used in this chapter were derived using the assumption that the material is metallic, that is that $k_F l >> 1$, where k_F is the Fermi wave vector and l is the mean free path. In a very disordered material the mean free path is on the order of the lattice constant and $k_F l \sim 1$, so that the applicability of the theory to this case is questionable. This would appear to be true for the three dimensional sample studied here. But the observed conductivity of this sample is metallic in nature so the theory may still give a good account of the observations. In the literature, other very disordered ($k_F l \sim 1$) three dimensional materials have been successfully analyzed using these theories [Mui et al (1984)]. The other two samples studied in detail here have longer mean free paths and the theory should apply to them.

Studying superconducting materials adds the complication of superconducting fluctuations to the effects of localization and electron-electron interactions. But it gives an additional

handle on the problem, since the diffusion constant and the electron-electron interaction constant can be determined from the superconducting critical fields and critical temperature. (The diffusion constant is affected by localization, which may introduce some error into our analysis.) This reduces the unknown parameters to only the inelastic scattering time and the spin orbit scattering time.

1) Analysis of a 3-D Material

a) Temperature dependence

Since three dimensional quantum conductivity corrections have not been studied as extensively as the two dimensional case, it will be analysed in detail here. Also, there has not been much success in analyzing the temperature dependence of the conductivity of superconducting materials. In this section, then the temperature dependence of a three dimensional material will be analysed. First the superconducting fluctuations will be considered, because they are better understood than the other quantum effects. It will be seen that there is a part of the conductivity that cannot be explained by superconcducting fluctuations and this will be attributed to localization and electron-electron interactions.

The sample which will be discussed in detail is a coevaporated Si:Nb film, on a sapphire substrate, with a composition of about 67% Nb and 33% Si (sample #50). Its

properties are given in Table 4-2. The coherence distance of 57 Å is much smaller than the film thickness of 850 Å so that the contribution to conductivity due to superconducting fluctuations should be three dimensional. Both Aslamasov-Larkin (A-L) and Maki-Thompson (M-T) terms depend on temperature as $[\ln(T/T_c)]^{-1/2}$. A plot of measured conductivity σ_{ex} vs $\epsilon^{-1/2} = [\ln(T/T_c)]^{-1/2}$ is shown in Fig. 5-1 for zero applied field and a field of 36.3 KOe. The data approach a functional dependence of $\epsilon^{-1/2}$ at low temperatures. At higher temperatures the data rises above an extrapolation of the low temperature behavior. The slope of the low temperature region is 35.04 $\Omega^{-1}cm^{-1}$. The theory gives [Aslamasov and Larkin (1968)]

$$\sigma'_{AL} = \frac{e^2}{32\hbar\xi}\frac{1}{\sqrt{\epsilon}} \qquad 5\text{-}3$$

for the A-L term. The theoretical slope of 13.25 $\Omega^{-1}cm^{-1}$ is much smaller than the observed slope.

The contribution of the M-T term [Thompson (1972)],

$$\sigma'_{MT} = \frac{e^2}{8\hbar\xi}\frac{1}{\sqrt{\epsilon}} \qquad 5\text{-}4$$

should be added to the A-L term. The total theoretical slope is then 66.25 $\Omega^{-1}cm^{-1}$, which is much larger than the experimental slope. The action of a superconducting pair breaker will reduce the magnitude of the M-T term. Maki (1971) gives the following formula,

$$\sigma'_{fl} = \sigma'_{AL} + \sigma'_{MT} = \frac{e^2}{32\hbar\xi\sqrt{\epsilon}}\left[1 + \frac{4}{1 + (b/\epsilon_o)^{1/2}}\right] \qquad 5\text{-}5$$

where $\epsilon_0=8(T-T)/\pi$ and δ is an intrinsic pair breaker. Keck and Schmid (1975) give

$$\delta = \frac{\pi\hbar}{8kT_c\tau_i} \qquad 5\text{-}6$$

A value of $\delta=0.38$ is needed to fit the low temperature data in Fig. 5-1. This implies an inelastic scattering time of τ_i = 1.7×10^{-12}s. At the end of this section, this value for τ_i will be compared with the value from the analysis of the magnetoconductance.

Studies of three dimensional superconducting fluctuations have been made by Johnson and Tsuei (1976) (MoRe, LaAuCu, and NbGe films) and Toyota et al (1984) (amorphous ZrIr films). Both groups find that their data near T approaches the value predicted by the A-L term alone. At higher temperatures, the data drops below the theory. Both studies were looking at amorphous metal alloys. In contrast to these two studies, the magnitude of the superconducting fluctuations observed in this work requires the M-T term and the high temperature data rises above the expected result.

It is possible to identify the source of the extra conductivity at higher temperatures observed in Fig. 5-1. Corrections to the conductivity due to electron-electron interactions and localization will increase the conductivity as the temperature gets larger (see Eqns. 5-7 and 5-8). Experimentally, at temperatures above T_c, a square root temperature dependence of conductivity has been observed by Chui

et al (1981) for granular Al films and by Werner et al (1982) for Nb/Cu multilayered films. Therefore, a contribution to the conductivity of $AT^{1/2}$ was subtracted from the data, which was then again compared to fluctuation theory. Fig. 5-2 shows a graph of $(\sigma_{ex} - AT^{1/2})$ vs $[\ln(T/T_c)]^{-1/2}$ for zero applied field, where A and T_c have been treated as fitting parameters. The low temperature data is most sensitive to variations of T_c, while the high temperature data is most sensitive to changing A. This makes an unambiguous fit possible. Plots for three values of A are drawn to show the quality of the fit. The lower solid line in the figure is for A = 13. At high temperatures the line drops below a straight line, indicating that 13 is too large a value for A. The upper line is for A = 9. It rises above a straight line, which shows that 9 is too small. The middle line uses A = 10 and it can be seen to be a straight line. It is not shown in the figure but a plot using A = 11 will also give a straight line. The best fitting parameters are A = 10.5 ± 0.5 and T_c = 4.61 ± 0.02 K.

The same analysis was performed on the temperature dependent conductivity in the presence of a constant magnetic field applied perpendicular to the film. Fig. 5-3 shows the result for an applied field of 36.3 KOe. Again the data can be fit assuming a $T^{1/2}$ contribution to conductivity on top of the fluctuations. Note that the slope of the line in Fig. 5-3 is less than that in Fig. 5-2. This is because the applied field has a pair breaking effect and hence reduces the magnitude of

the M-T term. Values of A and T_c for various values of applied field are given in Table 5-1.

The analysis so far has shown that the conductivity is composed of a part proportional to $\epsilon^{-1/2} = [\ln T/T_c]^{-1/2}$ and a part proportional to $T^{1/2}$. The first part is due to superconducting fluctuations. Other experimental results [Johnson and Tsuei (1976)][Toyota et al (1984)] show this temperature dependence only very near T_c. While it is usually assumed that the theory is only valid for small values of ϵ it is found here that the $\epsilon^{-1/2}$ behavior continues for larger values of ϵ. This identification of fluctuation conductivity will be given more weight if the $T^{1/2}$ part of the conductivity can be accounted for. This is discussed in the following.

Electron-electron interactions and weak localization can give corrections to the conductivity which are proportional to $T^{1/2}$. Table 5-1 gives the experimental coefficients of the $T^{1/2}$ term. In zero field the coefficient is 10.5 $\Omega^{-1}cm^{-1}K^{-1/2}$, and the value decreases with increasing field to 8.0 $\Omega^{-1}cm^{-1}K^{-1/2}$ in a field of 36.3 KOe. Application of a magnetic field has a large effect on localization. One can then attribute the 8 $\Omega^{-1}cm^{-1}K^{-1/2}$ part of the conductivity remaining at high fields to electron-electron interactions and the 2.5 $\Omega^{-1}cm^{-1}K^{-1/2}$ which was quenched by the field to weak localization. In the next section the magnetoconductance is examined in detail and it will show the above statement to be approximately true.

The magnitude of the conductivity correction due to electron-electron interaction in the particle-hole channel is [Altshuler and Aronov (1979)] [Lee and Ramakrishnan (1982)]

$$\sigma'_{ee} = \frac{e^2}{4\pi^2\hbar}\ \frac{1.3}{\sqrt{2}}\ \left(\frac{4}{3} - 2F\right)\left[\frac{2\pi kT}{\hbar D}\right]^{1/2} \qquad 5\text{-}7$$

F is an electron screening factor which approaches one for a short screening length and approaches zero for a long screening length. There will be an additional contribution from the particle-particle channel. This contribution is small compared to that of the particle-hole channel [Altshuler et al (1980)] [Lee and Ramakrishnan (1982)]. For sample #50 the diffusion constant is D = 0.49 cm^2s^{-1} and this gives for the conductivity σ' = 7.3(4/3-2F)T $\Omega^{-1}cm^{-1}$. This is about the same as the experimental value, for large H, of σ' = 8.0 T $\Omega^{-1}cm^{-1}$. Equating these gives F = 0.12. Bergmann (1984) has found for thin films that F is about 0.2 to 0.25. The value of F = 0.12 found here is of the same order.

The magnitude of the correction to conductivity due to weak localization is given by [Altshuler et al (1982)]

$$\sigma'_{loc} = \frac{e^2}{2\pi^2\hbar}\ \frac{1}{[D\tau_i]^{1/2}} \qquad 5\text{-}8$$

Since the inelastic scattering time $\tau_i \propto T^{-3/2}$, the conductivity should go like $T^{3/4}$. A dependence of $T^{1/2}$ was assumed in the analysis of the experimental data above. But over a small range of temperature, for such a small contribution due to localization, a $T^{3/4}$ dependence cannot be distinguished from $T^{1/2}$.

One can now make a comparison of the magnitudes of the theory and the experiment. The magnitude of the localization effect depends on the value of τ_i . The magnetoconductance which is studied in the next chapter gives $\tau_i(T=10K) = 1.2\times10^{-11}$ s and $\tau_i(T=7K) = 4.8\times10^{-11}$ s. Using these in Eqn. 5-8, one gets $\sigma'_{loc}(10K) - \sigma'_{loc}(7K) = 2.5\ \Omega^{-1}cm^{-1}$. This is about double the experimental result of $1.3\ \Omega^{-1}cm^{-1}$ which we obtained from the $T^{1/2}$ fits. The formula for localization used here is for the case of no spin orbit coupling. In the presence of spin orbit coupling the localization effect is reduced. Niobium, being in the middle of the periodic table, should have some spin orbit scattering. The observed correction to conductivity being about half of the theoretical maximum for localization seems reasonable.

In summary, this section examined the temperature dependence of the conductivity of a three dimensional Nb:Si film. It was found that the superconducting fluctuations are proportional to $[\ln(T/T)_c]^{-1/2}$ over a large range of temperature. Both A-L and M-T terms are needed to explain the observed magnitude. The large range of temperature over which the $\epsilon^{-1/2}$ dependence is observed is remarkable.

The theory for the M-T term with a pair breaker (Eqn. 5-5) does not give the full observed temperature dependence. It does fit at the low temperature end and gives $\tau_i = 1.7\times10^{-12}$s. The next section finds from the magnetoconductance that for T = 5 K, $\tau_i = 9\times10^{-11}$s. The two values do not agree. Since the magnetoconductance theory gives a good fit to the data, the

resulting value of τ_i should be reliable. Therefore the value of τ_i obtained using the M-T term is not correct. Bergmann (1984) studied the temperature dependent conductivity of a 2-D Al film. He found that the temperature dependence of the M-T term is not correctly reproduced by the theory. He concludes that the problem of calculating the M-T term from microscopic parameters (ie. τ_i) remains unsolved. Bergmann, then, draws the same conclusions for a 2-D Al film as were found here for a 3-D Nb:Si film.

At higher temperatures, we also found an additional conductivity above the superconducting fluctuation conductivity. As previously mentioned a $T^{1/2}$ dependence of conductivity for disordered metallic films has been reported in the literature. Chui et al (1981) studying granular Al films, find that the observed magnitude does not agree with localization or electron-electron theory. Werner et al (1982), on the other hand, find that their data can be explained if both localizations and electron-electron interactions are present in their Nb-Cu flims. The $T^{1/2}$ part of the conductivity observed here is explained using both localization and electron-electron interactions. By studying the temperature dependence of the conductivity in constant magnetic fields one can separate the contributions from each of the two theories.

Table 5-1

T_c values from resistive transitions for sample #50. The column labled "mp" contains values of T_c determined from the transition midpoints. The next two columns give the parameters from the ϵ fits. The final column gives T_c from the theoretical expression in Eqn. 5-34.

H(KOe)	T_c (K) "mp"	A	T_c (K) "ϵ"	T_c (K) "th"
0	4.47±0.02	10.5±0.5	4.61±0.02	4.61
4.84	4.23			
6.05		10.0	4.37	4.34
12.10	3.91	10.0	4.10	4.06
18.15		9.0	3.77	3.78
24.20		9.0	3.44	3.49
30.25		8.5	3.10	3.19
36.30	2.8±0.2	8.0	2.75	2.88

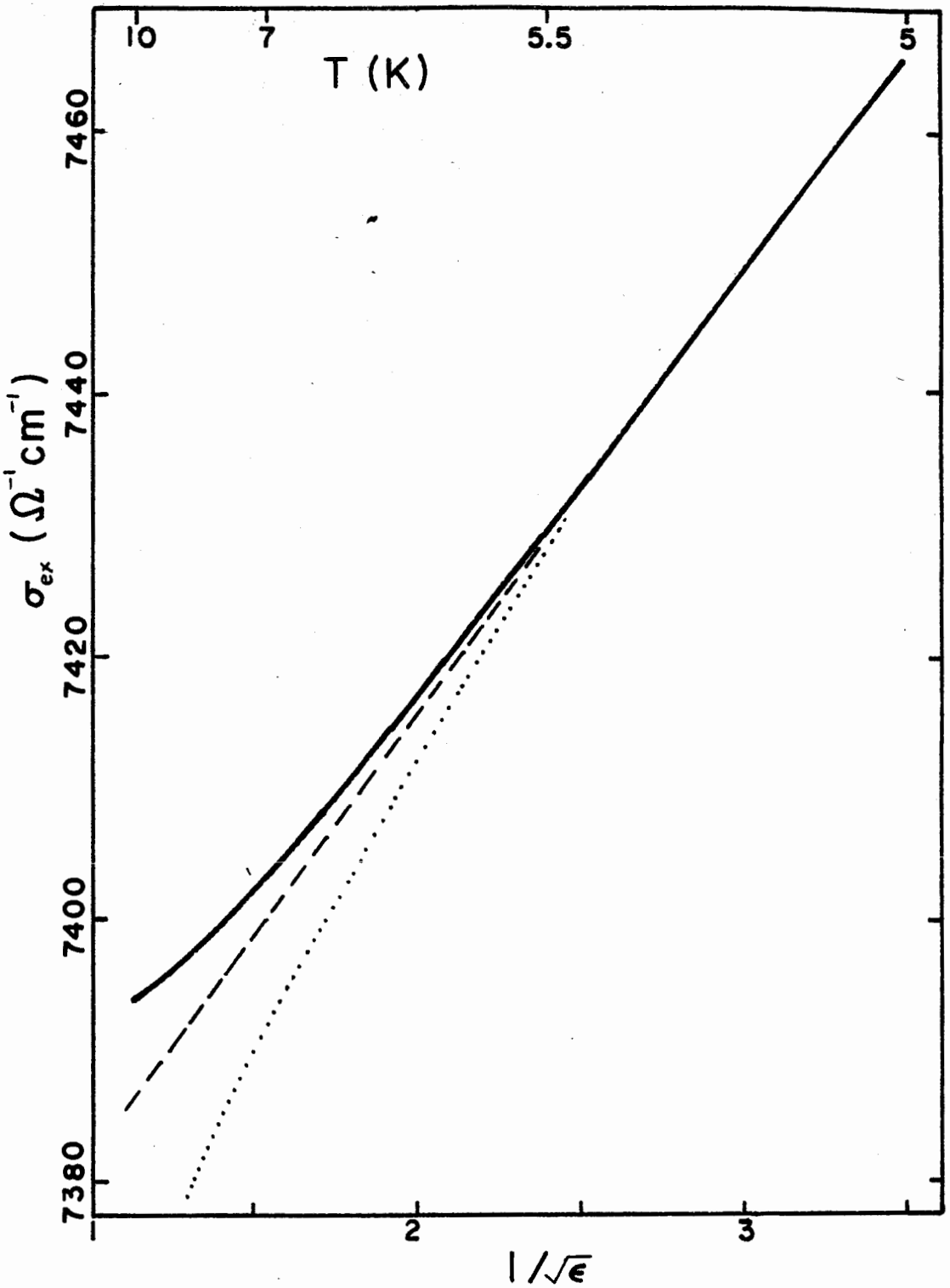

FIG. 5-1: σ_{ex} vs $\epsilon^{-1/2} = [\ln(T/T_c)]^{-1/2}$ in zero applied field for the 3-D sample #50. The data is shown as a solid line, the dashed line is a straight line, and the dotted line shows the fluctuation conductivity theory [Maki (1971)] for δ=0.38.

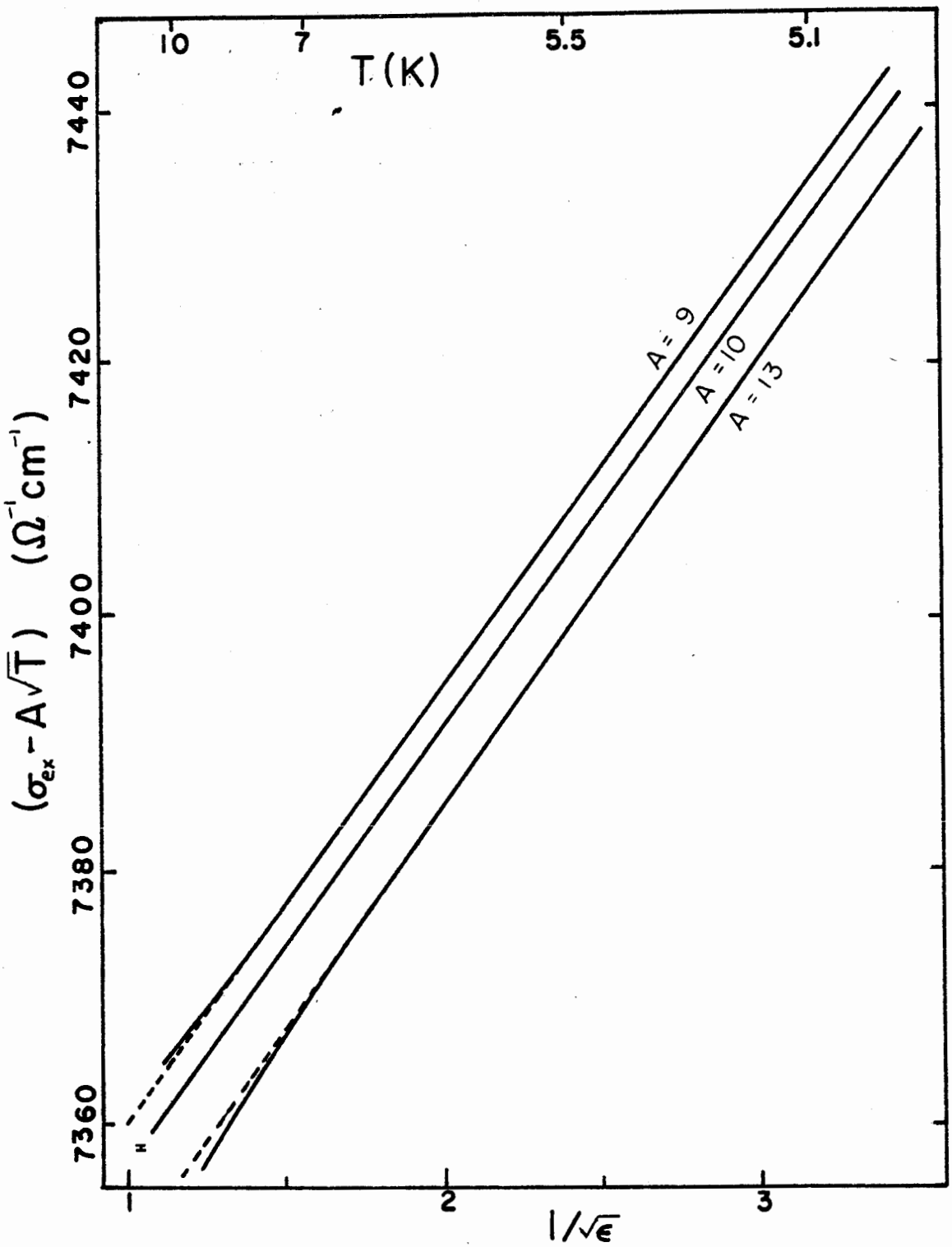

FIG. 5-2: $(\sigma_{ex}-AT^{1/2})$ vs $\epsilon^{-1/2}$ in zero applied field for sample #50. The parameters used are T_c = 4.61 K and three values of A, which are given on the figure. The data is shown as solid lines. Experimental uncertainty is shown by the error bar.

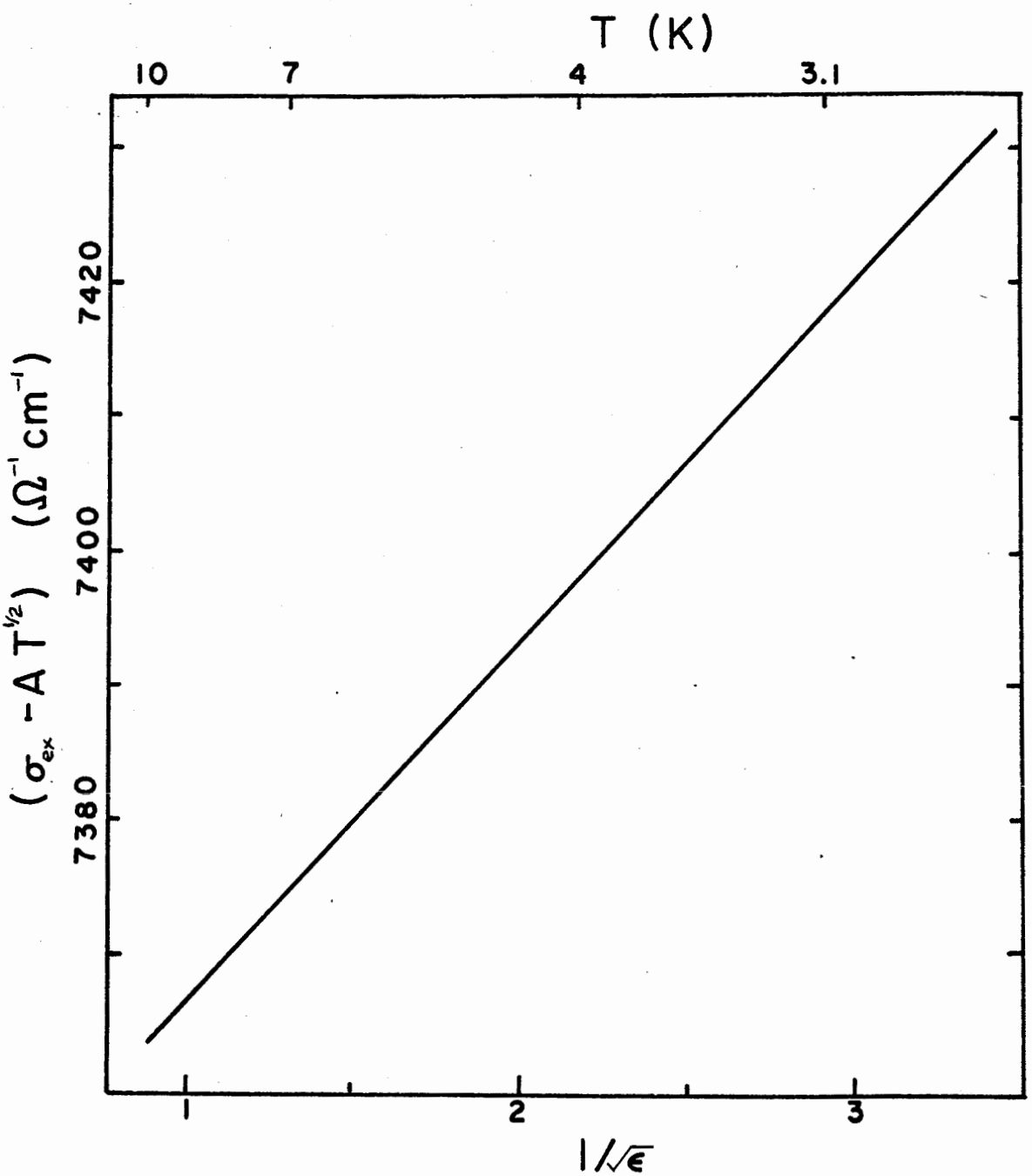

FIG. 5-3: $(\sigma_{ex}-AT^{1/2})$ vs $\epsilon^{1/2}$ with H = 36.3 KOe for sample #50. The parameters used are T = 2.75 K and A = 8, which give a straight line.

b) Magnetoconductance

The analysis of magnetoconductance can be more quantitative than the analysis of the temperature dependence. This is because there is a 3-D formula which includes the effect of spin orbit scattering on localization. In this section, the dimensionality of the sample is determined and the theoretical formulae which will be used to analyse the data are presented. The A-L fluctuation and the electron-electron interaction contributions are fully determined and are simply subtracted from the data. The unknown parameters τ_i and τ_{so} are found by fitting the remainder of the data to M-T fluctuation and localization theories.

Localization effects will be three dimensional if the film thickness is much larger than the inelastic diffusion length. For this sample, at T = 9 K, $\tau_i = 2\times10^{-11}$ which gives L = 250 Å, which is smaller than the thickness of 850 Å. So that this sample can be considered to be three dimensional. The theoretical expression is [Altshuler et al (1981)] [Mui et al (1984)]

$$\sigma'_{loc} = \frac{e^2}{2\pi^2\hbar}\left[\frac{eH}{\hbar c}\right]^{1/2}\left\{1.5\, f_3\left(\frac{4D\tau^* eH}{\hbar c}\right) - 0.5\, f_3\left(\frac{4D\tau_i eH}{\hbar c}\right)\right\} \qquad 5\text{-}9$$

where

$$\frac{1}{\tau^*} = \frac{1}{\tau_i} + \frac{4}{3}\frac{1}{\tau_{so}} \qquad 5\text{-}10$$

The function $f_3(x)$ is

$$f_3(x) = \sum_{n=0}^{\infty} \left\{ 2\left[\left(n + \tfrac{1}{x} + 1\right)^{1/2} - \left(n + \tfrac{1}{x}\right)^{1/2} \right] - \left(n + \tfrac{1}{2} + \tfrac{1}{x}\right)^{-1/2} \right\} \qquad 5\text{-}11$$

The magnetoconductivity due to the Maki-Thompson term for the superconducting fluctuations has the same functional dependence as the localization correction for weak magnetic fields. It is given by [Larkin (1980)] [Altshuler et al (1981)]

$$\sigma'_{MT} = -\frac{e^2}{2\pi^2\hbar}\left[\frac{eH}{\hbar c}\right]^{1/2} \beta \; f_3\left(\frac{4D\tau_i eH}{\hbar c}\right) \qquad 5\text{-}12$$

The function β gives the strength of the superconducting fluctuations. The temperature dependence of β is given in Table 5-2 [Larkin (1980)]. The limiting behavior of β is

$$\beta = \frac{-\pi^2}{4} g \quad , \text{ for } \; -g(T) \gg 1$$

$$\beta = \frac{\pi^2}{6} g^2 \quad , \text{ for } \; |g(T)| \ll 1 \qquad 5\text{-}13$$

where $g^{-1} = \ln(T_c/T)$, is the electron-electron interaction strength parameter.

Table 5-2

Larkin's β as a function of g, from Larkin (1980).

-g(T)	-0.1	+0.1	0.2	0.3	0.5	0.8	1	2	5	10
β(T)	0.017	0.015	.06	.13	.33	.73	1.05	3	9.8	22

If a constant β is used in Eqn. 5-12, σ'_{MT} will continue to increase with increasing H. Physically, however, the magnetic

field will quench the superconductivity at high fields so that σ'_{MT} should approach a constant value. McLean and Tsuzuki (1984) calculated the field dependence of Larkin's electron-electron interaction strength parameter g. It is

$$g^{-1} = \ln\left(\frac{T_{c0}}{T}\right) + \psi\left(\frac{1}{2}\right) - \psi\left(\frac{1}{2} + \frac{DeH}{2\pi ckT}\right) \qquad 5\text{-}14$$

where ψ is the digamma function. With no theoretical calculation available for $\beta(H)$, Mui et al (1984) assume Larkin's relation between β and g and use the field dependent g in Eqn. 5-14. This approximation of $\beta(H)$ gives a decreasing β as H increases, as it should. However for very large fields there is a problem with the calculated σ'_{MT} (see Mui et al (1984) Fig. 1). At a high field, σ'_{MT} reaches a minimum, and with a further increase in the field σ'_{MT} grows larger. This could only happen if superconducting fluctuations grew stronger again at very large fields. Clearly this is incorrect, but in the absence of a better theoretical calculation the method of Mui et al will be used. Since the M-T fluctuations are smaller compared to localization effects at temperatures well above T_c, the problem in calculating β will lead to less error at high temperatures than at temperatures near T_c.

The fluctuation conductivity due to the A-L term in the presence of a magnetic field was calculated by Mikeska and Schmidt (1970). They find, for small fields, that the equation of Aslamasov and Larkin (1968), vis. (Eqn. 5-3)

$$\sigma'_{AL} = \frac{e^2}{32\hbar\xi}\,\frac{1}{\sqrt{\epsilon}}$$

is still valid, but the field dependence comes through $\epsilon = \ln(T/T_c(H))$. The range of validity of the above equation is $\eta << \epsilon << 1$, where

$$\eta = \frac{DeH}{2\pi T_c} \qquad 5\text{-}15$$

For sample #50 and the largest field used, $\eta = 0.06$. The fields are small enough for Eqn. 5-3 to be valid. For a temperature of 8 K, $\epsilon = 0.7$. While the value of ϵ is less than one, it is rather large. However, as discussed in the previous section, the ϵ dependence of σ extends to larger values of ϵ than the theory suggests. Therefore, Eqn. 5-3 has been used to represent the A-L term. $T_c(H)$ will be taken from Table 5-1.

Electron-electron interactions also give a contribution to the magnetoconductance. The dimensionality is determined from the thermal diffusion length which is

$$L_T = \left[\frac{D\hbar}{kT}\right]^{1/2} \qquad 5\text{-}16$$

For a temperature of 8 K, L_T= 68 Å. This is much smaller than the film thickness (850 Å) and the 3-D theory must be used. The particle-particle channel gives [Altshuler et al (1981)]

$$\sigma'_{pp} = \frac{-e^2}{2\pi^2\hbar}\left[\frac{eH}{\hbar c}\right]^{1/2} g(T,H) \quad \phi_3\left(\frac{2DeH}{\pi c\, kT}\right) \qquad 5\text{-}17$$

g(T,H) is Larkin's electron-electron interaction strength parameter and is given by Eqn. 5-14. The function ϕ_3 is

$$\phi_3(x) = \left[\frac{\pi}{2x}\right]^{1/2} \int_0^\infty \frac{t^{1/2}}{\sinh^2 t}\left[1 - \frac{xt}{\sinh xt}\right] dt \qquad 5\text{-}18$$

In the limit where x<<1, ϕ_3 can be expressed as

$$\phi_3(x) \simeq 0.33\ x^{3/2} \qquad 5\text{-}19$$

For sample #50 discussed here the argument of ϕ_3 is x = 0.21 for the largest field. For this value of x the exact value of ϕ_3 is 0.0328 and the approximate value is ϕ_3 = 0.0332. Since the electron-electron interaction contribution to the magnetoconductance is small, the limiting form of ϕ_3 will be used.

Magnetoconductance in the particle-hole channel is given by [Lee and Ramakrishnan (1982)]

$$\sigma'_{ph} = \frac{-e^2}{2\pi^2\hbar}\left[\frac{kT}{8\hbar D}\right]^{1/2} F\, g_3\left(\frac{2\mu H}{kT}\right) \qquad 5\text{-}20$$

where μ is the Bohr magnetron. The characteristic field (ie. the field for which x = $2\mu H/kT$ = 1) is larger than the characteristic field for the particle-particle channel. The small field limit of g_3, which is

$$g_3(x) \simeq 0.053\ x^2 \quad , \text{ for } x \ll 1 \qquad 5\text{-}21$$

will be used in the analysis of the data.

The reports of other researchers in the literature do not use the contribution of the Aslamazov-Larkin term for superconducting fluctuations in their analysis of magnetoconductance of 3-D superconductors [Mui et al (1984)] [Bieri et al (1984)]. They give no reason why the A-L term should be neglected. In fact, in amorphous alloys [Toyota et al

(1984)] [Johnson and Tsuei (1976)] one expects that intrinsic pair breakers will greatly diminish the the M-T term. (This pair breaking effect may be included in Eqn. 5-12, through the τ_i dependence.) Only the A-L contribution will then remain and give a large contribution to the conductivity. This can be seen by looking at the data for sample #50 in Table 5-3 for a temperature of 8 K. In order to match the magnitude of the observed magnetoconductance using the M-T term (Eqn. 5-12) and localization (Eqn. 5-9) alone, an inelastic scattering time greater than 10^{-10} seconds must be used. This is much larger than typical inelastic scattering times observed in the literature. It also gives a very poor fit of the theory to the data points. The analysis of the data reported here must include the A-L term.

The quantitative analysis of the magnetoconductance at 8 K for sample #50 is given in Table 5-3. It can be seen that the A-L contribution is roughly equal to half of the entire observed magnetoconductance. It should not be neglected. The electron-electron interaction contributions are small. They are smaller than the experimental uncertainty except at the highest fields. These three contributions have no adjustible parameters since they are found from superconducting properties. They are subtracted from the data which gives the column labeled $\Delta\sigma_{ex-AL-ee}$, which should be due to the M-T fluctuations and localization.

The theoretical expressions for the M-T superconducting fluctuations and localizations have two undetermined parameters. These are the inelastic scattering time τ_i and the spin orbit scattering time τ_{so}. These can be determined by graphically fitting the theory to the data. Fig. 5-4 shows that good agreement is obtained in both the magnitude and the shape of the curve. The results of the fit are $\tau_i = (3.2\pm0.2)\times10^{-11}$s and $\tau_{so} = (8\pm1)\times10^{-12}$s.

The same analysis can be carried out at different temperatures. Fig. 5-5 shows magnetoconductance data (at T = 9.36 K) obtained from the series of temperature sweeps at constant field as studied above. It also shows data from a magnetic field sweep at constant temperature. The two sets of data agree at low fields. A fit of theory to the low field data is shown as a solid line. At fields above 25 KOe the field sweep data lags behind the temperature sweep data. We could not fit the theory to the high field part of the field sweep data. Since the theory agrees with the temperature sweep data, the field sweep data may be suspect. It is possible that the superconducting magnet was not charging properly during the field sweep operation. This has not been further investigated.

Fig. 5-6 shows the same analysis for temperatures of 7, 9 and 10 K. The results for τ_i and τ_{so} are given in Table 5-4.

There is a problem as the temperature approaches the superconducting critical temperature. The analysis proceeds as before to obtain $\Delta\sigma_{ex-AL-ee}$. But the M-T and localization theory

predicts a much different behavior than shown by $\Delta\sigma_{ex-AL-ee}$. The theory bends away from the data back towards $\Delta\sigma = 0$ at high fields. Very close to T_c the superconducting fluctuactions will dominate the magnetoconductance. The problem would appear to be that the assumed $\beta(H)$ decreases too fast as the field increases. This was mentioned in the discussion of Eqn. 5-12.

The evaluation of $\beta(H)$ merits further investigation. For large values of β Larkin (1980) gives (Eqn. 5-13)

$$\beta(T) = \frac{\pi^2}{4}\left(\frac{1}{\ln(T/T_c)}\right)$$

Using the experimental values of $T_c(H)$ (Table 5-1) in this formula gives about the same values of $\beta(H)$ as obtained using Eqns. 5-13 and 5-14. (This is not too surprising considering the similarity between McLean and Tsuzuki's (1984) formula for g(H) and the formula for $T_c(H)$ for a dirty superconductor, Eqn. 5-34.) These values are (Eqn. 5-13) given in Table 5-5, labeled as $\beta^{(2)}$. The parameter β gives the strength of the superconducting fluctuations. The temperature dependence of $\beta^{(2)}$, Eqn. 5-13, is the same as the temperature dependence of the A-L fluctuations in two dimensions. But the sample being studied here is three dimensional. It is reasonable that β should be related to the three dimensional superconducting fluctuations. Table 5-5 also gives $\beta^{(3)}$, which is proportional to $\bar{\epsilon}^{-1/2}$and normalized to Larkin's value of β for H = 0. It can be seen that $\beta^{(3)}$ decreases more slowly than $\beta^{(2)}$. Using $\beta^{(3)}$ the theory can be matched to the data at a temperature of 5 K, as shown in Fig. 5-7. Although the M-T

term is dominant, the localization contribution must be included to achieve good agreement between experiment and theory. The value of τ_i is 9.0×10^{-11}s (at T = 5 K). At this temperature $\tau_i >> \tau_{so}$ and the theory is close to the limit of strong spin order scattering so that a value of τ_{so} could not be determined.

Here we make a further note on dimensionality. The inelastic diffusion length for the value of τ_i at T = 5 K is L_i =660 Å. This is not much less than the film thickness (850 Å) and the film may not be 3-D. However, as discusssed by Bergmann (1983), the magnetic field introduces a time $t_H = hc/4eDH$. For strong fields this time replaces τ_i and the characteristic length for localization effects is $L_H = [Dt_H]$. If H = 5 KOe, then L_H = 180 Å. We see that for fields above 5 KOe this sample will be 3-D.

A summary of τ_i and τ_{so} for different temperatures is given in Table 5-4. A graph of τ_i vs $T^{-3/2}$ is shown in Fig. 5-8. The value of τ_i at T = 5 K sits only slightly below an extrapolation from the values of τ_i at higher temperatures. This suggests that the assumption that $\beta(H)$ varies like the 3-D A-L fluctuations is, at least approximately, correct. The figure shows that τ_i is proportional to $T^{-3/2}$. This theoretical dependence of τ_i due to electron-electron interactions was found by Altshuler et al (1982). We conclude, then, that the magnitude of the localization effects is determined by electron-electron interaction effects.

The results here can be compared to other work in the literature. Bieri et al (1984) studied a three dimensional amorphous CuZr thin film. They obtain values of τ_i which are about a factor of ten smaller than the values for the Nb:Si film studied here. They used a constant β rather than a field dependent β. Near T_c their data did not fit the theory for fields above 10 KOe. But they did get good fits for low fields. At higher temperatures β is less important and their fits were good to higher fields. But notice that since $\beta(H)$ is smaller than $\beta(0)$, the value of τ_i resulting from using $\beta(0)$ would be underestimated (see Eqn. 5-12). Bieri et al, also did not account for A-L fluctuations. Neglecting the A-L term would give values of τ_i which are too large. There is no other method of determining of τ_i and so one cannot comment further on the actual values. The temperature dependence of τ_i found by Bieri et al was $\tau_i \propto T^{-2}$. This is different from the $T^{-3/2}$ dependence found for the Nb:Si film and predicted by theory.

Mui et al (1984) studied a series of three dimensional granular Al films. Their values of τ_i range from about a factor of ten larger to a factor of ten smaller than that observed for the Nb:Si film. They only obtained good agreement between experiment and theory at temperatures well above T_c . They used a field dependent β but did not consider the A-L contribution. This suggests that their values of τ_i may be too large. They find, depending on the conductivity, that τ_i can have a temperature dependence ranging from T^{-1} (highest resistivity) to

T^{-2}(lowest resistivity). This interesting result cannot be compared to the present study which used only one sample.

The values of τ_{so} are also given in Table 5-4. Spin orbit scattering should not depend on temperature. The experimental values do agree within errors. The average value is τ_{so} = $(9\pm1)x10^{-12}$s.

Mui et al (1984) found τ_{so} = $1.8x10^{-11}$ to $1.3x10^{-10}$ s for Al. These are larger than τ_{so} found for the Nb:Si, as would be expected since Al is a lighter element than Nb. Bieri et al (1984) found a value of τ_{so} = $6x10^{-13}$ for CuZr, which is smaller than the τ_{so} found for Nb:Si. This is unexpected as Nb and Zr have about the same atomic number and should have the same amount of spin orbit scattering. Bergmann (1982) has found for a 2-D Cu film that τ_{so} = $3x10^{-12}$s and for a Au film that τ_{so} = $2x10^{-13}$s. This also is stronger spin orbit scattering than we see in Nb:Si.

Table 5-3

Experimental and theoretical magnetoconductances for sample #50 at T = 8 K. σ' is calculated using $\tau = 3.2\times10^{-11}$s and $\tau = 8\times10^{-12}$s. The conductivities are given in units of $\Omega^{-1}cm^{-1}$.

H(KOe)	$\Delta\sigma_{ex}$	σ'_{AL}	σ'_{pp}	σ'_{ph}	$\Delta\sigma_{ex-AL-ee}$	σ'_{loc+MT}
0	0	0	0	0	0	0
6.05	-2.1±0.1	-0.8	0.01	-0.00	-1.3	-1.3
12.10	-4.1	-1.6	0.03	-0.00	-2.5	-2.5
18.15	-5.8	-2.6	0.07	-0.00	-3.3	-3.4
24.20	-7.2	-3.4	0.13	-0.01	-3.9	-4.1
30.25	-8.5	-4.2	0.20	-0.02	-4.5	-4.4
36.30	-9.5	-5.0	0.27	-0.03	-4.7	-4.7

Table 5-4

Inelastic and spin orbit scattering times for sample #50.

T(K)	τ_i (s)	τ_{so} (s)
5.00	(9.5±0.5)x10^{-11}	
7.00	(4.8±0.3)	(8±1)x10^{-12}
8.00	(3.2±0.1)	8
9.00	(2.0±0.1)	10
9.36	(1.7±0.1)	10
10.00	(1.2±0.1)	7

Table 5-5

Values from the different calculations of $\beta(H)$ at T = 5K. β is obtained using Eqns. 5-13 and 5-14. $\beta^{(2)}$ is calculated from Eqn. 5-13 along with experimental values of T (H). $\beta^{(3)}$ is proportional to $\epsilon^{-1/2}$.

H(KOe)	β	$\beta^{(2)}$	$\beta^{(3)}$
0	30.4	30.4	30.4
6.05	15.8	18.3	23.6
12.10	10.8	12.4	19.4
18.15	8.2	8.7	16.3
24.20	6.6	6.6	14.2
30.25	5.4	5.2	12.5
36.30	4.6	4.1	11.2

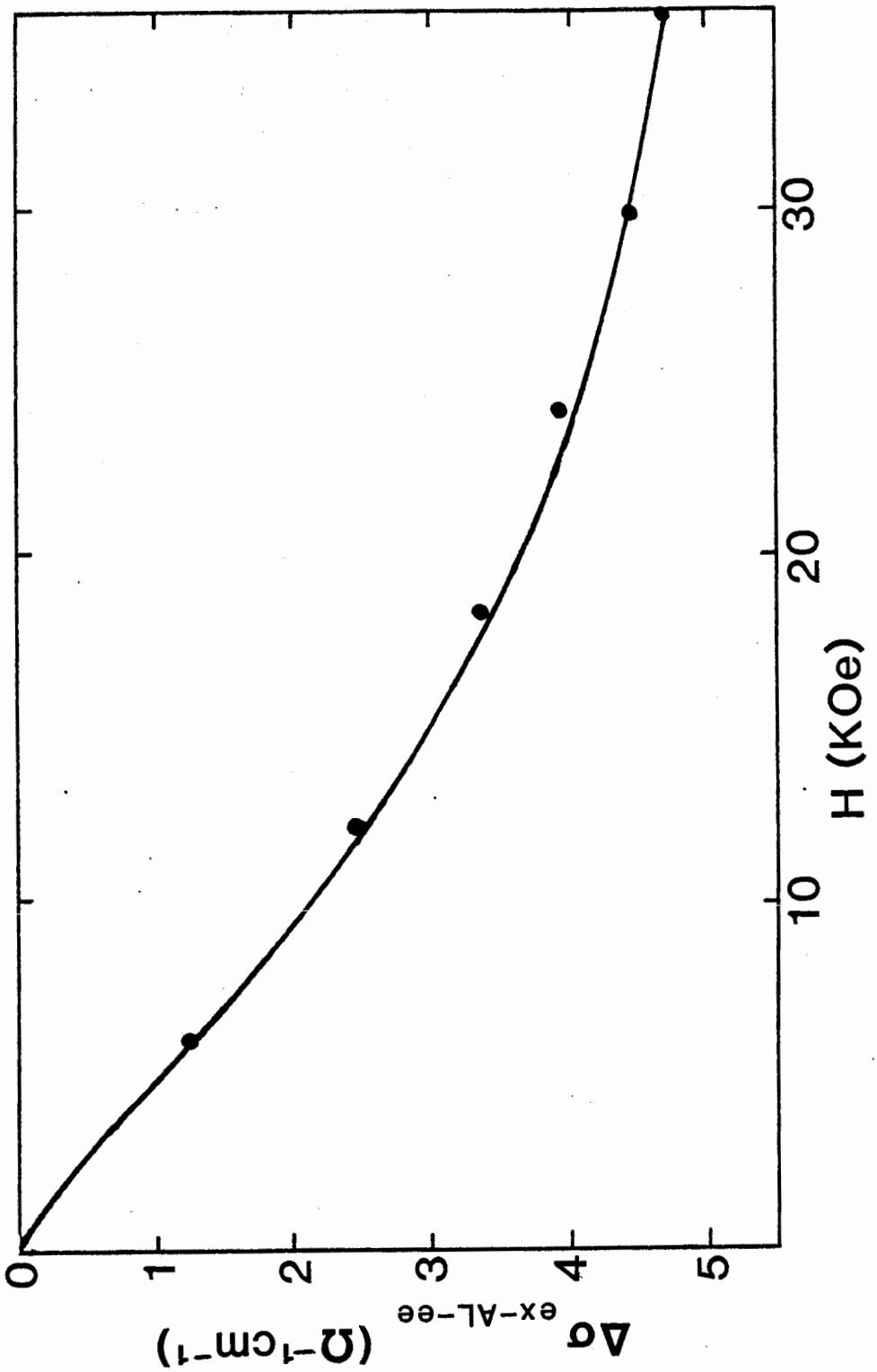

FIG. 5-4: $\Delta\sigma_{ex-AL-ee}$ vs H for sample #50. T = 8K. The line is the best fit to M-T fluctuations and localization theory, which gives τ_i = 3.2x10^{-11}s and τ_{so} = 8x10^{-12}s.

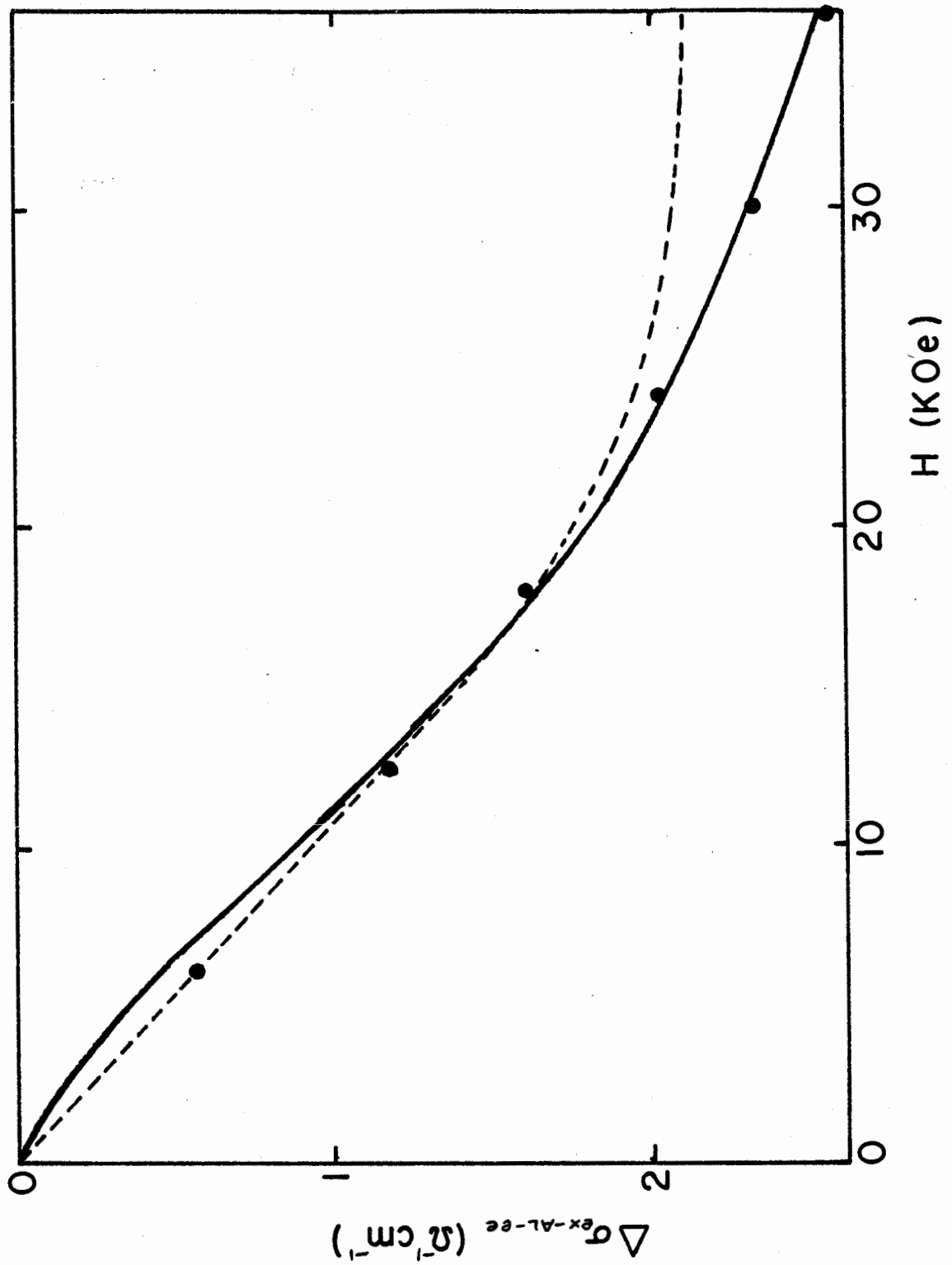

FIG. 5-5: $\Delta\sigma_{ex-AL-ee}$ vs H for sample #50, T = 9.36K. The dashed line is field sweep data. The circles are from the temperature sweep data. The solid line is the theoretical fit with τ_i = 1.7×10^{-11}s and τ_{so}= 1.0×10^{-11}s.

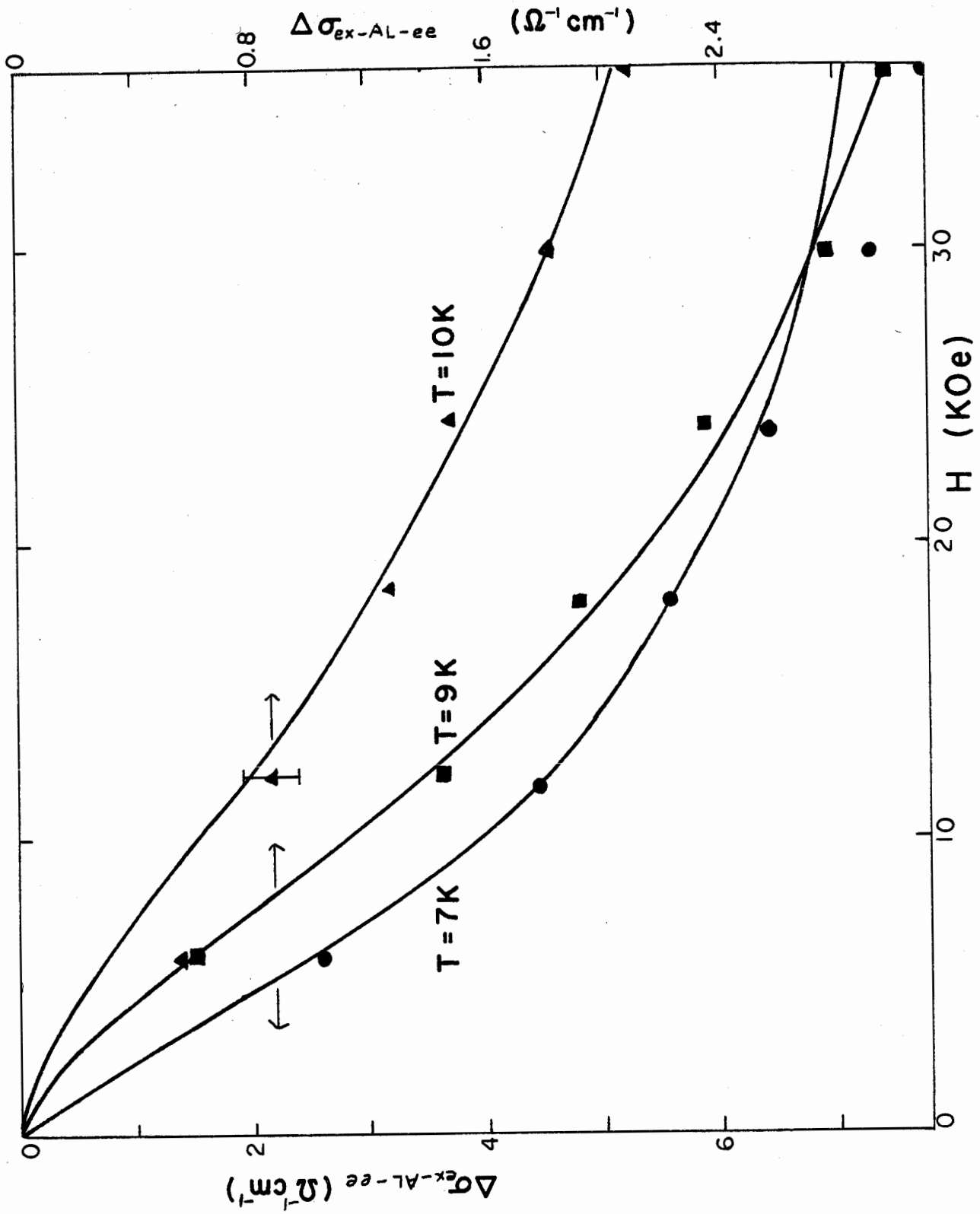

FIG. 5-6: $\Delta\sigma_{ex\text{-}AL\text{-}ee}$ vs H for sample #50, T = 7K, 9K, and 10K. The lines give the theoretical fits. The resulting values of τ_i and τ_{so} are given in Table 5-4.

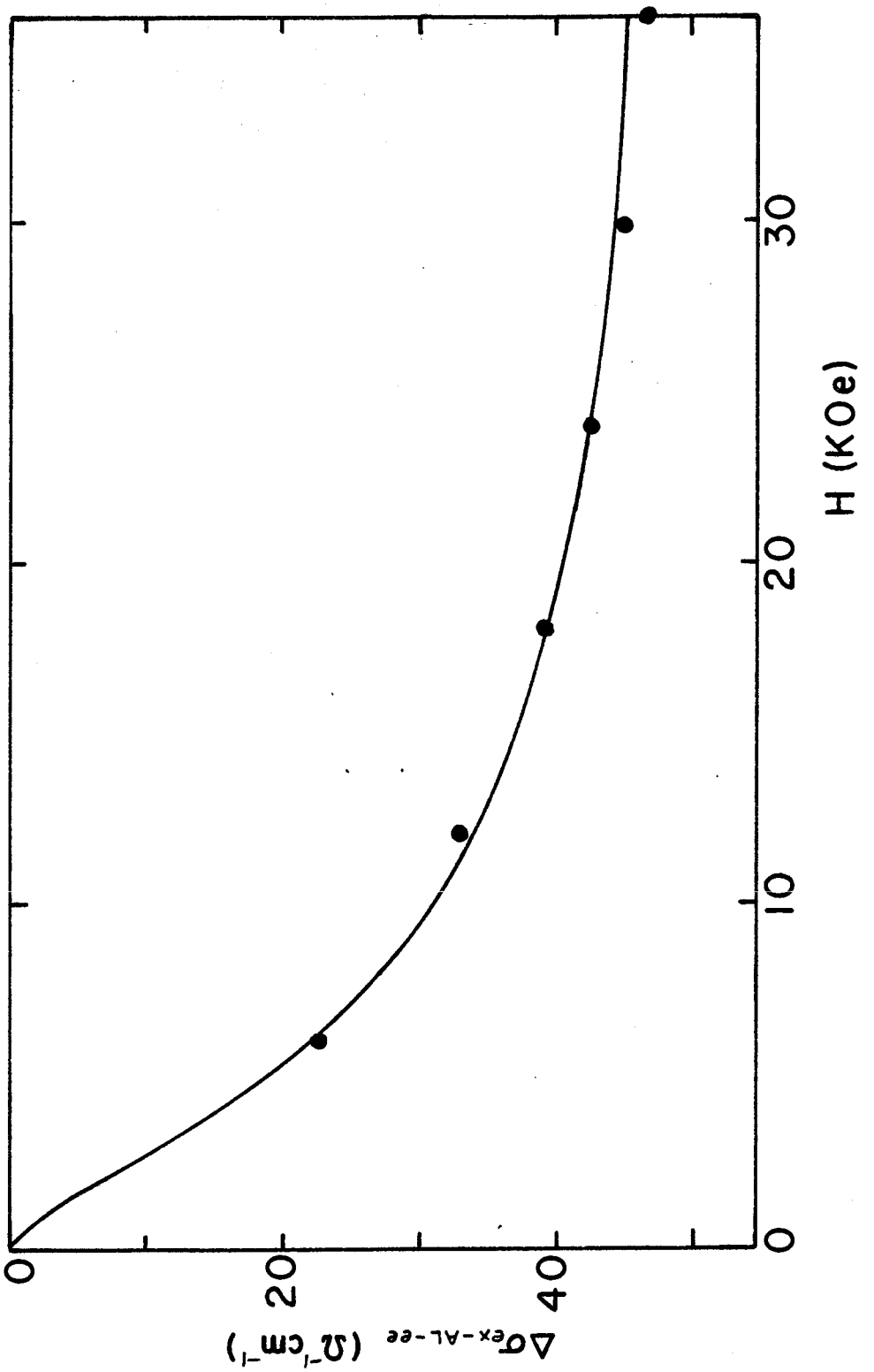

FIG. 5-7: $\Delta\sigma_{ex\text{-}AL\text{-}ee}$ vs H for sample #50, T = 5K. The line gives the theoretical fit, using $\beta^{(3)}$, with $\tau_i = 9.5 \times 10^{-11}$s and $\tau_{so} = 0$ (ie. the limit of strong spin orbit scattering).

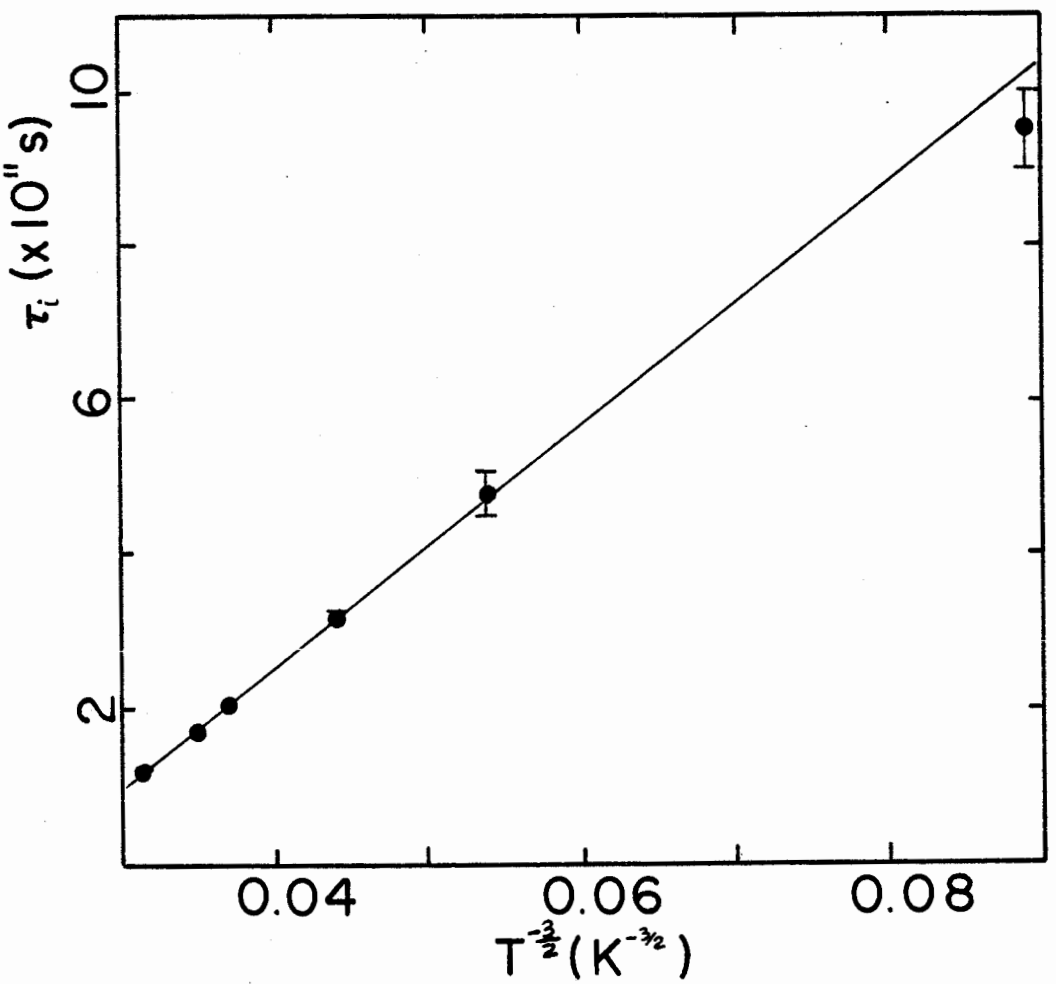

FIG. 5-8: τ_i vs $T^{-3/2}$ for sample #50.

2) Analysis of a 2-D material

The thin film analysed in this section has a temperature dependent conductivity at high temperatures even in high fields. This indicates that this sample (in contrast to the 3-D sample #50) has a contribution from classical conductivity due to inelastic scattering. This additional contribution makes the analysis of temperature dependence very difficult and it will not be carried out.

The magnetoconductance due to quantum corrections in 2-D has been well studied in the literature. In particular M-T fluctuations and localization, which give the largest contributions, seem to be well understood. The magnetoconductance of the 2-D Nb:Si film studied here can be explained with the 2-D theories. The method of analysis is the same as that used in the previous section.

Sample #51 is a coevaporated Nb:Si thin film on a sapphire substrate, made in the same way as sample #50. Its composition is approximately 80%Nb and 20%Si. It has a thickness of 140 Å and the diffusion constant is 1.34 $cm^2 s^{-1}$ (Table 4-2). Magnetoconductance measurements, in fields perpendicular to the film, were made at a constant temperature of 7.73 K. The characteristic length for localization effects is $L_i = [D\tau_i]^{1/2}$. If $\tau_i = 10^{-11}$s, then L_i = 370 Å which is much larger than the thickness of sample #51.

At 7.73 K the coherence length is determined using the value of $\xi(0)$ found in Chapter 4 and the theoretical temperature dependence which gives

$$\xi(T) = (93\ \text{Å}) \left(\frac{1}{\ln T/T_c} \right) = 180\ \text{Å} \qquad 5\text{-}22$$

which is larger than the film thickness. This film can be considered two dimensional as far as localization and superconducting fluctuations are concerned.

The formula for magnetoconductance due to localization in 2-D is [Hikami et al (1980)] [Maekawa and Fukuyama (1981)] [Santhanan and Prober (1984)]

$$G_{loc} = \frac{e^2}{2\pi^2\hbar} \left[-\frac{1}{2} \Psi\left(\frac{1}{2} + \frac{H_i}{H}\right) + \frac{3}{2} \Psi\left(\frac{1}{2} + \frac{H_2}{H}\right) - \ln\left(\frac{H_2}{H}\right) + \frac{1}{2} \ln\left(\frac{H_i}{H}\right) \right] \qquad 5\text{-}23$$

where $\psi(x)$ is the digamma function, and G is the conductance per square. It has been customary to express the arguments of the above functions in terms of characteristic fields,

$$H_i = \frac{\hbar c}{4\pi D \tau_i} \qquad 5\text{-}24$$

$$H_{so} = \frac{\hbar c}{4\pi D \tau_{so}} \qquad 5\text{-}25$$

$$H_2 \quad H_i + \frac{4}{3} H_{so} \qquad 5\text{-}26$$

The formula for M-T fluctuations in two dimensions is [Larkin (1980)] [Santhanan and Prober (1984)]

$$G_{MT} = \frac{-e^2}{2\pi^2\hbar} \beta \left[\Psi\left(\frac{1}{2} + \frac{H_i}{H}\right) + \ln\left(\frac{H}{H_i}\right) \right] \qquad 5\text{-}27$$

The parameter β will be discussed later in this section.

The magnetoconductance due to the A-L fluctuations is smaller for two dimensions than for three dimensions. The theory calculated by Redi (1977) gives the temperature and field dependent conductivity correction

$$G_{AL}(T,H) = \frac{\gamma^2 e^2}{2\ln(T/T_{c0})}\left[\psi\left(\gamma+\tfrac{1}{2}\right) - \psi(\gamma+1) + \frac{1}{2\gamma}\right] \qquad 5\text{-}28$$

where

$$\gamma = \frac{2\epsilon kT}{\pi DeH} \qquad 5\text{-}29$$

The A-L contribution to the magnetoconductance is calculated from

$$G_{AL}(H) = G_{AL}(T,H) - G_{AL}(T,0) \qquad 5\text{-}30$$

The dimensionality of electron-electron interaction effects is determined from the thermal diffusion length, which at T = 7.73 K is L_T= 115 Å. This is somewhat smaller than the film thickness of 140 Å. The three dimensional formulae Eqn. 5-17 and Eqn. 5-20 will be used. While this sample may not be strictly three dimensional the corrections due to electron-electron interactions are small (in 3-D or 2-D) and will not affect the analysis of the data.

The contributions due to the electron-electron interaction and A-L fluctuation magnetoconductivities are small. They become of the same order as the experimental uncertainties only at the largest fields. These corrections are subtracted from the data

giving $\Delta G_{ex\text{-}AL\text{-}ee}$ which is plotted in Fig. 5-9. The data in this figure is then fitted to the M-T fluctuation and weak localization theories. The parameter β is a source of problems again. If a field dependent $\beta(H)$ is calculated using Eqn. 5-13 and Eqn. 5-14, the "+" in Fig. 5-9 are the result. This approach does not fit the data. Using a constant value of $\beta = \beta(H=0)$ gives the solid line. It fits the data reasonably well. Both of these choices of β were used by Santhanan and Prober (1984), who investigated two dimensional Al films. They came to the same conclusion as obtained here; a constant value of β gives a better fit to the data.

While a constant β fits the data, it is clear from physical arguments that β must eventually decrease with increasing fields. As seen in the analysis of the three dimensional material, $\beta(H)$ may have a similar field dependence as the A-L fluctuations. The dashed line in Fig. 5-9 is calculated using $\beta(H)$ proportional to G (H) given in Eqn. 5-30. This fit gives the same value of τ_i (1.4×10^{-11}s) as the fit using a constant value of β. However the two theoretical fits give different values of τ_{so} (β=constant yields $\tau_{so}=5\times10^{-12}$s wheras β G gives $\tau_{so}=3\times10^{-13}$). It is not clear which is the better value.

The value of τ_i found for this 2-D film is smaller than the value for the 3-D film of $\tau_i(8K) = 3.2\times10^{-11}$s. This means that the inelastic scattering is larger in the cleaner (higher conductivity) material. Mui et al (1984) found that the opposite is true in Al films. This may be explained by the difference in

band structure of the two materials. The difference is that Nb has a large contribution to electron-electron scattering from the interaction between s and d orbitals.

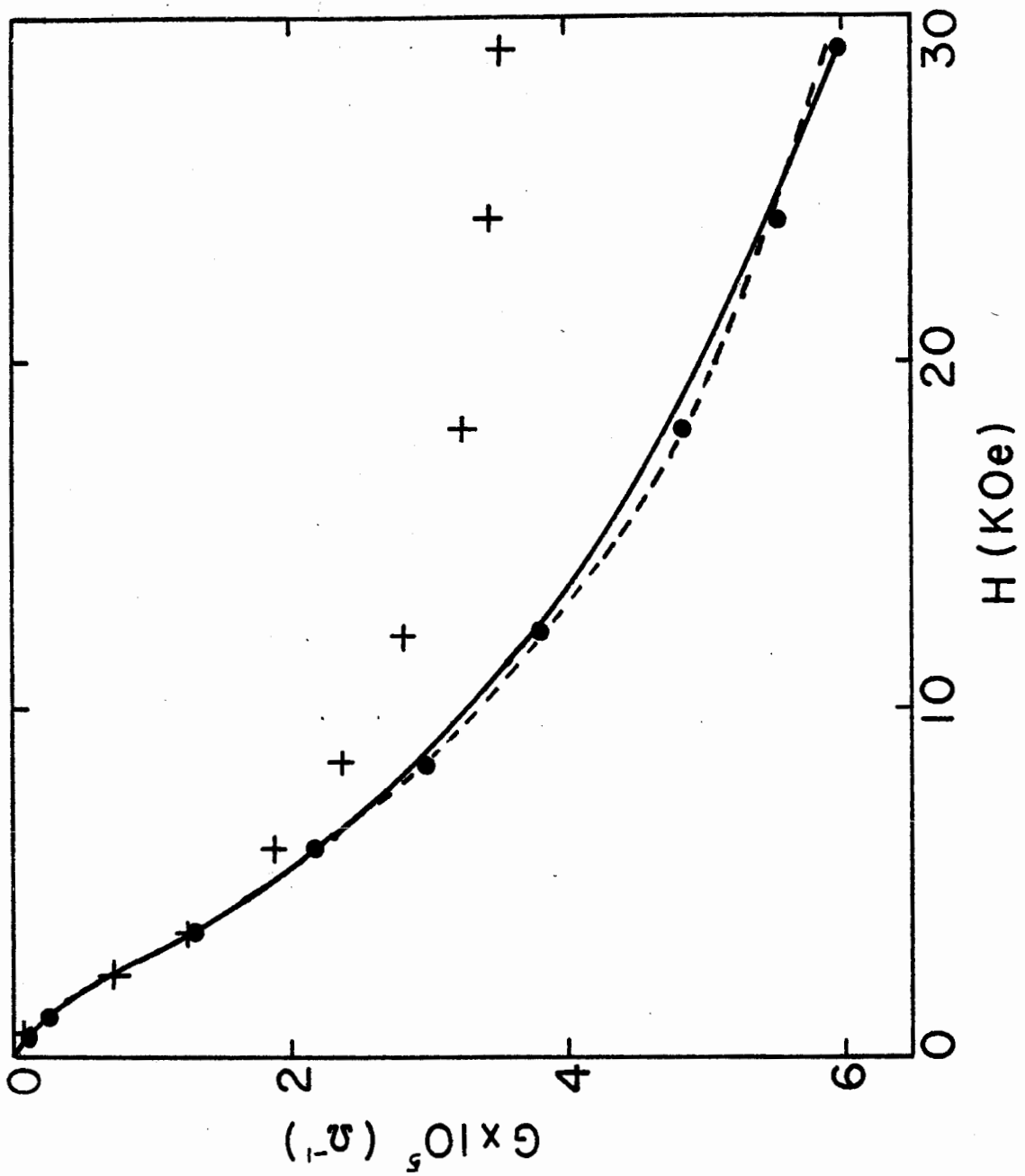

FIG. 5-9: $\Delta G_{ex\text{-}AL\text{-}ee}$ vs H for sample #51, T = 7.73 K. The data are given by the circles. The crosses are theory with $\beta(H)$ given by Eqns. 5-13 and 5-14, $\tau_i = 1.4\times10^{-11}$s, and $\tau_{so} = 4\times10^{-13}$s. The solid line is theory with β = constant, $\tau_i = 1.4\times10^{-11}$s, and $\tau_{so} = 5\times10^{-12}$s. The dashed line is theory with $\beta \propto G_{A\text{-}L}$, $\tau_i = 1.4\times10^{-11}$s, and $\tau_{so} = 3\times10^{-13}$s.

3) Analysis of a layered material

So far magnetoconductance have been fit to theory for both a three dimensional sample and a two dimensional sample. Data for a layered material will now be examined. The magnetoconductance is analysed following the method of the previous sections. It is found that the dimensionality of localization effects is uncertain for this sample. Two different values of τ_i are obtained depending on whether a dimensionality of 2 or 3 is assumed. It is not clear from the magnetoconductance which is the better value. The influence of τ_i on the temperature dependent conductivity is also investigated. This shows that a better value of τ_i is obtained by assuming that localization is 2-D.

Sample #24 consists of four layers of Si each about 25 Å thick, separated by three Nb layers each about 72 Å thick. The total thickness is 310 Å. The superconducting coherence length is anisotropic, with the coherence length perpendicular to the layers, $\xi_\perp$, being equal to 38 Å. The superconducting fluctuations will be three dimensional in nature.

The dimensionality of localization effects is determined by the inelastic diffusion length. If we assume $\tau_i = 2\times10^{-11}$ with a diffusion constant perpendicular to the layers $D_\perp = 0.57\ cm^2s^{-1}$, then $L_i = 340$ Å. This implies a two dimensional behavior. Since the magnetoconductance of the M-T fluctuations depend on L_i in

the same way as localization, they will be assumed to be two dimensional even though the A-L fluctuations are three dimensional.

The characteristic length for electron-electron interactions is L_T= 107 Å. Therefore the three dimensional corrections for electron-electron interactions will be used. As before, these corrections are small.

The dimensionality of the different phenomenon in this sample is questionable. During the following analysis the consistency of the above choices of dimensionality will be discussed.

First the contribution of the A-L term is calculated. In the three dimensional formula of Eqn. 5-3 the coherence distance must be the average over the anisotropy elipsoid

$$\xi = [\xi_{//}^2 \xi_{\perp}]^{1/3} = 70 \text{ Å} \qquad 5\text{-}31$$

As pointed out in the previous section, the field dependence of the A-L term comes through the field dependence of the critical temperature. The T_c(H) measurements were made only down to temperatures of 2.37 K (H = 16.94 KOe). A linear extrapolation was used to extend T_c(H) down to 0 K (which gives $H_{c2}(0)$ = 35.4 KOe). For fields higher than $H_{c2}(0)$ no value of σ'_{AL} was calculated. The formula used here for the magnetoconductivity of the A-L term is only valid for small $\epsilon = \ln T/T_c$. The calculation is therefore suspect at high fields where T_c approaches zero.

Note that the magnetoconductance data in Fig. 4-8 shows a kink at H = 35 KOe, indicating a qualitative change in the magnetoconductance when the superconductivity is completely quenched. This is a very interesting feature. The theories which give magnetoconductance due to superconducting fluctuations, localization, and electron-electron interactions predict a smoothly changing magnetoconductance as the field increases. These theories give no mechanism to produce such a kink. We will come back to this in the discussion at the end of this chapter.

The 3-D A-L contribution accounts for about half of the observed magnetoconductance. A two dimensional calculation gives a much smaller contribution. If the two dimensional A-L formulas were used, the remaining magnetoconductance is too large to be accounted for by the localization and M-T corrections. Therefore the A-L fluctuations must be three dimensional in this film.

In calculating the electron-electron interaction contributions for an anisotropic material [Altshuler et al (1981)], one must multiply the formula in Eqn. 5-17 and 5-20 by $D_{//}/D^{(3)}$, where $D^{(3)} = [D_{//} D_{//} D_{\perp}]^{1/3}$ for three dimensions. For this sample $D_{//} = 1.42\ cm^2 s^{-1}$ and $D^{(3)} = 1.05\ cm^2 s^{-1}$. $D_{//}$ and $D_{\perp}$ are given in Table 4-2.

Again the above calculations are subtracted from the data to give $\Delta\sigma_{ex\text{-}AL\text{-}ee}$, which is shown in Fig. 5-10. The magnetoconductance due to two dimensional M-T fluctuations and localization is found using Eqn 5-27 and Eqn. 5-23 corrected for anisotropy by multiplying by [Altshuler et al (1981)] $D_{//}/D^{(2)}$,

where $D^{(2)} = [D_{//} D_{\perp}]^{1/2} = 0.90\ cm^2 s^{-2}$. The calculation using a field dependent $\beta(H)$ as given by Eqns. 5-13 and 5-14 is shown using a dashed line. A very small value of τ_{so} is needed to give a reasonable fit to the data. Results from the previous section suggest that it is better to use a constant value for β. This is shown as a solid line. It too agrees fairly well with the data, although it is not within the error bar of every data point. The fitting parameter for the spin orbit scattering time is $\tau_{so} = 5 \times 10^{-12} s$, which is close to the value of $\tau_{so} = 9 \times 10^{-12} s$ found for sample #50, as expected. The other fitting parameter, the inelastic scattering time is $\tau_i = 4.0 \times 10^{-12} s$ (for both $\beta = \beta(H)$ and β = constant). The dimensionality must be checked using this result to calculate the inelastic scattering length. It gives $L_i = 150$ Å which is smaller than the film thickness of 310 Å. This implies that this film may be three dimensional rather than two dimensional.

The magnetoconductance will now be analysed assuming that this sample is 3-D. Fig. 5-11 shows the data compared to three dimensional theory. The M-T and localization contributions are given by Eqn. 5-12 and Eqn. 5-9 multiplied by $D_{//}/D^{(3)}$. The solid line is for $\tau_i = 2.0 \times 10^{-11} s$ and $\tau_{so} = 0$ (strong spin orbit scattering). This curve does not fit the data as well as the two dimensional theory does. Including a finite amount of spin orbit scattering (dashed line) gives more disagreement between theory and data. The resulting inelastic diffusion length of $L_i = 340$ Å would imply that the film may be two dimensional.

There are now two contradictory results. If 2-D M-T fluctuations and localization are assumed, the resulting value of L implies that the film is 3-D. However, if 3-D M-T fluctuations and localization are assumed, the resulting value of L implies that the film is 2-D. Calling this sample either two dimensional or three dimensional is questionable. The actual behavior may be something in between. Only for the A-L fluctuations do we obtain a definite 3-D behavior.

A further comparison between the assumption of 2-D or 3-D can be made by considering the magnitude of the resulting values of τ_i . For a fixed τ_i, the effect of localization is larger in two dimensions than in three dimensions. This means that, in fitting experimental data, the 2-D formula will give a smaller τ_i than the 3-D formula. This is seen to be true from the above values of τ_i. In the following, it is shown that only one of these values of τ_i is consistent with the observed temperature dependence of conductivity.

At high temperatures and high magnetic fields this sample has a conductivity which increases as temperature decreases (see Fig. 4-6). Since the superconducting fluctuations are now quenched, this must be due to inelastic scattering τ_i in the classical theory, since the conductivity due to quantum effects (localization and electron-electron interactions) would result in the opposite temperature dependence. The classical conductivity is given by

$$\sigma = (\text{const})\,\tau \qquad 5\text{-}32$$

where $\tau^{-1} = \tau_o^{-1} + \tau_i^{-1}$. If $\tau_i >> \tau_o$, then the conductivity due to the inelastic scattering can be written

$$\sigma_i' = \sigma_o \frac{\tau_o}{\tau_i} \qquad 5\text{-}33$$

where σ_o = (const)τ_e . The change of conductivity observed between T = 10 K and T = 15 K is $\Delta\sigma_{ex}$ =15.5 $\Omega^{-1}cm^{-1}$. Assuming that $\tau_i \propto T^{-3/2}$ and using the two dimensional result that τ_i (T=8.94K) = $4x10^{-12}$s, gives τ_i (10K) = $3.4x10^{-12}$ and τ_i (15K) = $1.9x10^{-12}$s. Table 4-2 gives the values τ_o = $1.3x10^{-15}$s and σ_o = 20,800 $\Omega^{-1}cm^{-1}$. Putting these into Eqn. 5-33 gives $\Delta\sigma'$= 10.0 $\Omega^{-1}cm^{-1}$. This is nearly as large as the experimental result. It is good agreement considering the uncertainty in the value of τ_o . The same calculation using the value τ_i = $2x10^{-11}$s from the three dimensional fit gives $\Delta\sigma$ = 2.0 $\Omega^{-1}cm^{-1}$. This is much smaller than the experimental value. Only the value of τ_i obtained using the 2-D magnetoconductance theory is consistent with the observed temperature dependence. This would confirm that the layered sample #24 behaves two dimensionally as far as localization and M-T fluctuations are concerned.

A further check on the consistancy of the results found in this chapter can be made. Applying the above method of calculation (Eqn. 5-33) to the 3-D sample #50 gives $\Delta\sigma_i'$ (7K to 10K) = 0.20 $\Omega^{-1}cm^{-1}$. This is too small to be seen by the measurements and so is consistent with the flat curves at high temperatures and high fields in Fig. 4-4.

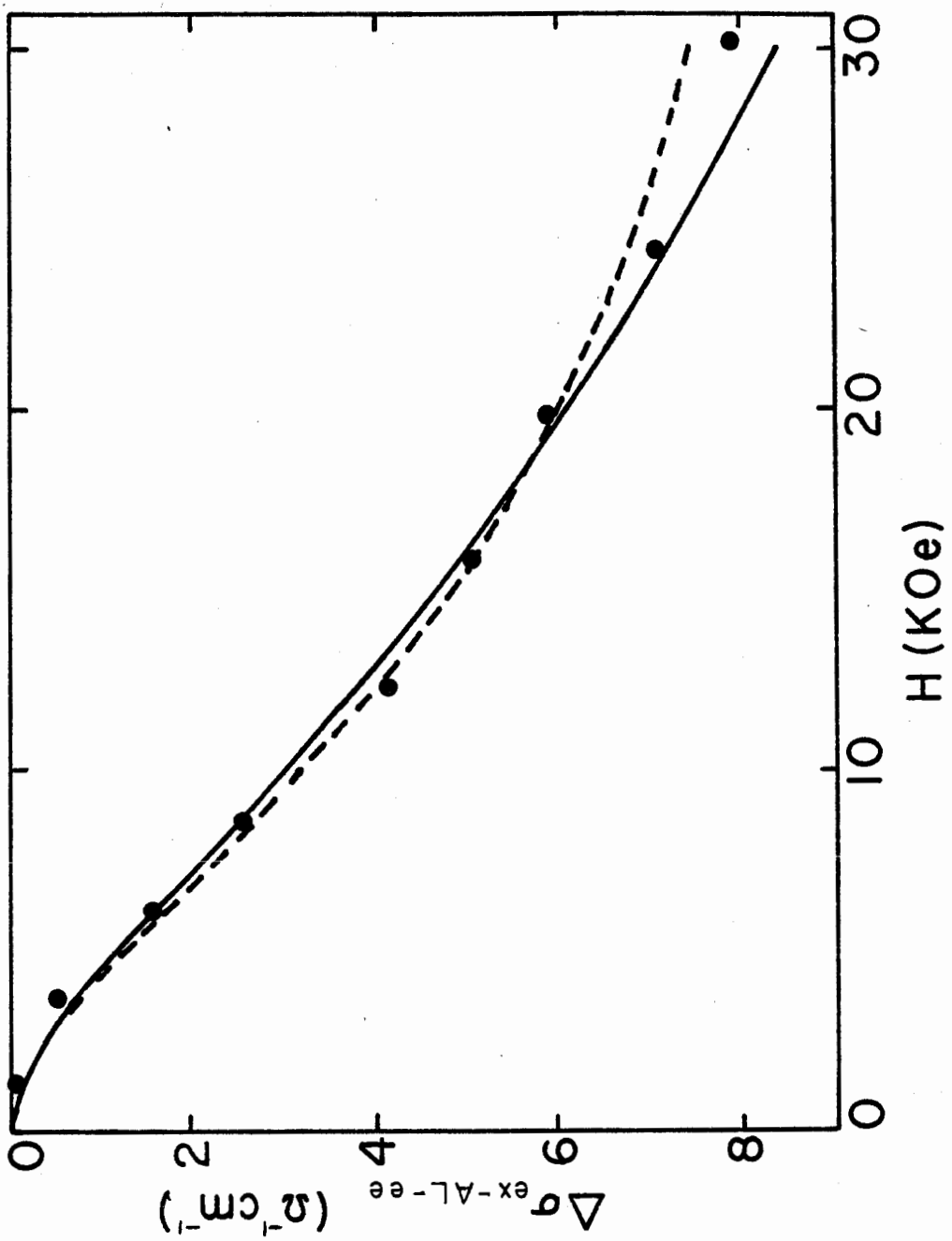

FIG. 5-10: $\Delta\sigma_{ex\text{-}AL\text{-}ee}$ vs H for sample #24, T = 8.94 K. The solid line is the 2-D theory with β = constant, τ_i =4.0x10^{-12}s, and τ_{so} = 5x10^{-12}s. The dashed line is the 2-D theory with β = β(H), τ_i = 4.0x10^{-12}s, and τ_{so} = 0.

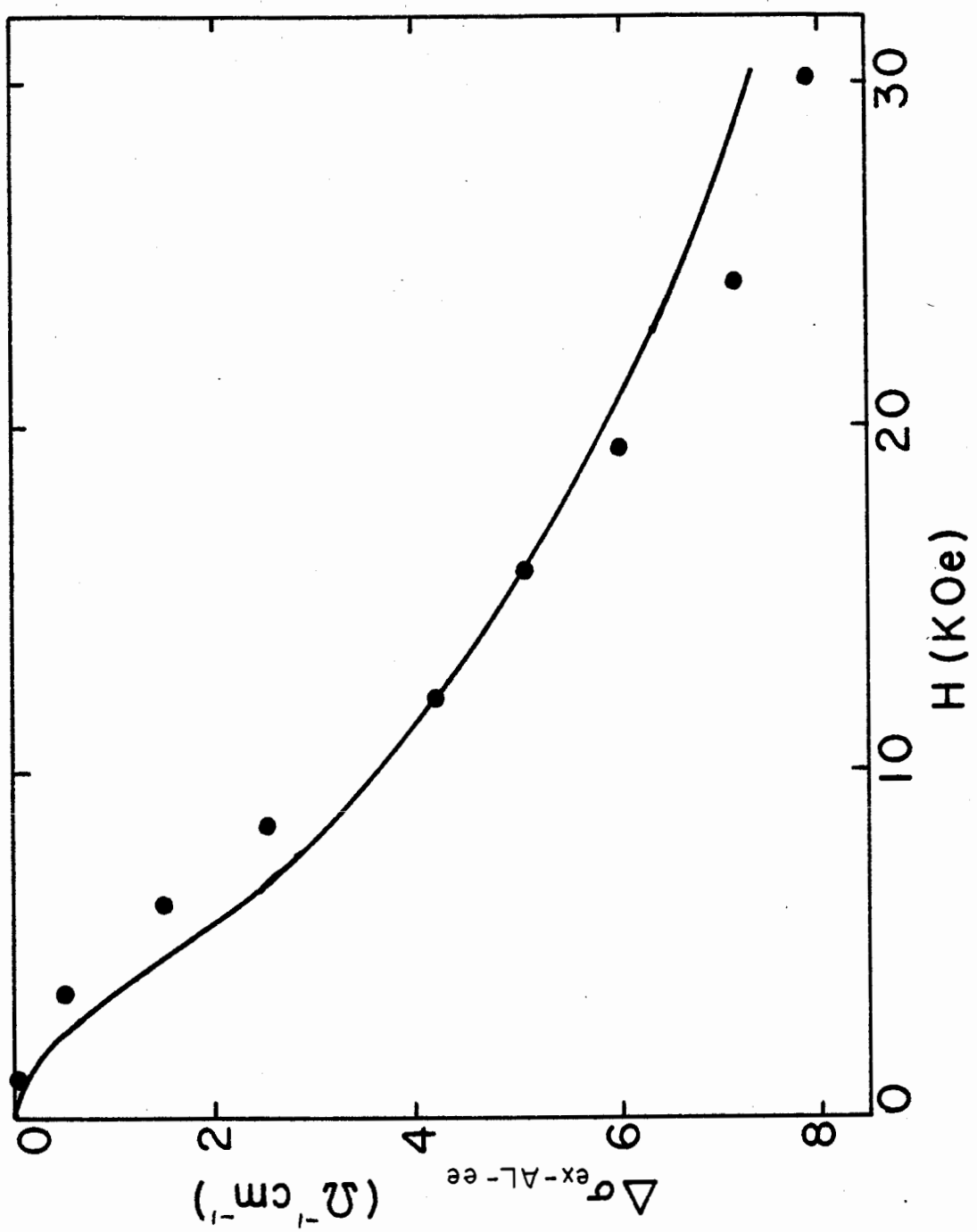

FIG. 5-11: $\Delta\sigma_{ex-AL-ee}$ vs H for sample # 24, T = 8.94 K. The line is the 3-D theory with τ_i = 2.0x10^{-11}s and τ_{so} = 0.

4) Upper critical fields

The upper critical fields of samples #50 and #24 can give important additional information about these films. In this section, the data for $H_{c2}(T)$ is presented. In the case of the layered sample #24, both parallel and perpendicular critical fields are given. The shapes of these H_{c2} curves differ from the standard three dimensional theory. Two explanations for the observed character of H_{c2} are considered. One is the dimensionality and the nature of the coupling between superconducting multilayers. The other is the possible effects that localization can have on superconductivity.

a) 3-D Nb:Si film

The values of T_c obtained from the fit of fluctuation conductivity in the analysis of the temperature dependence of the previously studied 3-D sample #50 are used to make the plot of H_{c2} vs T in Fig. 5-12. Values of T_c determined from the midpoint of the resistive transitions are slightly lower than T_c from the fluctuation conductivity fits, but both sets of data give the same slope (the important quantity) of H_{c2} near T_{co}. The solid line in Fig. 5-12 is the theoretical curve for H_{c2} in a dirty superconductor given by [deGennes (1966)]

$$\ln\left(\frac{T}{T_{co}}\right) + \psi\left(\frac{1}{2} + \frac{D e H_{c2}}{2\pi c k T}\right) - \psi\left(\frac{1}{2}\right) = 0 \qquad 5\text{-}34$$

Here ψ is the digamma function. The experimentally determined

value of 0.49 cm^2s^{-1} was used for the diffusion constant D. T_{c0} was taken to be 4.61 K as determined by the fluctuation conductivity fits. Although the theory fits the data quite well, it can be seen that the experimental points rise more steeply than the theoretical curve near T_{c0}, but at lower temperatures the data fall below the prediction. A smaller value of D could have been chosen to give a good fit near T_{c0}, but then the low temperature data would be even further below the theory. Conversely, the theory could be fit to the low temperature data using a larger value of D. In this case, the theory would fall above the data near T_{c0}, giving in particular, a larger value of T_{c0}. It is not imediately clear what the proper choice of the diffusion constant should be.

b) Layered Nb/Si film

We now consider the layered material. The critical fields parallel and perpendicular to the layers of sample #24 are presented in Fig. 5-13. This data was obtained from the midpoints of the resistive transitions. The anisotropy of this material is evident in the $H_{c2}(T)$ curves. The slope of $H_{c2//}$ is about three times larger than the slope of $H_{c2\perp}$. There are interesting features in the shapes of the curves near T_{c0}. In a bulk superconductor H_{c2} is linear near T_{c0}(see the theoretical curve in Fig. 5-12). But here neither $H_{c2//}$ nor $H_{c2\perp}$ is linear near T_{c0}. $H_{c2\perp}$ shows a slight upwards curvature, while $H_{c2//}$ has a strong downward curvature.

The critical fields of Nb/Ge multilayered thin films were studied in detail by Ruggiero et al (1982). Their results will be used to interpret the H_{c2} data given here. They studied parallel critical fields using the theory of superconductivity in layered materials by Klemm et al (1975). For a material with ξ much larger than the layer thickness $H_{c2//}$ (T) will have the standard 3-D shape which is linear near T_{co}. Materials where the layer separation is greater than ξ have Josephson-coupled superconducting layers. $H_{c2//}$ of these samples has a strong negative curvature and approaches the shape expected for isolated 2-D films, $H_{c2//} \propto (T_c - T)^{1/2}$. Some of their Nb/Ge samples had a 3-D behavior near T_{co} and crossed over to a 2-D behavior at lower temperatures when $\xi_\perp$(T) decreases to lengths shorter than the layer separation. $H_{c2//}$ for sample #24 in Fig. 5-13 has the same shape as a quasi-2-D layered material. This shows that the Nb layers are decoupled, as far as superconductivity is concerned, and have a 2-D behavior. (This is not consistent with our use of 3-D A-L fluctuations.)

$H_{c2\perp}$ for sample #24 has a slight upwards curvature near T_{co}. An upwards curvature of $H_{c2\perp}$ seems to be a universal feature of layered superconductors: both natural (Coleman et al (1983)) and synthetic (Ruggiero et al (1982)). Neither group were able to explain the upward curvature, but Ruggiero et al show that it is likely a property of isolated, individual layers.

While the shape of $H_{c2//}$ of sample #24 can be explained, the upward curvature of $H_{c2\perp}$ has not been explained. Also the

deviations of H_{c2} of sample #50 from the 3-D theory have not been explained. It has been shown in this chapter that the phenomena of localization exists in these films. Theoretically, localization should affect the critical fields. This is discussed in the following.

c) Effects of localization

The presence of localization is expected to reduce T_c of a superconductor. From this, Coffee et al (1984) predict an enhancement of H_{c2} over the standard theory for dirty superconductors (Eqn. 5-34). Their argument assumes that if the field did not influence localization, then $H_{c2}(T)$ would follow the standard theory. But since a magnetic field diminishes the effects of localization, T_c (H) will be higher than the prediction of the standard theory. This argument says that if the standard theory is fitted to experimental data near T_c (0), the data will rise above the theory at lower temperatures. This is opposite from what we observed for sample #50, Fig. 5-12.

It may be more natural to take the opposite starting point from the above argument of Coffey et al. That is, assume that at high fields the effects of localization are essentially quenched. Then, H_{c2} at high fields will follow the standard theory. As the field is decreased, localization effects will begin to be important. This will lower T_c below the standard theory. This argument does agree with our measurements on sample #50.

Maekawa et al (1983 and 1984) give a theory for H_{c2} in dirty superconductors for two and three dimensions. Their equation giving H_{c2} is

$$\ln\left(\frac{T}{T_{c0}}\right) = \Psi\left(\frac{1}{2}\right) - \Psi\left(\frac{1}{2} + \frac{e D H_{c2}}{2\pi c kT}\right) + R \qquad 5\text{-}35$$

This equation differs from the standard result for H (Eqn. 5-34) in two ways. First, the function R is due to the modification of the electron-electron Coulomb interaction by the disorder. Maekawa et al give complicated expressions for R which depend on both T and H_{c2}. The function R will affect H_{c2} and it will lower T in the absence of a field. Second, the diffusion constant D is modified by localization to give

$$D = \begin{cases} D_0\left[1 - \dfrac{3\sqrt{3}\,\pi}{(2\pi E_F \tau_0)^2}\right] & , \text{ for 3-D} \\ D_0\left[1 - \dfrac{3}{4\tau_0 E_F k_F t} \ln\left(\dfrac{1}{2\pi T \tau_0}\right)\right] & , \text{ for 2-D} \end{cases} \qquad 5\text{-}36$$

where k_F is the Fermi wave vector and t is the film thickness. (Note that the 3-D expression does not depend on temperature while the 2-D expression does.) Localization effects reduce the size of D, which will, in turn, increase the size of H_{c2}. But a change in D will not affect $T_c(H=0)$.

While the theory of Maekawa et al can give H_{c2} curves with an upward curvature, this curvature persists at high fields. This is unlike the behavior we observed for perpendicular critical fields of samples #50 and #24. We note that the above expressions for the modified diffusion constant have no dependence on magnetic field. Yet localization effects are

quenched by a field and this would increase D. Considering this, it is possible that H_{c_2} could show an upward curvature at low fields, but at large fields, as the localization is quenched, H_{c_2} would approach the shape predicted without localization effects. This is roughly what we observed for our Nb/Si films. From our sketchy arguments we cannot conclude that the shape of our observed H_{c_2} curves is due to localization. But they suggest that localization effects may be the cause of the anomalous upward curvature in H_{c_2}. More theoretical and experimental work is needed.

d) Summary

The shape we observed for $H_{c_{2\parallel}}$ for the layered sample #24 was explained by the theory for superconductivity in layered materials. It shows that (except very near T_{c_0}) sample #24 is quasi-2-D with decoupled superconducting layers.

This suggests a solution to the problem we had in the analysis of the magnetoconductivity of the layered sample. There we assumed 2-D localization which leads to an inelastic diffusion length (L_i = 150Å) which is smaller than the total film thickness (310A) in apparent contradiction to the original assumption. But the individual layers are thinner (72Å) than L_i, which implies that the layers are isolated as far as localization is concerned. This interpretation also gives an explanation for the observed kink in the magnetoconductivity (Fig. 4-8). In a high magnetic field the characteristic length

for localization is given by $L_H = [\hbar c/4eH]$ rather than by L_i. The kink occurs at a field of H = 35 KOe corresponding to L_H = 69 Å. This is about the same as the individual layer thicknesses. Which means that the kink in the magnetoconductance is the result of the change from 2-D localization at low fields to 3-D localization at high fields. This type of behavior has not been reported in the literature.

The observed H_{c2} curves for both the layered sample #24 and the 3-D sample #50 do not agree with the standard theory. This may be due to the effects of localization and electron-electron interactions, but the quantitative theory does not agree in detail with our observations. An examination of the theory shows that it is not yet complete as it doesn't include the effect of magnetic field on the diffusion constant.

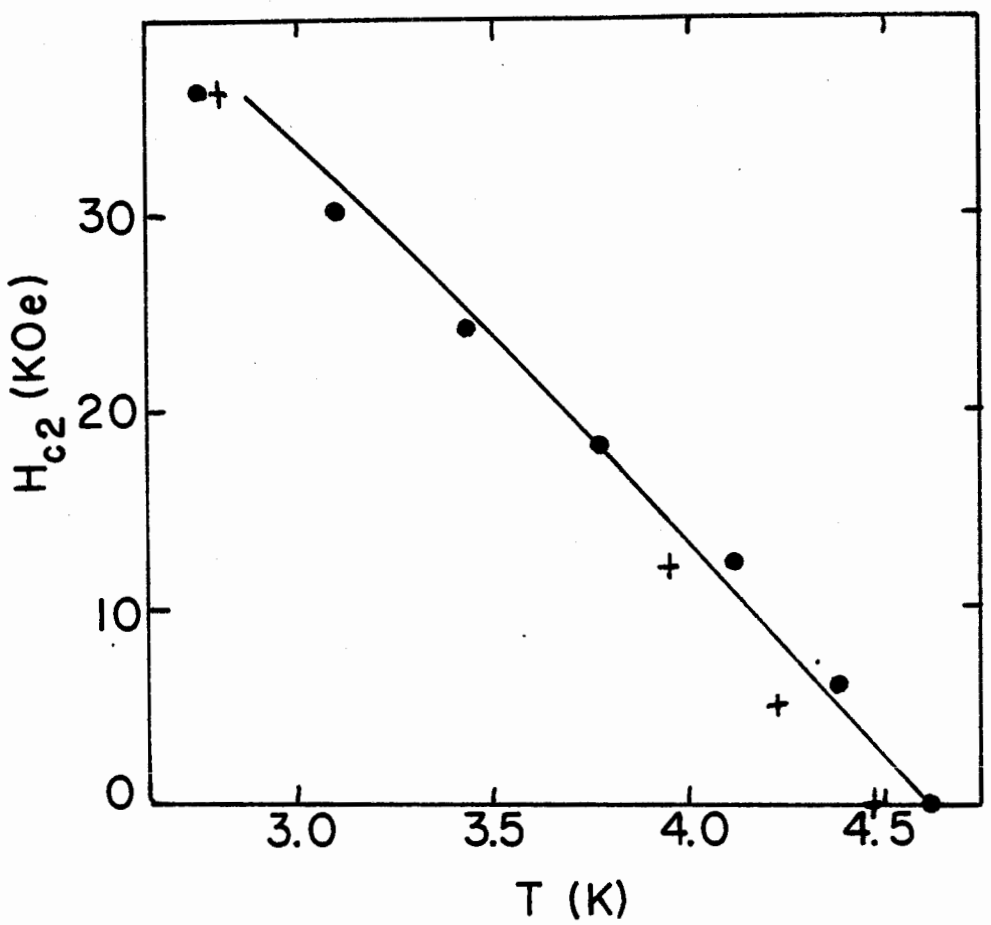

FIG. 5-12: Upper critical fields for sample #50. The circles are obtained from fits to fluctuation conductivity. The crosses are from the midpoints of resistive transitions. The line is the standard theory for dirty superconductors (Eqn 5.34).

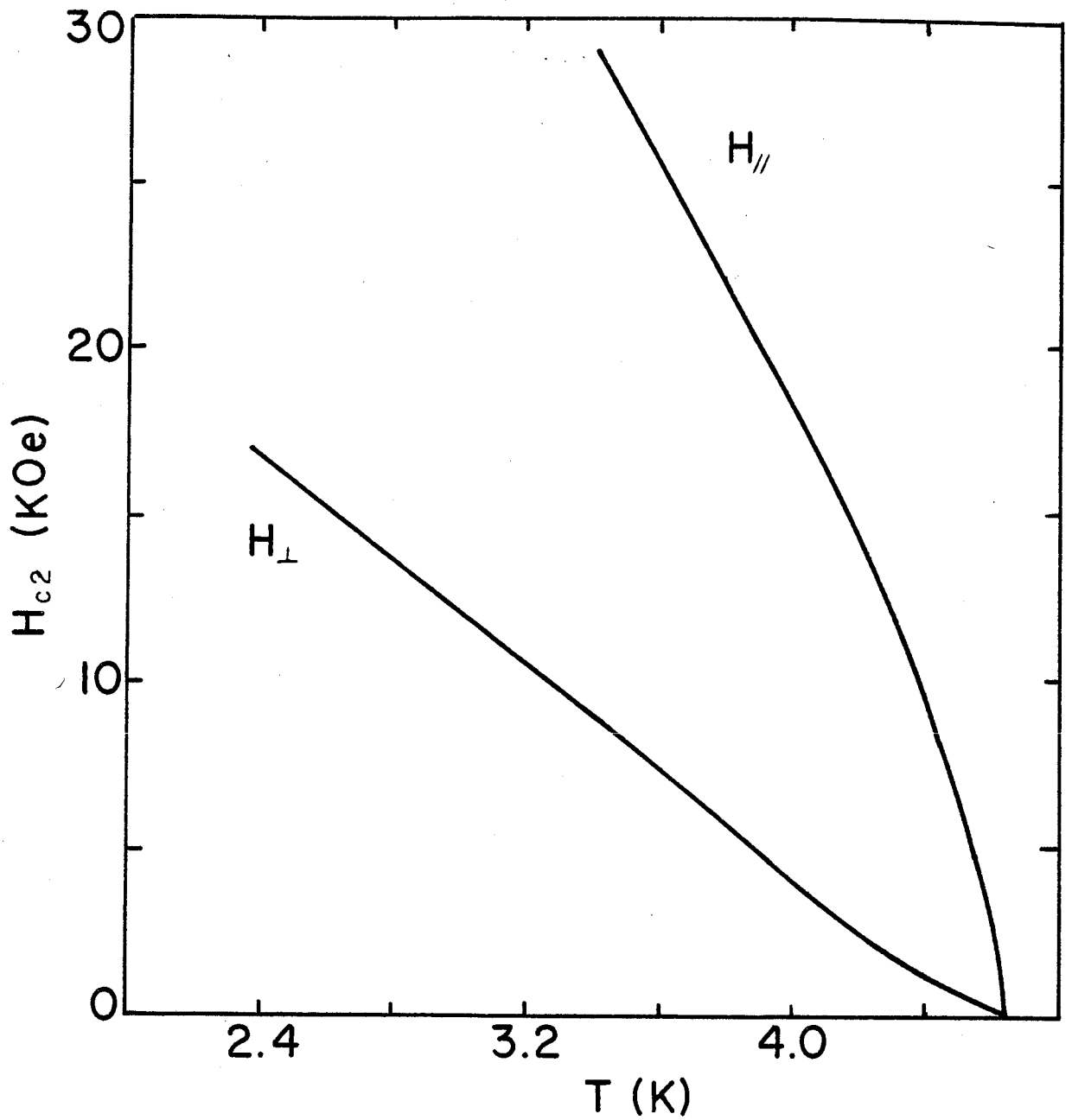

FIG. 5-13: Parallel and perpendicular critical fields for sample #24. The data is from the midpoints of resistive transitions.

VI. Discussion and Conclusions

We have built an ultra high vacuum evaporation system. Its features include an ion pumped vacuum chamber, two e-gun evaporation sources, an introduction chamber, a substrate oven, and a quartz crystal thickness monitor. This system was used to make a series of Nb-Si thin films. Some of these films had a layered composition while others were coevaporated and presumably uniform in composition. The superconducting properties and the conductivity above T_c were studied for these materials.

The structure of the Nb-Si films was studied using transmission electron microscopy and Auger/sputter depth profiles. We found that the Nb in the films had a continuous polycrystalline structure, while the Si remained amorphous. In the coevaporated material, the Si may sit between the Nb grains. A very thin Nb layer (57Å) had some amorphous regions, suggesting that even thinner films would be amorphous. The Auger/sputter depth profiles showed a sharp interface for Nb evaporated onto a [100] Si single crystal. But it showed that a large amount of diffusion occurs at the interface of evaporated Nb and amorphous Si. The multilayered materials do not have discrete layers but rather a diffused structure with a modulated composition.

We found a relationship between T_c and ρ for the Nb-Si films. There is a rapid decrease of T_c with increasing ρ for $\rho<20$ $\mu\Omega$cm. This observation is quite well explained by the lifetime broadening theory of Testardi and Mattheiss (1978). For larger ρ the results depend on the substrate material. Films on sapphire substrates continued to follow the lifetime broadening theory. But films on glass substrates showed a slower decrease of T_c as ρ is increased. The reason for this is not understood.

The observed relationship between T_c and ρ encouraged further investigation of the electronic properties. We chose to investigate in detail a thick (3-D) coevaporated film, a thin (2-D) coevaporated film, and a multilayered film. Four probe measurements were made to determine ρ, T_c, and H_{c2} for these films. From these measurements the electronic parameters in Table 4-2 were determined. We could then proceed to analyse fine details of the conductivities above T_c.

Careful, high sensitivity measurements of conductivity above T were made. These are given in Figs. 4-4 and 4-5 for the coevaporated samples. Qualitatively these two films behave as would be expected. The conductivity grows as T_c is approached and T_c is reduced by the application of a field. A quantitative analysis of the temperature dependent conductivity for the 3-D film gave two results. First, the superconducting fluctuations consist of both A-L and M-T contributions and they are proportional to $[\ln(T/T_c)]^{-1/2}$ over a large range of temperature. Other studies in the literature report a $[\ln(T/T_c)]^{-2}$ dependence

only very near T_c. Second, we found a contribution to conductivity in addition to the fluctuation conductivity. This is proportional to $T^{1/2}$ and is due to electron-electron interactions and localization. By studying the conductivity in various constant applied fields, the contributions from electron-electron interactions and localization could be separated. The magnitudes of both of these contributions agree with the prediction of theory. We note that the temperature dependence shows that the electron-electron interactions are important in these films even though they do not contribute much to the magnetoconductivity.

The temperature dependent conductivity of the layered film (Figs. 4-6 and 4-7) has very interesting qualitative features. These can be explained in light of the analysis in Chapter 5. The most obvious feature is the maximum in conductivity that appears in large values of perpendicular field. The increasing conductivity at high temperatures is due to the decreasing inelastic scattering as the temperature drops. At low temperatures and high fields, where the superconductivity is essentially quenched, the quantum corrections to conductivity begin to dominate and the conductivity decreases. In these large fields the effects of localization will be diminished so that we expect the decreasing conductivity to be mainly due to electron-electron interactions.

The magnetoconductivity was analyzed quantitativity for all three samples. First we discuss the 3-D sample. The analysis

shows that the contribution from the A-L fluctuations is important and must be included. This has not been done by other researchers in the literature. We also discussed in detail the calculation of the field dependence of Larkin's fluctuation strength parameter β. The method of calculating $\beta(H)$ used by Mui et al (1984) was found to give satisfactory agreement for theory and experiment for temperatures well above T_c. But it did not work for temperatures near T_c. We found that assuming β was proportional to the 3-D superconducting fluctuations (ie. to $[\{\ln(T/T_c)\}^{-1/2}$ resulted in) a satisfactory fit to the data. Some theoretical work is needed to find a formula for $\beta(H)$ and this formula should be at least approximately proportional to $[\ln(T/T_c)]^{-1/2}$.

The fits of theory to our data give the values of τ_i and τ_{so} in Table 5-4. They have reasonable magnitudes. A final result for the 3-D film is that $\tau_i \propto T^{-3/2}$. This agrees with the theory for electron-electron scattering in a disordered material by Altshuler et al (1982).

The magnetoconductivity of the 2-D film was studied only at one temperature. The analysis followed exactly the procedure used in recent work in the literature. In 2-D, the contribution from the A-L term is small, contrary to the 3-D case. It also seems best, in the 2-D case, to use a constant value of β. In principle, β should depend on H but this must be only a small effect. The value of τ_i found for the lower resistive 2-D film is smaller than τ_i for the higher resistive 3-D film. This is the reverse of the finding of Mui et al (1984) for Al films. Nb has

a large contribution to electron-electron scattering by interactions between the d and s bands. This is not the case for Al. It is known that in pure Nb the electron-electron scattering goes like T^{-2}. But we have shown for the very disordered 3-D sample that $\tau_i \propto T^{-3/2}$. It is reasonable to assume that the less disordered 2-D sample is inbetween these two behaviours, and that its τ_i has a stronger temperature dependence than $T^{-3/2}$. The 2-D sample would then have a larger amount of inelastic scattering than the 3-D sample in agreement with our observations.

Having suceeded in analyzing the magnetoconductance for 2-D and 3-D localization, we proceeded to a layered material. Such an analysis has not yet been presented in the literature. The question of dimensionality comes to the forefront. Considering only the magnetoconductivity, both 2-D and 3-D localization and M-T fluctuations could be fit to the data. But in both cases the 3-D A-L contribution was needed. We found that the magnitude of the temperature dependent conductivity was only consistant with the value of τ_i from the 2-D fit. The inelastic scattering length is smaller than the overall thickness of the film which would seem to contradict the assumption of 2-D localization. But L_i is larger than the thickness of the individual layers and this suggests that the layers are isolated as far as localization is concerned. This assumption allows us to make the prediction that localization should change from 2-D to 3-D when the field characteristic length becomes smaller than a layer thickness.

This would occur for an applied field of 35 KOe and we observed a kink in the magnetoconductance at this field (Fig. 4-8).

The critical fields we measured for these films do not agree with the standard theory for a dirty superconductor. The shape of $H_{c2//}$ of the layered sample can be explained if the sample is a quasi-2-D superconducting material where the layers are decoupled. $H_{c2\perp}$ has an upward curvature which is common to layered superconductors. The physical cause of this has not been determined in the literature. We suggest that it may be due to localization. This would agree with the conclusion of Ruggiero et al (1982) that the upward curvature is due to a property of an isolated layer.

The critical field measured for the 3-D sample also does not agree with the standard theory. The deviation can be explained if there is a reduction of T_c at low fields due to localization effects. Unfortunately we have not been able to show to what extent localization affects T_{co}.

The main result of this thesis is the successful analysis of the magnetoconductance for three thin films. One was 3-D, one was 2-D, and the third was layered. One must be careful to treat each contribution to the conductivity properly. The theories are complicated and the effects are small. It is remarkable that the theory both predicts the functional form of the data and yields reasonable values of τ_i and τ_{so}. But there is still the outstanding problem of the calculation of $\beta(H)$.

It would be interesting to study the effects of localization on $T_c(0)$. This is difficult because the theory [Fukuyama et al (1984)] depends on a large number of parameters. By studying a series of MoGe films of constant composition but different thicknesses, Graybeal and Beasley (1984) showed that localization effects do depress T_c in 2-D. With a constant composition, but different thicknesses, the electronic properties are unchanged for the series of films and the effect of 2-D localization is increased by decreasing the thickness of the films. This cannot be done in 3-D. One would have to control localization by changing the resistivity, which could also change other electronic properties, making the problem very complicated. It would seem that in 3-D it is more promising to study H_{c2} where the localization is controlled by applying a magnetic field. In order to do this the theory must be further developed.

REFERENCES

Abrahams, E. and J. W. F. Woo (1968), Phys. Lett. 27A, 117.

Altshuler, B. L. and A. G. Aronov (1979), Zh. Eksp. Teor. Fiz. 77, 2028 [Sov. Phys.-JEPT 50,968].

Altshuler, B. L., D. Khmelnitzkii, A. I. Larkin, and P. A. Lee (1980), Phys. Rev. B22,5142.

Altshuler, B. L., A. G. Aronov, A. I. Larkin, and D. E. Khmelnitskii (1981),Zh. Eksp. Teor. Fiz. 81, 768 [Sov. Phys. JEPT 54,411].

Altshuler, B. L., A. G. Aronov, and D. E. Khmelnitzkii (1982), J. Phys. C: Solid State Phys. 15,7367.

Anderson, H. H. and H. L. Bay (1981), in Topics in Applied Physics, vol. 47 (Ed. R. Behrish), Springer Verlag, Heidelberg, p. 145.

Anderson, P. W., K. A. Muttalib, and T. V. Ramakrishnan (1983), Phys. Rev. B 28, 117.

Aslamasov, L. G. and A. I. Larkin (1968), Fiz. Tverd. Tela. 10, 1104 [Sov. Phys. - Solid State 10, 875].

Bergmann, G. (1982), Z. Phys. B. Condensed Matter 48, 5.

Bergmann, G. (1983), Phys. Rev. B 28, 2914.

Bergmann, G. (1984),Phys. Rev. B 29, 6114.

Bieri, J. B., A. Fert, G. Creuzet, and J. C. Ousset (1984), Solid State Commun. 49, 849.

Coffey, L., K. A. Muttalib, and K. Levin (1984), Phys. Rev. Lett. 52, 783.

Coleman, R. V., G. K. Eiserman, S. J. Hillenius, A. T. Mitchell, and J. L. Vincent (1983), Phys. Rev. B 27, 125.

de Gennes, P. G. (1966), Superconductivity of Metals and Alloys, Benjamin, New York.

de Trey, P., S. Gygax, and J.-P. Jan (1973), J. of Low Temp. Phys. 11, 421.

Denhoff, M., S. Gygax, and J. R. Long (1981), Cryogenics 21,400.

Denhoff, M. W. and Suso Gygax (1982), Phys. Rev. B 25, 4479.

Denhoff, M., B. Heinrich, A. E. Curzon, and S. Gygax (1985), submitted to Solid Thin Films.

Ebisawa, H., S. Maekawa, and H. Fukuyama (1983), Solid State Commun. 45, 75.

Fukuyama, H. (1982), Surface Science 113, 489.

Fukuyama, H., H. Ebisawa, and S. Maekawa (1984), Technical Report of The Institute for Solid State Physics, Ser. A, No. 1444.

Gladstone, G., M. A. Jensen, and J. R. Schrieffer (1969), in Superconductivity, (Ed. R. D. Parks), Marcel Dekker, Inc., New York.

Graybeal, J. M. and M. R. Beasley (1984), Phys Rev. B 29, 4167.

Hammond, R. H. (1975), IEEE Trans. Mag. MAG-11, 201.

Hikami, S., A. I. Larkin, and Y. Nagaoka (1980), Prog. Theor. Phys. 63, 707.

Imry, Y. and M. Strongin (1981), Phys. Rev. B 24, 6353.

Johnson, W. L. and C. C. Tsuei (1976), Phys. Rev. B 13, 4827.

Keck, B. and A. Schmid (1975), Solid State Commun. 17, 799.

Klemm, R. A., A. Luther, amd M. R. Beasley (1975), Phys. Rev. B 12, 877.

Kulik, I. O. (1971), Pis'ma Zh. Eksp. Teor. Fiz. 14, 341 [JEPT Lett. 14, 228].

Larkin, A. I. (1980), Pis'ma Zh. Eksp. Teor. Fiz. 31,239 [JEPT Lett. 31, 219].

Lawrence, E. D., N. C. MacDonald, P. W. Palmberg, G. E. Riach, and R. E. Weber (1978), Handbook of Auger Spectroscopy, 2nd Ed., published by Physical Electronics Div., Perkin Elmer Co., Eden Prairie, Minnesota.

Lee, P. A. and T. V. Ramakrishnan (1982), Phys. Rev. B 26, 4009.

Maekawa, S. and H. Fukuyama (1981), J. Phys. Soc. Jpn. 50, 2516.

Maekawa, S., H. Ebisawa, and H. Fukuyama (1983), J. Phys. Soc. Jpn. 52, 1352.

Maekawa, S., H. Ebisawa, and H. Fukuyama (1984), J. Phys. Soc. Jpn. 53, 2681.

Maki, K. (1968), Progr. Theoret. Phys. (Kyoto) 39, 897; 40, 193.

Maki, K. (1971), Progr. Theoret. Phys. (Japan) 45, 1016.

Mattheiss, L. F. (1970), Phys. Rev. B 1, 373.

Mayadas, A. F., R. B. Laibowitz, and J. J. Cuomo (1972), J. Appl. Phys. 43, 1287.

McLean, W. L. and T. Tsuzuki (1984), Phys. Rev. B 29, 503.

Mikeska, H.-J., and H. Schmitt (1970), Z. Phys. 230, 239.

Moehlecke, S. and Z. Ovadyahu (1984), Phys. Rev. B 29, 6203.

O'Hanlon, J. (1980), A Users Guide to Vacuum Technology, John Wiley and Sons, Inc., New York.

Redi, M. H. (1977), Phys. Rev. B 16, 2027.

Ruggiero, S. T., T. W. Barbee Jr. and M. R. Beasley (1982), Phys. Rev. B 26, 4894.

Sanathanam, P. and D. E. Prober (1984), Phys. Rev. B 29, 3733.

Shapira, Y. and D. Lichtman (1979) in Methods of Experimental Physics vol. 14, Eds. G. L. Weissler and R. W. Carlson, Academic Press, New York.

Sigmund, P. (1981) in Topics in Applied Physics, vol 47, Ed. R. Behrish, Springer Verlag, Heidelberg.

Testardi, L. R. and L. F. Mattheiss (1978), Phys. Rev. Lett. 41, 1612.

Thompson, R. S. (1970), Phys. Rev. B 1, 327.

Tinkham, M. (1975), Introduction to Superconductivity, McGraw-Hill, New York.

Toyota, N., A. Inoue, K. Matsuzaki, T. Fukase, and T. Masumoto (1976), Phys. Rev. B 13, 4827.